ERS-2 GOME GDP 3.0 Implementation and Delta Validation

Validation Report for GOME Level-1-to-2 Data Processor Upgrade to Version 3.0

Contributors: D. S. Balis, C. Fayt, P. Gerard, J. F. Gleason, J. Granville, G. Hansen, J-C. Lambert, G. Labow, D. Loyola, V. Soebijanta, W. Thomas, J. H. G. van Geffen, R. F. van Oss, M. Van Roozendael, C. Zehner, and C. S. Zerefos

Document: ERSE-DTEX-EOAD-TN-02-0006
Issue: Version 1.0, November 2002
Editor: J-C. Lambert – IASB, Brussels, Belgium
Authorised: C. Zehner – ESA/ESRIN, Frascati, Italy

Space Aeronomy Institute of Belgium

Norwegian Institute for Air Research

German Aerospace Agency

Aristotle University of Thessaliniki

NASA Goddard Space Flight Center

ERS-2 GOME GDP 3.0 Implementation and Delta Validation

Validation Report for GOME Level-1-to-2 Data Processor Upgrade to Version 3.0

CONTENTS

ACRONYMS AND ABBREVIATIONS

AMF	Air Mass Factor, optical enhancement factor
AZM	azimuth angle
BIRA	Belgisch Instituut voor Ruimte-Aëronomie
DLR	German Aerospace Centre
DOAS	Differential Optical Absorption Spectroscopy
D-PAF	German Processing and Archiving Facility
DU	Dobson Unit
ERS-2	European Remote Sensing Satellite-2
ESA/ESRIN	European Space Agency/European Space Research Institute
F&K	Fortuin and Kelder climatology
FWHM	Full Width Half Maximum
GAW	WMO's Global Atmospheric Watch programme
GDP	Off-line GOME Data Processor
GOME	Global Ozone Monitoring Experiment
GOFAP	GOME Fast Delivery Service
GVC	Ghost Vertical Column
HALOE	HALogen Occultation Experiment
IASB	Institut d'Aéronomie Spatiale de Belgique
ICFA	Initial Cloud Fitting Algorithm
IMF	Remote Sensing Technology Institute
ITCZ	Inter Tropical Convergence Zone
KNMI	Royal Dutch Meteorological Institute
LIDORT	Linearized Discrete Ordinate Radiative Transfer model
LOS	Line Of Sight
LUT	Look Up Table
MPI	Max Planck Institute in Mainz
NDSC	Network for the Detection of Stratospheric Change
NILU	Norwegian Institute for Air Research
NLLS	Non Linear Least Squares fitting
NO_2	Nitrogen Dioxide

O_3	Ozone
POAM	Polar Occultation and Aerosol Measurement
SAOZ	Système d'Analyse par Observation Zénithale
SCD	Slant Column Density
SPOT	Satellite Pour l'Observation de la Terre
SZA	Solar Zenith Angle
TOMS	Total Ozone Mapping Spectrometer
UARS	Upper Atmosphere Research Satellite
UV	ultraviolet
VCD	Vertical Column Density
VIS	visible
WMO	World Meteorological Organization
XST	cross section temperature

I INTRODUCTION

I.1 GOME OPERATION AND OFF-LINE DATA PROCESSOR

Operating aboard the ESA ERS-2 polar platform launched in April 1995, the Global Ozone Monitoring Experiment (GOME) [1-3] is the successful predecessor of a series of new generation sensors aiming at the needed global measurement of key ozone-related species to assess current and future changes of the atmosphere. Providing the global picture of atmospheric ozone (O_3), GOME is also the first and currently the only spaceborne instrument having the capability to measure the vertical column amount of nitrogen dioxide (NO_2), a trace species playing a crucial role in the ozone photochemistry. Since August 1996, GOME total O_3 and NO_2 data are routinely retrieved at the German Processing and Archiving Facility (D-PAF) on behalf of ESA with the off-line GOME Data Processor (GDP) [4-6].

The accurate derivation of total ozone and NO_2 from GOME data presents several difficulties and is still a matter of research. Since the release in summer 1995 of its first developmental version, GDP was upgraded on many occasions and the quality of both ozone and NO_2 products has improved significantly (e.g., [7,8]). Nevertheless, many studies have highlighted the need to revisit several aspects of the GDP retrieval algorithms. In late 2001, DLR-IMF upgraded GDP level-0-to-1b to version 2.2 and GDP level-1b-to-2 to version 3.0 focusing on the ozone slant column retrieval and the estimation of the ozone air mass factor.

I.2 GDP 3.0 DELTA VALIDATION CAMPAIGN 2002

Before proceeding to the implementation of any major GDP changes in the operational processing chain, it is essential to verify the accuracy and effectiveness of the modification and to assess the quality of the new data product. Such 'delta' validation campaigns have been executed after every major GDP upgrade by a sub-group of the GOME Validation Group, with a limited but representative set of orbits.

Organised by ESRIN and IASB, the GDP 3.0 Implementation and Validation Campaign was set up to provide an independent characterisation of the recent upgrade to version 3.0 of the GDP level-1-to-2 segment (see Chapter II). Main emphasis was given to the global quality assessment of new O_3 column amounts, but other major GDP changes were investigated as well.

The campaign involved the following institutes (by alphabetical order):

- DLR/Remote Sensing Technology Institute (DLR-IMF), Oberpfaffenhofen, Germany
- Dutch Royal Meteorological Institute (KNMI), De Bilt, The Netherlands
- ESA/European Space Research Institute (ESRIN), Frascati, Italy (coordinator)
- Laboratory of Atmospheric Physics, Aristotle University of Thessaloniki, Greece
- NASA/Goddard Space Flight Center (GSFC), Greenbelt, Maryland, USA
- Norwegian Institute for Air Research (NILU), Troms¢, Norway
- Space Aeronomy Institute of Belgium (IASB-BIRA), Brussels, Belgium (coordinator)

The composition of the team was defined according to the following objectives:

- To insure the availability of correlative data sets suitable for global-scale investigation;
- To insure the availability of independent level-1-to-2 retrieval algorithms;
- To get independent studies and data quality assessments;
- To combine complementary expertise.

Results were presented at ESRIN in July 2001, during the GOME User Consultation meeting on January 28-29, 2002, and during the GDP 3.0 Implementation and Validation Final Meeting on April 10, 2002. The present document outlines the main outcome of the GDP 3.0 Implementation and Validation Campaign held in 2002. This outcome consists of:

- Characterisation of the new total ozone level-2 data product by comparison with correlative measurements from ground-based networks – the Network for the Detection of Stratospheric Change (NDSC), the Norwegian ozone monitoring network, and the WMO/GAW Dobson network – and from Earth Probe TOMS satellite sensor;
- Characterisation of the new total nitrogen dioxide level-2 data product by comparison with correlative measurements from the ground-based Network for the Detection of Stratospheric Change and from UARS HALOE, SPOT-3 POAM-II, and SPOT-4 POAM-III satellite sensors;
- Using the WinDOAS software tool, further investigation of DOAS-related errors affecting the accurate retrieval of ozone, namely: choice of ozone absorption cross-section reference data, determination of GOME slit function, accuracy of wavelength calibration of both reference data and measured GOME spectra, determination of ozone absorption effective temperature, treatment of the Ring effect, and calculation of the ozone air mass factor at a single wavelength (325 nm) over a 10 nm broad fitting window;
- Update of the existing documentation on GDP data products, including the upgrade of the GOME Technical Notes, GOME Data Disclaimer and of the GOME validation web page.

Relevant GDP modifications are listed in Chapter II. A more detailed description of the GDP upgrades is given in [5]. The issue of reference data sets for delta validation studies is addressed in Chapter III, including a description of the data sets actually selected during the present campaign and the new data selection methodology. Individual contributions about level-2 data are reported in Chapter IV for total ozone and Chapter V for total nitrogen dioxide, respectively. Issues peculiar to the DOAS spectral analysis technique used in GDP are addressed in Chapter VI. The updated 'GOME Data Disclaimer' document resulting from the campaign is provided in the Annexe.

I.3 FURTHER GDP UPGRADE TO VERSION 3.1

A few months after implementation of the GDP 3.0 upgrade, an additional feature was discovered in the reprocessed GOME data set. Under very occasional circumstances of high ozone values (> 500 DU) at low sun elevation (SZA > 85°), the iterative AMF algorithm might not converge to a realistic AMF value, leading to unrealistically high ozone values (e.g. 700 DU) that could be identified and filtered out easily. The affected ground pixels are estimated to be in the order of 0.01% of a single orbit, randomly distributed on 1% of the GOME products from 1995 through 2001. Therefore no reprocessing of those historical data is foreseen in the near future. This problem has been solved and the data from 2002 onwards will be (re)processed with a new GDP level-2 version 3.1. Delta validation results presented hereafter will obviously not be affected by this further GDP upgrade.

I.4 REFERENCES

[1] GOME Interim Science Report, ESA SP-1151, 59 pp., 1993.

[2] GOME Users Manual, ESA SP-1182, 200 pp., 1995.

[3] Burrows, J.P., M. Weber, M. Buchwitz, V. Rozanov, V. Ladstätter-Weißenmayer, A. Richter, A. De Beek, R. Hoogen, K. Bramstedt, K.U. Eichmann, and M. Eisinger, The Global Ozone Monitoring Experiment (GOME): Mission concept and first Scientific Results, *J. Atmos. Sci.*, **56**, pp. 151-175, 1999.

[4] GOME Level 0 to 1 Algorithms Description, Technical Note, ER–TN–DLR–GO–0022, Iss./Rev. 5/B, July 31, 2002.

[5] GOME Level 1 to 2 Algorithms Description, Technical Note, ER–TN–DLR–GO–0025, Iss./Rev. 3/A, July 31, 2002.

[6] Product Specification Document of the GDP, ER-PS-DLR-GO-0016, Iss./Rev. 4/A, April 2002.

[7] GOME Data Improvement Validation Report, B. Greco (Ed.), ESA/ESRIN APP/AEF/17/GB, 58 pp. 1998.

[8] ERS-2 GOME Data Products Delta Characterisation Report 1999, J.-C. Lambert and P. Skarlas (Eds.), IASB, issue 1, November 1999.

[9] GOME Geophysical Validation Campaign: Final Results Workshop Proceedings, ESA-ESRIN, Frascati 1996, ESA WPP-108, 268 pp., 1996.

II SUMMARY OF GOME DATA PROCESSOR UPGRADES

By Werner Thomas and Diego Loyola
German Aerospace Agency
DFD/IMF, Oberpfaffenhofen, D-82234 Weßling, Germany
Contact: Werner.Thomas at dlr.de

The main changes in the new GDP system are related to the level 1-to-2 processing system. Some minor changes were implemented into the level 0-to-1 system: There are processor changes (changes with impact on the binary level 1 product) and changes of the extractor software.

II.1 GDP LEVEL 0-TO-1 PROCESSOR VERSION 2.2

The following listing gives an overview about the implemented updates since GDP level 0-to-1 version 2.0.

- Inclusion of a test to reject Sun calibrations with improper illumination. (ERS-2 EBM problem starting in 17th January 2001)
- Geolocation:
  - Correction of the geolocation of ground pixels in the static view mode.
  - Closing of geolocation gaps. Interpolate centre coordinates of ground pixel.

II.2 GDP LEVEL 0-TO-1 EXTRACTOR VERSION 2.2

- New option (-k) for calculating the solar spectrum wavelength using the cross-correlation algorithm [A5]. This option is active by default.

II.3 GDP LEVEL 1-TO-2 PROCESSOR VERSION 3.0

A more detailed description of Algorithm changes can be found in [A6].

- **General**
  In order to provide as much as useful L2 results to the user community the product philosophy has changed. In previous versions of GDP the pixel results were deleted if any error in the algorithm chain occurred. Thus, a failure in e.g., the ozone retrieval suppressed the following independent NO_2 retrieval and no result was transferred to the product. Now the ozone results structure will be filled with zeros but all other reliable retrieval results will be written to the product.

- **ERS-2 orbit propagator**
  The calculation of footprint coordinates (4 corners, centre position) for „static-view" pixels (static scan mirror) were calculated erroneously. The interpolation scheme in place assumed subsequent ground pixels in across-track direction, while subsequent static-view pixels follow in along-track direction. The interpolation scheme is now able to handle also static-view pixels correctly.

The minimum line-of-sight angle has changed from 0.1 degree to 0.001 which is in line with the value used in GDP L01 processing.

- **Pre-processing algorithms**

As a consequence of recent problems with improperly calibrated measured spectra (mainly earth-shine spectra) the earth-shine wavelength grid is not used anymore; instead, the sun wavelength grid is assigned to backscatter measurements on a pixel-to-pixel basis. The choice of the reference wavelength grid is controlled by a flag in the static input file of the GDP [A3].

The derivation of cloud-top reflectances from data base entries has been corrected for negative azimuth differences (between the Sun and the satellite's position) which may be present as valid input for the single scattering radiative transfer model in place.

- **Data Bases**

More information about GDP data bases can be found in [A1]. Here, a brief summary of recently integrated data bases is given.

A bi-modal undersampling correction spectrum for BrO fitting has been implemented [A12]. This spectrum is not used operationally but can be selected for BrO retrieval by a keyword in the static input file of the GDP.

A bi-modal Ring spectrum for ozone fitting has been implemented. It was derived from GOME sun measurements of Orbit 17296 (August 1998) and a theoretical Ring spectrum as described in [A10].

A new reference data set of ozone cross-sections based on FTS measurements has been integrated [A25]. The data set is not used in the operational context.

The GOME-BBM sulphur dioxide spectrum [A24] has been integrated. The data set is not used in the operational context.

A new reference data set of BrO cross-sections based on FTS measurements has been implemented [A26]. The data set is not used in the operational context.

A new reference data set of HCHO cross-sections based on FTS measurements has been implemented [A10]. The data set is not used in the operational context.

The O_2-O_2 reference data set [A14] has been modified (hand-shifted by about 0.1 nm towards longer wavelengths, smoothed) according to [A18].

The TOMS V7 ozone profile climatology [A17] has been implemented and can be used for off-line AMF computation. Interfaces for LIDORT [A22] and GOMETRAN [A20] have been programmed. This climatology is not used for the on-line calculation of single scattering AMFs of NO_2.

An alternative ozone profile climatology [A13] has been implemented and can be used for AMF computation. Interfaces for LIDORT [A22] and GOMETRAN [A20] have been generated. It is used operationally for the on-line calculation of single scattering AMFs for NO_2 in the NO_2 fitting window at 437.5 nm.

A trace gas profile climatology with enhanced tropospheric loading of O_3, NO_2, SO_2 and HCHO has been implemented. It is partially based on scenarios defined in [A2]. This data base is not used operationally but can be selected by a keyword in the static input file of the GDP.

- **Initial Cloud Fitting Algorithm module (ICFA)**

  A new flag is defined that indicates a failure of the least-square fitting routine used for cloud coverage retrieval. If the normalised cloud coverage is greater than 1. or less than 0., the corresponding flag is set and a warning message is generated. This flag is written to the ICFA flag array and is part of the GOME level 2 product (see [A4]).

  A calibration check module which is part of the DOAS module chain is now called also in the algorithm chain of ICFA. The spectral beginning of each channel should lie inside a wavelength interval which is defined in a static data base. If the check fails, a warning message is generated. A flag is implemented that indicates the failure and this flag is part of the ICFA flag array and is written to the GOME level 2 product (see [A4]).

- **Spectral analysis module (DOAS)**

  The GOME FM ozone cross-sections [A9] are now used in the standard UV fitting window (usage controlled by keyword).

  Nitrogen dioxide at 241K [A8] has been added as interfering species in the ozone fitting window in the UV (usage controlled by keyword).

  An undersampling correction spectrum [A21] has been added to the ozone fitting window in the UV (usage controlled by keyword).

  The GOME FM Ring spectrum used in the UV window has been superseded by a bi-modal theoretical Ring spectrum [A10]. Only it's first component is applied to ozone retrieval, as suggested by [A19].

  A recent Ring spectrum provided by SAO in 1997 that was used for NO_2 fitting has been superseded by a bi-modal theoretical Ring spectrum [A10]. Only it's first component is applied to nitrogen dioxide retrieval [A19].

  All shifts/squeeze operations for reference spectra are now switched off for ozone and nitrogen dioxide retrieval, except for the static undersampling correction spectra. These spectra are available on a static wavelength grid and the fitting is improved if shift/squeeze operations are allowed.

  A „warm“ ozone spectrum and an ozone difference spectrum calculated from the difference of ozone cross-sections at different temperatures are now fitted simultaneously in the UV ozone fitting window [A18]. This option is used operationally.

  The fitted ozone temperature may be used internally as a diagnostic variable [A19] but is not part of the GOME level 2 product.

  Extraction of reference spectra is now done only once per processing order.

  The theoretical Doppler-shift of the sun spectrum can now be calculated for the centre wavelength of each fitting window and can be used to limit shift/squeeze operations of the sun spectrum. This option is not used in the operational context.

  Application of a pre-shift of +0.02nm to measured GOME-FM reference spectra (O_3, NO_2) is recommended in Ch2. Recent studies indicate that a pre-shift of +0.012 nm give lowest fit residuals. Thus, the GOME-FM spectra (O_3, NO_2) in Ch2 are pre-shifted by about 0.012 nm towards longer wavelengths for ozone fitting in the UV. The pre-shift is set in the static input file of GDP.

- **Air Mass Factor module (AMF)**

The profile data base mentioned in [A13] is now used operationally for the calculation of single scattering AMFs for NO_2 in the NO_2 fitting window at 437.5 nm.

A look-up table (LUT) of ozone AMFs at 325 nm has been generated using LIDORT [A22]. It is based on TOMS V7 ozone profiles [A17], i.e. total column content and latitude and corresponding T-p- profiles; other variables are albedo, height above sea-level, land/sea mask (i.e., aerosol types "rural"/"maritime"), and viewing geometry (SZA, LOS, rel. AZM). The LUT is not part of the operational data bases.

A neural network approach [A15] [A16] was established to calculate AMFs for ozone at 325 nm, as function of the above-mentioned variables. The LUT was used as training data set for the neural network. The training network itself is part of GDP.

New formulas for calculating the Rayleigh scattering coefficient and the Rayleigh phase function as suggested by [A10] replace the formula given by [A7]. The Rayleigh phase function is now computed as function of a wavelength-dependent depolarization factor. The new formulas are used for both pre-calculated ozone AMFs (the training data set) and on-line single scattering AMFs for NO_2 in the VIS fitting window.

Geometric AMFs are calculated now by default for other species besides O_3 and NO_2. This option is not used in the operational context.

The so-called cut-off parameter was re-set to SZA = 90° (92° in previous versions) because there are no ozone AMFs available (in the neural network training data set) under twilight conditions (SZA > 90°). This will lead to a reduced number of ground pixel per orbit.

- **Vertical Column Density (VCD)**

An iterative scheme following [A23] has been implemented to derive the ozone vertical content.

The ghost column computation is now done also by the neural network. It uses the initial TOMS V7 ozone profiles, the total column content, latitude and the cloud-top height as input. The column content is finally derived by integrating the layer content between the ground and the cloud-top.

A new flag has been implemented that indicates the usage of the iterative scheme for total ozone computation. This flag will be written to the AMF flag array and is part of the GOME level 2 product [A4].

The intensity weighting of AMFs across the footprint is now controlled by a flag in the static input file of GDP. It is switched on by default.

II.4 REFERENCES

[A1] GOME Data Bases (Level 1 to 2 Processing), ER-TN-IFE-GO-0018, Iss./Rev. 3/A, July 2002

[A2] A Study of Methods for Retrieval of Atmospheric Constituents, Final Report, ESA/SERCO, December 1993

[A3] Interface Specification Document of the GDP, ER-IS-DLR-GO-0004, Iss./Rev. 3/A, July 2002.

[A4] Product Specification Document of the GDP, ER-PS-DLR-GO-0016, Iss./Rev. 4/A, April 2002.

[A5] GOME Level 0 to 1 Algorithms Description, Technical Note, ER–TN–DLR–GO–0022, Iss./Rev. 5/B, July 31, 2002.

[A6] GOME Level 1 to 2 Algorithms Description, Technical Note, ER–TN–DLR–GO–0025, Iss./Rev. 3/A, July 31, 2002

[A7] Brasseur G. and S. Solomon, Aeronomy of the middle atmosphere, second edition, D. Reidel Publishing Company, Dordrecht, Holland, 1986.

[A8] Burrows J.P., A. Dehn, B. Deters, S. Himmelmann,A. Richter, S. Voigt and J. Orphal, Atmospheric Remote-Sensing Reference Data from GOME: Part 1. Temperature-dependent Absorption cross-sections of NO_2 in the 231-794nm range, *J. Quant. Spec. Radiat. Trans.*, 60, 1025-1031, 1998.

[A9] Burrows J.P., A. Richter, A. Dehn, B. Deters, S. Himmelmann, S. Voigt and J. Orphal, Atmospheric Remote-Sensing Reference Data from GOME: Part 2. Temperature-dependent Absorption cross-sections of O_3 in the 231-794nm range, *J. Quant. Spec. Radiat. Trans.*, 61, 509-517, 1999.

[A10] Cantrell C.A., J.A. Davidson, A.H. McDaniel, R.E. Shetter, and J.G. Calvert, Temperature–dependent formaldehyde cross sections in the near–ultraviolet spectral region, *J. Phys. Chem.*, 94, 3902–3908, 1990

[A11] Chance K.V. and R.J.D. Spurr, Ring Effect Studies, Appl. Opt., 36, 5224-5230, 1997.

[A12] Chance K.V., Analysis of BrO Measurements from the Global Ozone Monitoring Experiment, *Geophys. Res. Lett.*, 25, 3335-3338, 1998.

[A13] Fortuin J.P.F. and H. Kelder, An ozone climatology based on ozonesonde and satellite measurements, J. Geophys. Res., 103, 31709-31734, 1998.

[A14] Greenblatt G.D., J.J. Orlando, J.B. Burkholder, and A.R. Ravishankara, *J. Geophys Res.*, 95, 18577–18582, 1990.

[A15] Loyola D., Using Artificial Neural Networks for the Calculation of Air Mass Factors, ESAMS'99 - European Symposium on Atmospheric Measurements from Space, 1999.

[A16] Loyola D., Combining Artificial Neural Networks for Parameterization of Radiative Transfer Models, IEEE International Geoscience and Remote Sensing Symposium, IGARSS'2000, 2000.

[A17] McPeters R.D., P.K. Bhartia, A.J. Krueger, J.R. Herman, B.M. Schlesinger, C.G. Wellemeyer, C.J. Seftor, G. Jaross, S.L. Taylor, T. Swissler, O. Torres, G. Labow, W. Byerly and R.P. Cebula, Nimbus-7 Total Ozone Mapping Spectrometer (TOMS) Data Products User's Guide, NASA Reference Publication, 1996.

[A18] Richter A., personal communication, IUP, 2000.

[A19] Van Roozendael M., Technical Note: Ring effect study: Test of available data sets for DOAS fitting of GOME spectra in the O_3 and BrO intervals, IASB Technical Note, May 2000.

[A20] Rozanov V., D. Diebel, R.J.D. Spurr and J.P.Burrows, GOMETRAN : Radiative Transfer Model for the Satellite Project GOME, the Plane-Parallel Version, *J. Geophys. Res.*, 102, 16683-16695, 1997.

[A21] Slijkhuis S., A. v. Bargen, W. Thomas and K.V. Chance, Calculation of Undersampling correction spectra for DOAS spectral fitting, ESAMS'99 - European

Symposium on Atmospheric Measurements from Space, ESA WPP-161, Noordwijk, The Netherlands, 1999.

[A22] Spurr R.J.D, T.P. Kurosu, and K.V. Chance, A Linearized Discrete Ordinate Radiative Transfer Model for Atmospheric Remote Sensing Retrieval, *J. Quant. Spec. Radiat. Trans.*, 68, 689-735, 2001.

[A23] Spurr R.J.D, Improved climatologies and new air mass factor look-up tables for O_3 and NO_2 column retrievals from GOME and SCIAMACHY backscatter measurements, ESAMS'99 - European Symposium on Atmospheric Measurements from Space, Noordwijk, The Netherlands, ESA WPP-161, 277-284, 1999.

[A24] Tuerk A., B. Deters and J.P. Burrows, SO_2 Absorption cross–sections at 298K, unpublished, 1994

[A25] Voigt S., J. Orphal, K. Bogumil, and. J.P. Burrows, The temperature dependence (203¯293 K) of the absorption cross sections of O_3 in the 230-850 nm region measured by Fourier-transform spectroscopy, *J. Photochem. Photobiol. A: Chem.*, 143, 1-9, 2001.

[A26] Wilmouth D., T.F. Hanisco, N.M. Donahue, and J.G. Anderson, Fourier Transform Ultraviolet Spectroscopy of the $A^2\,\Pi_{3/2} \leftarrow X^2\,\Pi_{3/2}$ Transition of BrO, *J. Phys. Chem. A*, 103, 8935-8945, 1999.

III DELTA VALIDATION ORBITS

By Jean-Christopher Lambert and José Granville

Space Aeronomy Institute of Belgium (IASB-BIRA)
Avenue Circulaire 3, B-1180 Brussels, Belgium
Contact: J-C.Lambert at iasb.be

Starting from the list of 399 orbits used for the delta validation of GDP upgrade to version 2.7 [ESA, 1999], we have selected an additional list of 1858 validation orbits with the twofold objective to optimise validation studies relying on ground-based network data and to allow long-term verification. The resulting list of 2257 validation orbits represents a good compromise between minimum processing time and maximum representativeness of GDP characteristics.

The current selection of orbits is based on histograms of GOME/NDSC comparisons performed with GDP 2.7 data record since January 1996. Orbits have been selected when leading to closest values to the median value of the relative difference in total ozone.

The selection has been constrained for both ozone and NO_2 in such a way that the sampling of the column range and of its cyclic variations - with season, latitude and solar zenith angle - complies with both Nyquist and Central Limit theorems. Most of data records have been limited to the period of 1996-1997, that is, limited in terms of instrumental degradation. For long-term verification purposes, data records have been extended from 1996 through 2001 at a few representative stations. Figure 1 shows coincidences resulting from the selection of orbits at the Antarctic station of Halley (76°S). The selected set of 321 coincidences – out of a total of 1180 coincidences within the 1996-2001 timeframe – capture quite well major GDP features such as the strong season/SZA dependence observed at polar stations and the drastic column dependence observed during ozone hole conditions. It is remarkable that, at this polar station, GDP dependences on the ozone column and on the solar zenith angle do not interfere, allowing their easy discrimination.

Finally, the subset of validation orbits has also be designed in order to sample sufficiently seasonal and meridian structures of the effective temperature to be used in the ozone spectral analysis. Figure 2 shows the improvement of the sampling gained with the new set of validation orbits, compared to the previous one. In this Figure, GOME/ozonesonde coincidences are identified on top of a latitude-month cross-section of the estimated error of GDP 2.7 total ozone related to the temperature dependence of the ozone absorption cross-section.

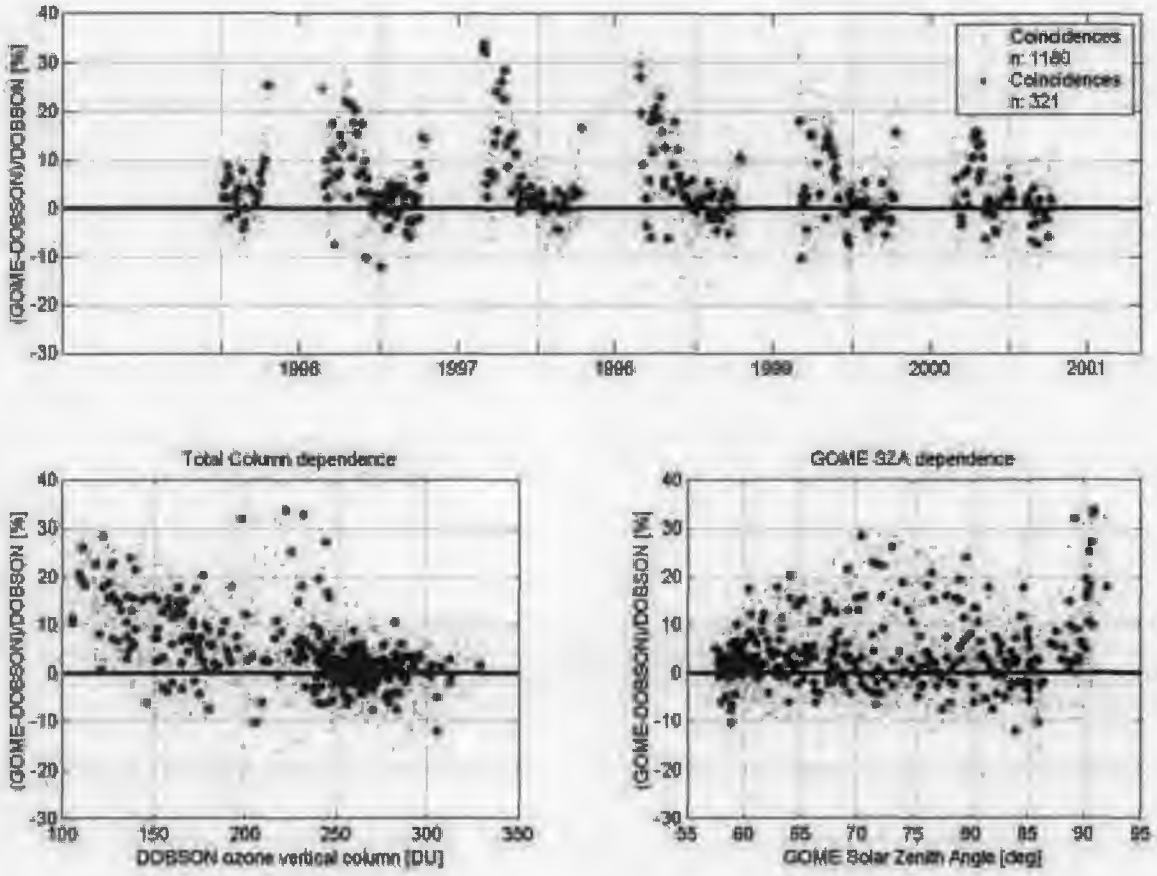

Figure 1 - Selected GOME/Dobson coincidences (bold dots) on top of all coincidences (light dots) at the Antarctic station of Halley (76°S), showing the sampling of seasonal (upper panel), column (lower left) and SZA (lower right) dependences. During the springtime ozone 'hole', the respective phases of dependences on the ozone column and on the solar zenith angle do not interfere together, allowing easy discrimination.

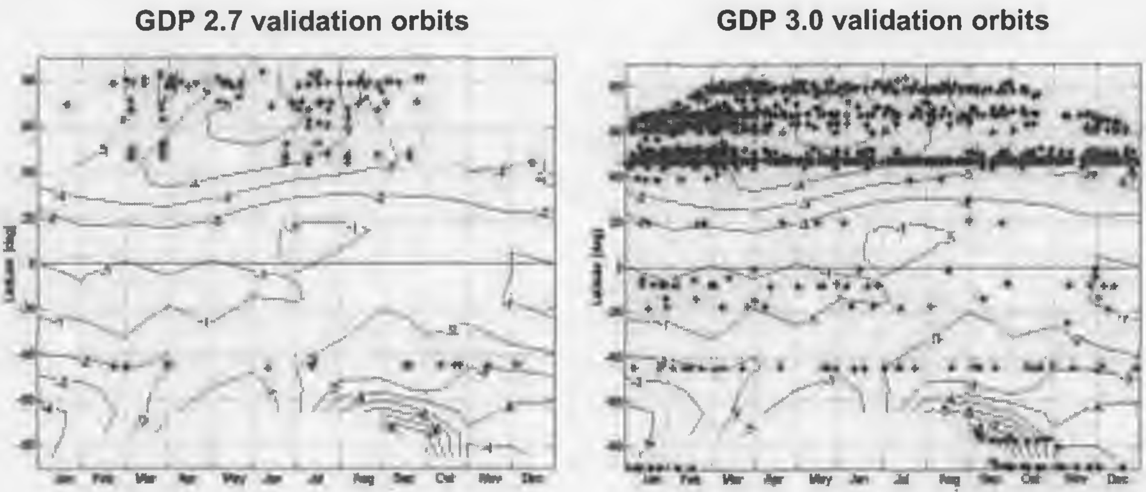

Figure 2 - Coincidences with ground-based ozone profile data offered by the old 399-orbit (left plate) and new 2257-orbit (right plate) sets of delta validation orbits, respectively. Coincidences are highlighted by red crosses on top of a latitude-time cross-section of the estimated percentage relative error of GDP 2.7 total ozone, associated with the temperature dependence of the ozone absorption cross-section.

Practically, the new set of validation orbits allows:

- Validation studies at about 25 monitoring stations from the Arctic to the Antarctic, for both total ozone and total nitrogen dioxide;
- Accurate investigation of major stratospheric features: seasonal variation, meridian structure, winter-spring polar photochemistry and ozone depletion, midnight sun conditions;
- Accurate investigation of major GDP-generated features: dependences on season, latitude, SZA, ozone column, and ozone/temperature profile shape;
- Only limited information on day-to-day variability and zonal structures;
- Long-term verification from 1996 through 2001;
- Possible studies requiring the use of ground-based profile data records, e.g., for effective temperature and air mass factor calculations.

Reference:

ESA, 1999: ERS-2 GOME Data Products Delta Characterisation Report 1999 / Validation Report for GOME Data Processor Upgrade: Level-0-to-1 Version 2.0 and Level-1-to-2 Version 2.7, J.-C. Lambert and P. Skarlas (Eds.), Issue 1, 103pp.

IV TOTAL OZONE

IV.1 RESULTS FROM BIRA-IASB

By Vincent Soebijanta, Jean-Christopher Lambert, José Granville, Michel Van Roozendael, and Caroline Fayt

Contact: *J-C. Lambert*
Space Aeronomy Institute of Belgium (BIRA-IASB)
Avenue Circulaire 3, B-1180 Brussels, Belgium
E-mail: j-c.lambert at iasb.be

NDSC-Based Correlative Study of GOME GDP Total Ozone Upgrade From Version 2.7 to 3.0

V. Soebijanta, J-C. Lambert, J. Granville, M. Van Roozendael, and C. Fayt

Space Aeronomy Institute of Belgium (IASB-BIRA), Brussels, Belgium

Abstract: : Preliminary delta validation of the GOME Data Processor level-1b-to-2 upgrade from version 2.7 to version 3.0, is reported for the total ozone product. The investigation relies on cross-correlation studies of intermediate GDP products – slant column, air mass factor, ghost column – and on comparisons with correlative ground-based measurements of total ozone associated with the quasi-global Network for the Detection of Stratospheric Change (NDSC).

IV.1.1 Introduction

IV.1.1.1 Objectives

The level-1b-to-2 segment of off-line GOME Data Processor (GDP) established at DLR-IMF retrieves total column amounts of ozone (O_3) and nitrogen dioxide (NO_2), and cloud information from GOME radiometric measurements. The processor was upgraded in 2001 from version 2.7 to version 3.0. Consequently, a delta validation campaign was organised in 2002 in order to provide an independent verification and characterisation of the upgrade. The main goals of this campaign were (1) to verify the correctness of implemented changes, (2) to investigate their impact on the total column products, (3) to draw a preliminary quality assessment of the new data products, and (4) possibly, to propose further improvement. This document reports on such delta validation studies carried out during the campaign by means of correlative ground-based observations associated with the international Network for the Detection of Stratospheric Change (NDSC).

The present document reports on total O_3 related changes. NO_2 is studied in Chapter IV of this issue. Based on previous validation results that used the same instrumentation, the status of GDP 2.7 total O_3 is summarised in Sub-Section 1.2. The adopted methodology and selected data sets are described in Section 0. Major changes between GDP 2.7 and GDP 3.0 and their expected effect are outlined in Section 3. The impact of the new ozone cross-section temperature determination is studied in Section 4. In Section 5, the ground-based measurements acquired at various NDSC stations are used as correlative data to assess the geophysical consistency of the GDP 3.0 total ozone product. General conclusion and recommendations for further improvement are proposed in Section 6.

IV.1.1.2 Performance of GDP 2.7

Since its delta validation compared to GDP version 2.4, numerous validation studies of GDP version 2.7 have been carried out, among others by comparison with well understood and documented ground-based measurements associated with the NDSC (Lambert *et al.*, 1999), a main contributor to the WMO's Global Atmospheric Watch (GAW) programme.

Figure 1 shows the seasonal and latitudinal bias of the level-2 total ozone GDP 2.7 data product as revealed by the confrontation with GAW ground-based ozone data (NDSC/UV-visible, Dobson and Brewer networks). The monthly mean agreement is about ±4% in the Tropics and ±5% at middle latitudes. At higher latitudes, a solar zenith angle (SZA) dependent difference appears. The monthly mean deviation of GOME GDP from ground-based data rarely exceeds ±5% for SZA below 70°. Above SZA values of 70°, the difference ranges from -10% to +5% depending on the season and the year. Lowest total ozone values can be overestimated by GDP by 15% and even more during ozone hole conditions.

Further studies have investigated possible origins of the SZA/latitude/column dependence, among them the inaccurate treatment of the atmospheric profile shape effect in GDP AMFs, the partial unsuitability of the particular spectral analysis when the atmosphere becomes optically thick, and other issues peculiar to the DOAS technique.

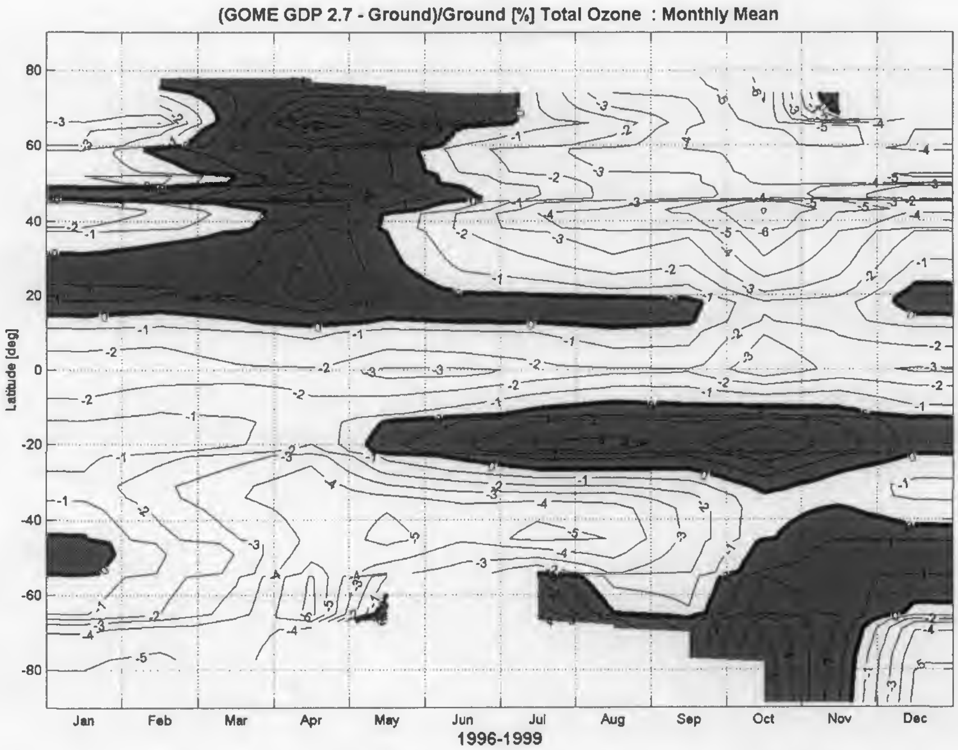

Figure 1 - ***Mean relative difference between ERS-2 GOME GDP 2.7 and GAW ground-based networks (NDSC/UV-visible, Dobson and Brewer) total ozone. Shaded areas highlight positive deviations of GOME from ground-based data (from Lambert et al., 2001).***

IV.1.2 Methodology and Data Sets

IV.1.2.1 Method of Investigation

The main analyses of the present study are to quantify the impact of each GDP changes and to verify the evolution from GDP 2.7 to GDP 3.0 by comparison with NDSC correlative measurements as a standard transfer.

A new level-1b product (spectral radiance) based on cross-calibration technique (xcorr) has been proposed by DLR-IMF. We compare the level-2 data obtained by both the recalibrated spectra and the old calibration technique (no-xcorr) values in order to quantify the effect of this change.

The level-1-to-2 segment of the GDP off-line processor is based on a two-step approach. The first step consists in retrieving the apparent slant column density (SCD) from the measured spectra using differential optical absorption spectroscopy (DOAS). This value represents the number of absorbing molecules along the optical path of the radiation observed by GOME. The second step consists in converting the slant column into a vertical column (VCD) by means of an geometrical enhancement, or air mass factor (AMF). The latter is estimated using a radiative transfer model. It depends on the solar zenith angle (SZA) and atmospheric parameters controlling the path of the radiation through the atmosphere. An important parameter is the cloud fractional cover value derived from GOME spectra with the Initial Cloud Fitting Algorithm (ICFA).

Several major changes have been implemented in the GDP version 3.0, that could affect the total ozone product significantly. Compared to GDP 2.7, GDP 3.0 includes a new determination of effective absorption temperature (XST) derived by spectral analysis, instead of the previous deterministic estimation based on climatological grounds. Further details are given in Section 4. AMFs are now determined iteratively using a neural network trained on column- and latitude-classified atmospheric profiles. Profiles are taken from the TOMS v7 climatological database (Wellemeyer *et al.*, 1997), instead of the MPI-2D modelling results used by GDP 2.7 (Bruhl, 1994). The same profiles are then used for the determination of the so-called Ghost Vertical Column (GVC) amount of ozone standing below the clouds.

In GDP 3.0, the ozone slant column amount and the ozone effective absorption temperature are retrieved simultaneously. Due to the absence of the retrieved effective temperature values in the GDP data files, we used hereafter the effective temperature retrieved with the WinDOAS off-line processor developed at IASB (Fayt and Van Roozendael, 2001). IASB and DLR have worked closely to enable WinDOAS to match within 0.5% the temperature values produced by GDP 3.0 (Thomas and Van Roozendael, 2002).

To investigate separately the impact of GDP upgrades for each module of the level-1b-to-2 processor (SCD, ICFA, AMF, and GVC), we have generated four hybrid VCD products hereafter referred to as preGDP_x and outlined in Table 1. These products are obtained by substituting one after the other 3.0 values with 2.7 values.

Table 1 ***Details of the four total ozone hybrid products generated in this study. Each product is calculated by mixing intermediate products (SCD, AMF, ICFA and GVC) from GDP 2.7 and 3.0 data sets. For each hybrid product (PreGDP_x), the table indicates which GDP version of intermediate products has been used.***

Intermediate Product	PreGDP_1	PreGDP_2	PreGDP_3	PreGDP_4
SCD	3.0	3.0	2.7	2.7
ICFA	2.7	2.7	2.7	3.0
GVC	2.7	2.7	2.7	3.0
AMF	2.7	3.0	3.0	2.7

IV.1.2.2 Correlative Data

Studies reported hereafter rely on comparisons of GOME data with ground-based GAW/NDSC measurements. Contributing ground-based instruments are listed in Table 2.

Table 2 ***Characteristics of total ozone monitoring instruments contributing to the present study: station name, geographical location, coordinates, responsible institute, and type of instrument.***

Station	Location	Lat.	Long.	Institute	Instrument
Ny-Ålesund	Spitsbergen	79°N	12°E	NILU	SAOZ
Thule	Western Greenland	77°N	69°W	DMI	SAOZ
Scoresbysund	Eastern Greenland	70°N	22°W	CNRS/DMI	SAOZ
Sodankylä	Finland	67°N	27°E	CNRS/FMI	SAOZ
Zhigansk	Eastern Siberia	67°N	123°E	CNRS/CAO	SAOZ
Harestua	Norway	60°N	11°E	BIRA-IASB	DOAS
Oslo	Norway	60°N	11°E	U. Oslo	Dobson
Hohenpeißenberg	Germany	48°N	11°E	DWD	Brewer, Dobson
Jungfraujoch	Swiss Alps	47°N	8°E	BIRA-IASB	SAOZ
Arosa	Swiss Alps	46°N	9°E	ETHZ	Brewer, Dobson
O. H. P.	French Alps	44°N	6°E	CNRS	Dobson, SAOZ
Mauna Loa	Hawaii	20°N	156°W	NOAA/CMDL	Dobson
Tarawa	Kiribati	01°N	172°E	CNRS	SAOZ
Nairobi	Kenya	01°S	37°E	SMI/DMK	Dobson
Natal	Brazil	05°S	35°W	INPE	Dobson
Bauru	Brazil	22°S	48°W	CNRS/UNESP	SAOZ
Cachoeira Paulista	Brazil	23°S	45°W	INPE	Dobson
Lauder	New Zealand	45°S	170°E	NIWA	Dobson,
Kerguelen	Indian Ocean	49°S	70°E	CNRS	SAOZ
Faraday/Vernadsky	Antarctic Peninsula	65°S	64°W	BAS, KTSU	Dobson, SAOZ
Dumont d'Urville	Antarctica	66°S	140°E	CNRS	SAOZ
Rothera	Antarctic Peninsula	68°S	68°W	BAS	SAOZ
Halley	Antarctica	76°S	27°W	BAS	Dobson
Arrival Heights	Antarctica	78°S	167°E	NIWA	Dobson
Amundsen Scott	Antarctica	90°S	25°W	NOAA/CMDL	Dobson

Measurements of the ozone vertical column amount at twilight have been collected from the SAOZ/DOAS UV-visible network of the NDSC (Pommereau and Goutail, 1988; Roscoe *et al.*, 1999). Total ozone data throughout the day have also been monitored by Dobson and Brewer ultraviolet spectrophotometers. Combined together, the various ozone observation techniques used in the frame of the NDSC provide powerful complementary information for satellite validation, each observation technique extending capabilities of the others, and ensure internal consistency of the ground-based data records (Lambert *et al.*, 1999a).

IV.1.2.3 GOME Validation Orbits

Starting from the list of 399 orbits used for the delta validation of GDP upgrade to version 2.7 (Lambert *et al.*, 1999b), we have selected an additional list of 1858 validation orbits with the twofold objective to optimise validation studies relying on ground-based network data and to allow long-term verification. The resulting list of 2257 validation orbits is a good compromise between minimum processing time and maximum representativeness.

The selection of orbits is based on histograms of GOME/NDSC comparisons performed with the GDP 2.7 data record since January 1996. Orbits have been selected when leading to closest values to the median value of the relative difference in total ozone.

The selection has been constrained in such a way that the sampling of the ozone column range and of its cyclic variations - with season, latitude and solar zenith angle - complies with both Nyquist and Central Limit theorems. Most of data records have been limited to the period of 1996-1997, that is, limited in terms of instrumental degradation. For long-term verification purposes, data records have been extended from 1996 through 2001 at a few representative stations.

Practically, the new set of validation orbits allows:

- Validation studies at about 25 monitoring stations from the Arctic to the Antarctic, for both total ozone and total nitrogen dioxide;
- Accurate investigation of major stratospheric features: seasonal variation, meridian structure, winter-spring polar photochemistry and ozone depletion, midnight sun conditions;
- Accurate investigation of major GDP-generated features: dependences on season, latitude, SZA, ozone column, and ozone/temperature profile shape;
- Only limited information on day-to-day variability and zonal structures;
- Long-term verification from 1996 through 2001;
- Studies requiring the use of ground-based profile data records, e.g., for effective temperature and air mass factor calculations.

IV.1.3 Effect of Individual GDP Module Changes

The ozone vertical column is calculated by dividing the apparent slant column by an appropriate air mass factor. However, the presence of clouds in the field of view of the instrument complicates the calculation of the vertical column. GDP approximates clouds as Lambertian reflecting surfaces. Two AMFs are calculated: one down to the ground surface (AMF_{clear}) and one down to the cloud top (AMF_{cloudy}). A correction is introduced to account for the ozone amount below the cloud top (the so-called ghost vertical column, GVC).

Total vertical column values are determined in GDP using the following equations:

$$VCD = \frac{SCD + F.GVC.AMF_{cloudy}}{AMF_{total}} \qquad \textbf{(Eq. 1)}$$

where F is the cloud fraction and where :

$$AMF_{total} = (1-F).AMF_{clear} + F.AMF_{cloudy} \qquad \text{(Eq. 2)}$$

According to the description of GDP changes given in Chapter II of the present issue, GDP upgrade to version 3.0 should produce insignificant cloud fraction change, minor GVC changes, and major SCD and AMF changes. Hereafter, the sensitivity of GDP total ozone modifications to those various terms of Equation 1 is investigated.

IV.1.3.1 Vertical Columns

A selection of about 300 orbits in 1996, that is, about one million GOME pixels have been used to estimate the changes between GDP version 2.7 and 3.0. Figure 2 shows the monthly mean relative difference of the vertical column amount on a 5-degree latitude grid. Grid cells containing less than 50 pixels have been removed to ensure statistical significance.

The standard deviation (1σ) of the difference between those GDP versions are represented in Figure 3, which shows clearly that globally, the mean difference is higher than the 1σ variation. GDP changes in the low and middle latitudes can be studied obviously in a statistically consistent manner. Only a small area near the Antarctic terminator has a significant monthly standard variation higher than the monthly mean by 1.5%, that can reach a value of 4-5%.

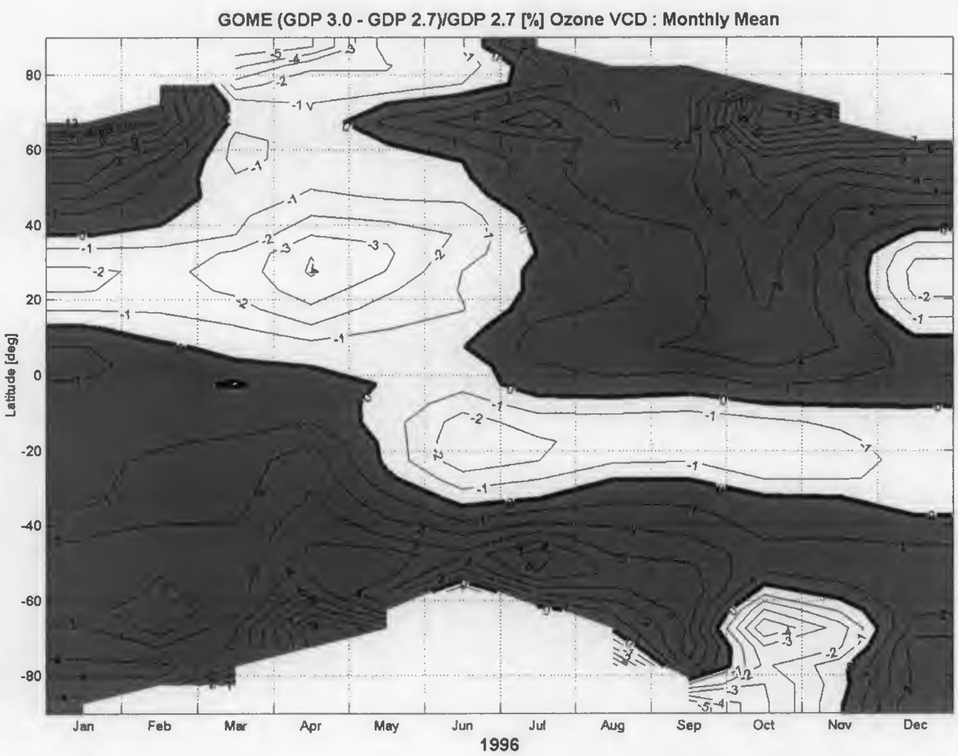

Figure 2 *Latitude-month cross-section of the percentage relative difference between GDP 2.7 and 3.0 total ozone. Shaded areas highlight an increase of total ozone from GDP 2.7 to GDP 3.0.*

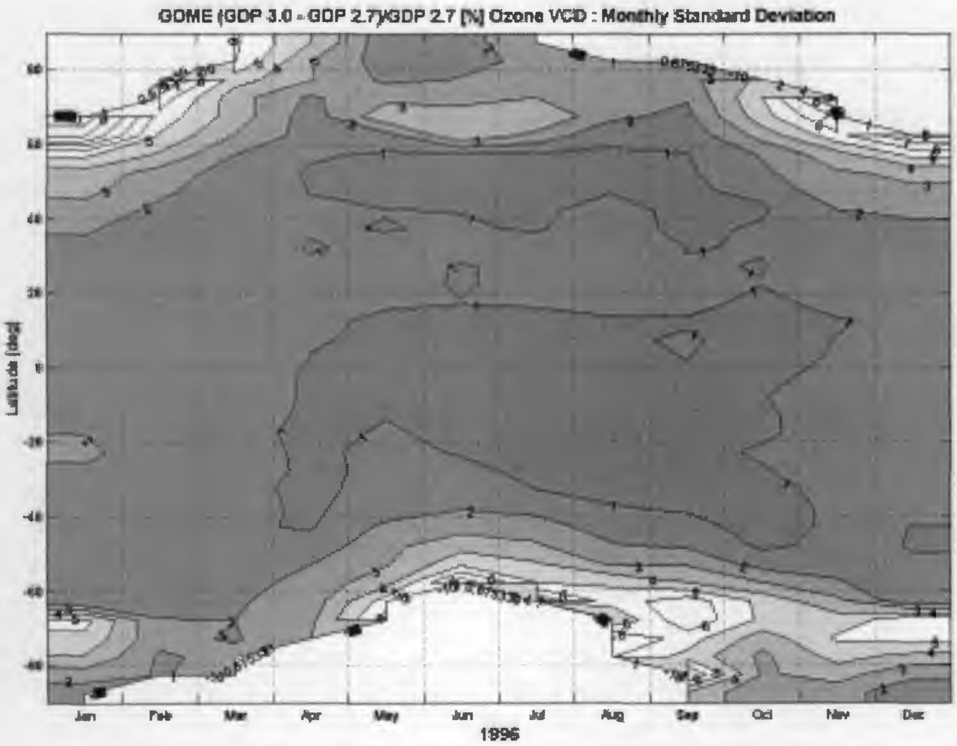

Figure 3 ***Latitude-month cross-section of the percentage standard deviation (1σ) difference between GDP 2.7 and 3.0 total ozone.***

With the same data set, it is also possible to estimate the agreement between GDP 3.0 and ground-based data (Figure 4) by multiplying the GDP 2.7/ground ratio with GDP 3.0/GDP 2.7 ratio. The comparison of Figure 1 with Figure 4 shows that seasonal variations of the GDP-ground difference are slightly smoothed (clearly visible at northern mid and high latitude and at the southern tropic). The comparison is easier to make with the latitudinal cross-section of the GDP-NDSC relative difference depending on season, presented in Figure 5-a and 5-b. From those plots, we observe that the meridian variations remain significant. Major structures of the difference between GDP 2.7 and NDSC data (Figure 1) persist in the GDP 3.0-ground comparison, but sometimes appear to be shifted to upper values like in the southern mid to high latitude (Figure 5-b).

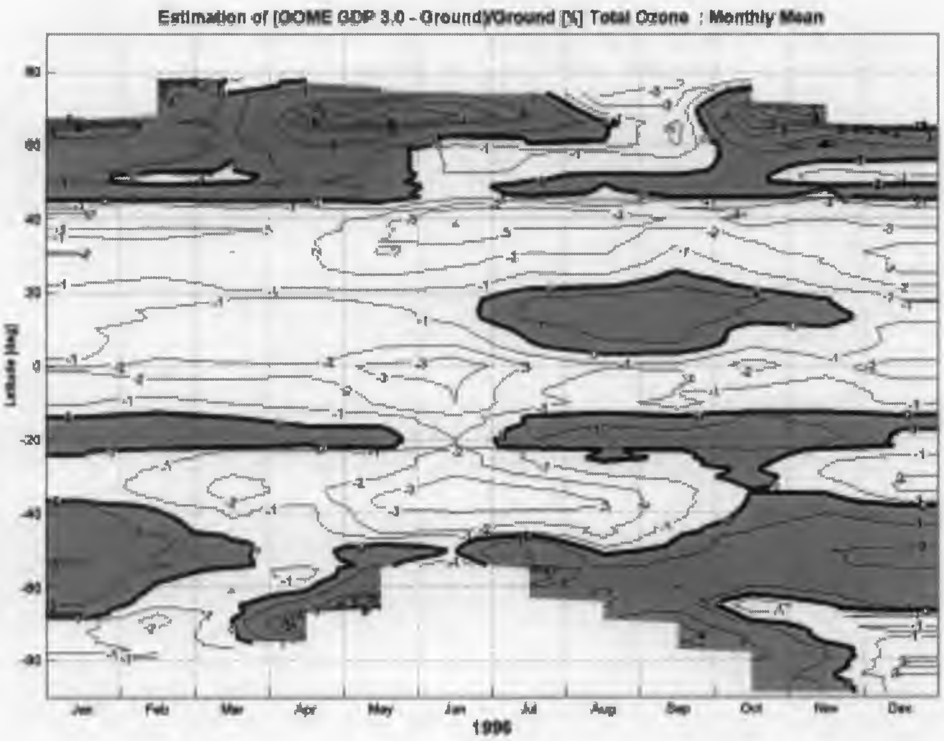

Figure 4 ***Latitude-month cross-section of the estimated percentage relative difference between GDP 3.0 and GAW networks (NDSC/UV-visible, Dobson and Brewer) total ozone. Shaded areas highlight positive deviations of GOME from ground-based data.***

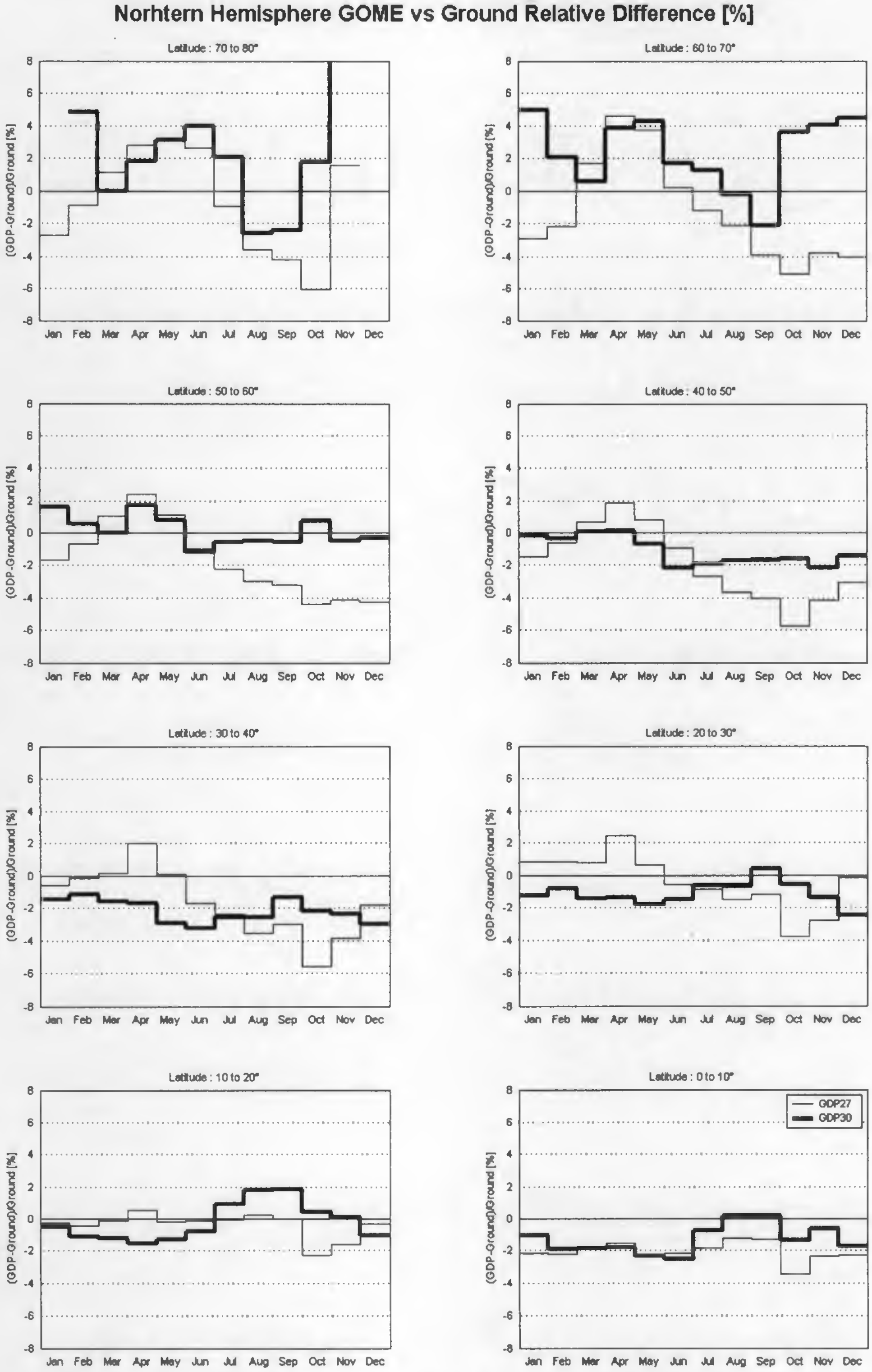

Figure 5-a *Estimation of the seasonal mean relative difference between GOME GDP (2.7 thin/3.0 thick lines) and GAW ground-based networks (NDSC/UV-visible, Dobson and Brewer) total ozone in the Northern hemisphere.*

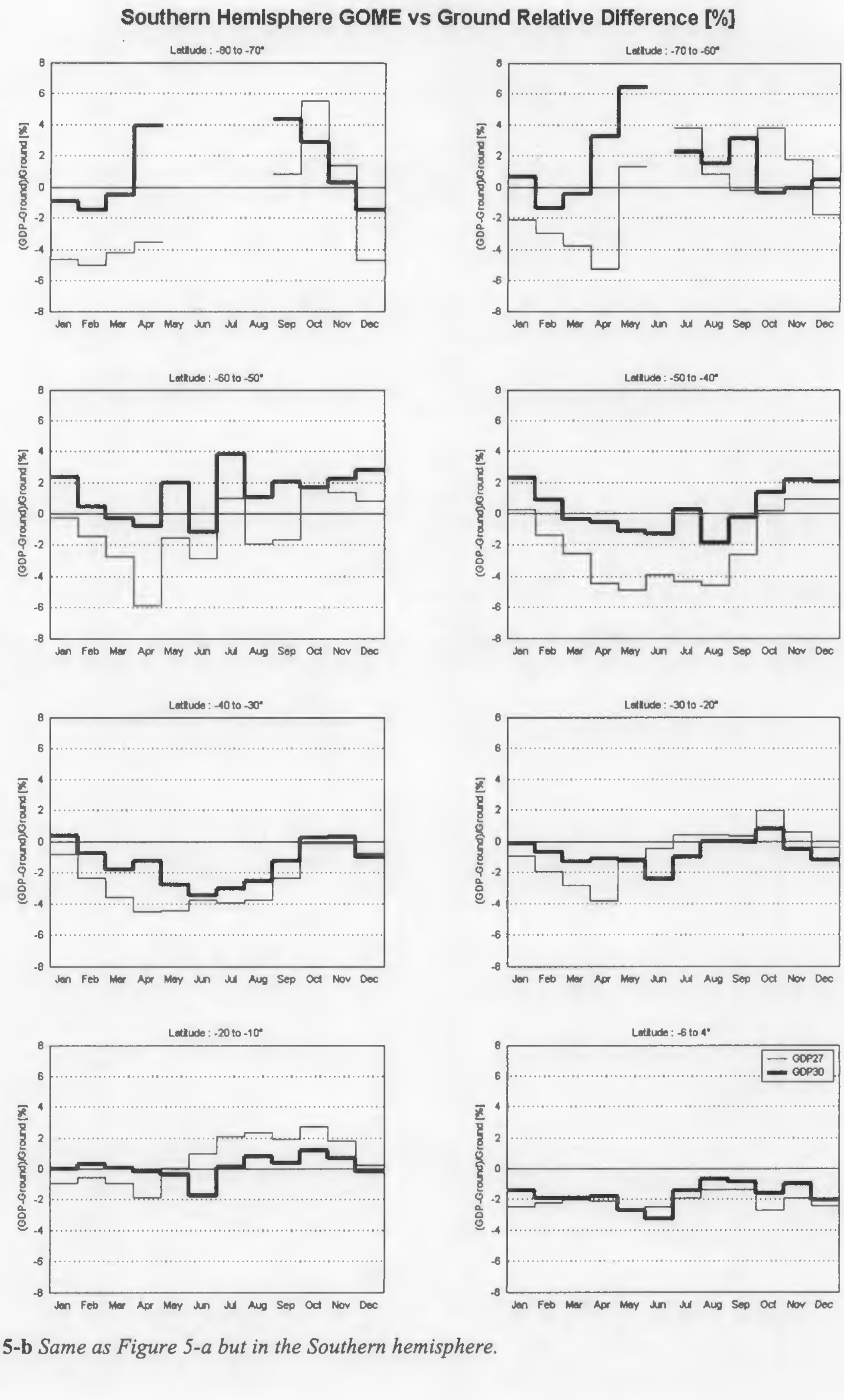

Figure 5-b *Same as Figure 5-a but in the Southern hemisphere.*

IV.1.3.2 Cloud Fraction

The absolute difference between GDP 2.7 and 3.0 monthly mean cloud fraction values, illustrated in Figure 6, generally is less than 0.02 except in regions of high cloudiness at very high latitudes where it can reach 0.03-0.04. Obviously, changes in ICFA outputs will have no significant impact on the new total ozone product.

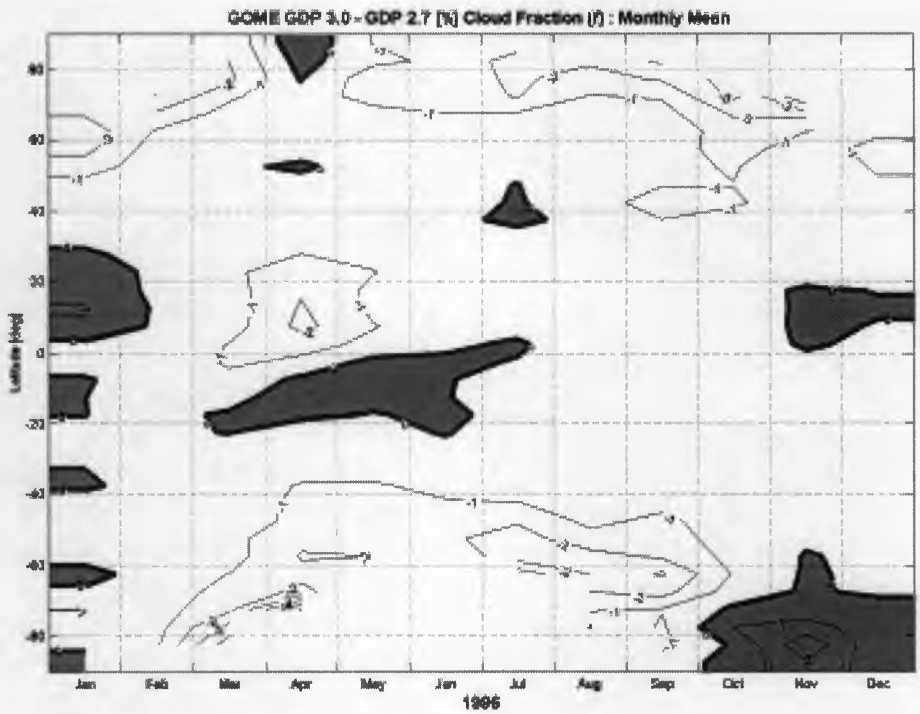

Figure 6 ***Latitude-month cross-section of the absolute difference between GDP 2.7 and 3.0 percentage cloud fraction (F). Shaded areas indicate an increase of the ICFA cloud fraction from GDP 2.7 to GDP 3.0.***

IV.1.4 Slant Column

The absorption cross-sections of ozone in the Huggins bands, where GDP ozone is retrieved, depend on the temperature. In former GDP versions, the cross-sections temperature was selected as the temperature corresponding to a maximum of ozone concentration in MPI-2D modelled profile (DLR, 2002c). The cross-section temperature dependence was expressed through the empirical quadratic interpolation formula of Bass & Paur (Paur and Bass, 1984, Bass and Paur, 1984).

With GDP 3.0, the cross-section temperature is derived from the spectra by fitting simultaneously effective temperature and SCD with a direct linear equation, assuming a linear dependence of the ozone cross-section on the temperature between 221K and 241K.

Figure 7 displays the monthly and meridian mean difference between GDP 2.7 and 3.0 SCDs. Globally no large change occurs, evolution of more than 1% can be seen only at latitude higher than 40° in both hemisphere. A seasonal variation of about 2% of the SCD evolution can be observed at almost every latitude. According to Equation 1, the evolution of the SCD will increase the VCD values, excepted in the inter-tropical region between December and June where a slight decrease of the SCD is observed.

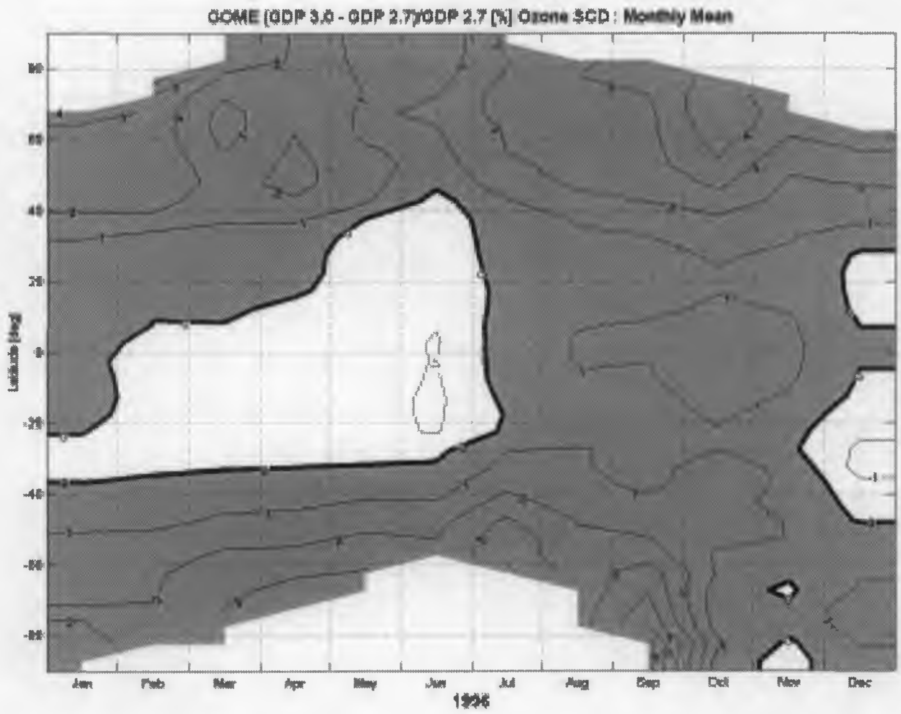

Figure 7 ***Latitude-month cross-section of the percentage relative difference between GDP 2.7 and 3.0 ozone slant column. Shaded areas indicate an increase of the slant column from GDP 2.7 to GDP 3.0.***

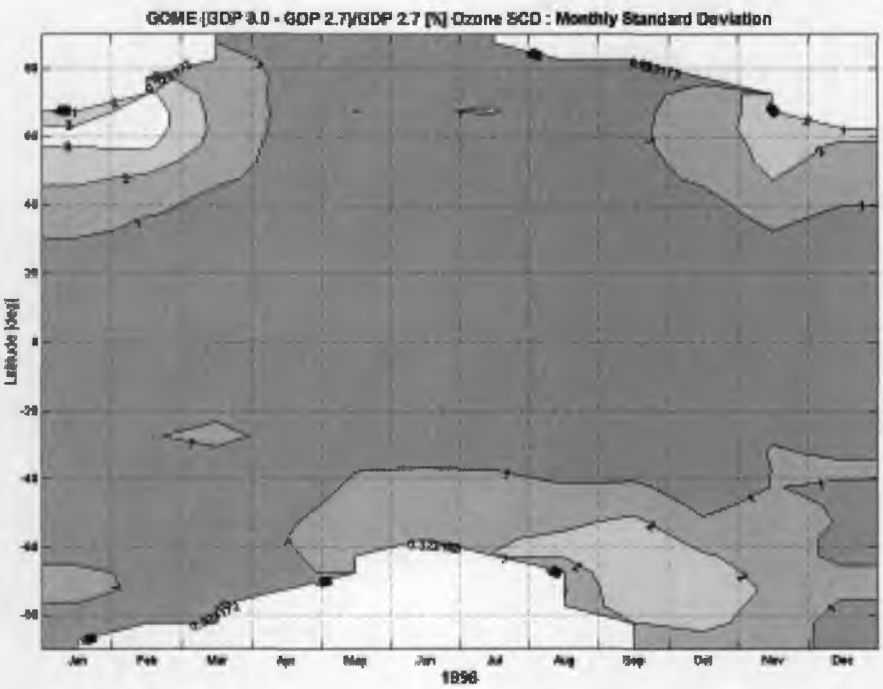

Figure 8 ***Latitude-month cross-section of the standard deviation between GDP 2.7 and 3.0 ozone slant column.***

The monthly standard deviation of the SCD GDP evolution, displayed in Figure 8, shows globally a very low variability, excepted in January and February at Northern middle to high latitudes where those values can be slightly higher than the monthly mean.

IV.1.4.1 Air Mass Factor

Total air mass factor (AMF_{total}) is calculated considering the clear sky air mass factor (AMF_{clear}), the cloudy sky air mass factor (AMF_{cloudy}), and the cloud fractional cover inside the GOME ground pixel (F). Total AMF is changed by a new AMF_{clear} and AMF_{cloudy}. However, the new cloud fraction product F, as demonstrated in a previous subsection, has a negligible impact on AMF_{total}. The MPI ozone profile database used in GDP 2.7 has also been replaced in the new GDP version by climatological profiles selected from the TOMS v7 database using a neural network.

Figure 9 illustrates the difference between GDP 2.7 and 3.0 total air mass factors. This difference is more dominated by the AMF_{clear} evolution than by the AMF_{cloudy} evolution. Nevertheless due to the cloud fraction distribution which tend to be high at the inter-tropical convergence zone (ITCZ) and also at polar latitudes, the evolution of AMF_{cloudy} has a significant impact on AMF_{total} at those latitudes.

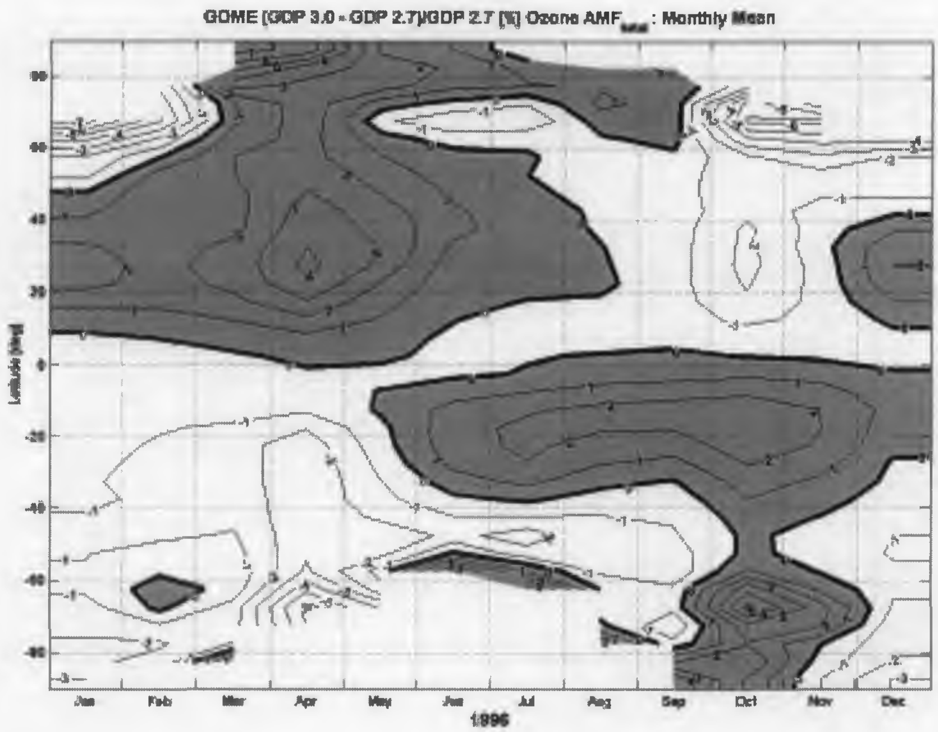

Figure 9 ***Latitude-month cross-section of the percentage relative difference between GDP 2.7 and 3.0 ozone air mass factor. Shaded areas indicate an increase of the air mass factor from GDP 2.7 to GDP 3.0.***

Figure 10 displays the monthly and latitudinal mean evolution of the SCD/AMF$_{total}$ ratio from GDP 2.7 and GDP 3.0, corresponding to the first part of the right term of the VCD formula (Eq. 1). The monthly and latitudinal changes of VCD seen in Figure 2, is generally not different from the considered ratio by more than ± 0.5%, except only in the southern high latitudes in August and September where a decrease which can reach 5% is observed (more details in the next sub-section). This excellent correlation demonstrates that VCD has changed mainly due to SCD and/or AMF. More, considering that SCD has slightly increased between the two GDP versions (see Sub-section 3.3), we may assume that globally the major changes of VCD are due to the new determination of the ozone AMF.

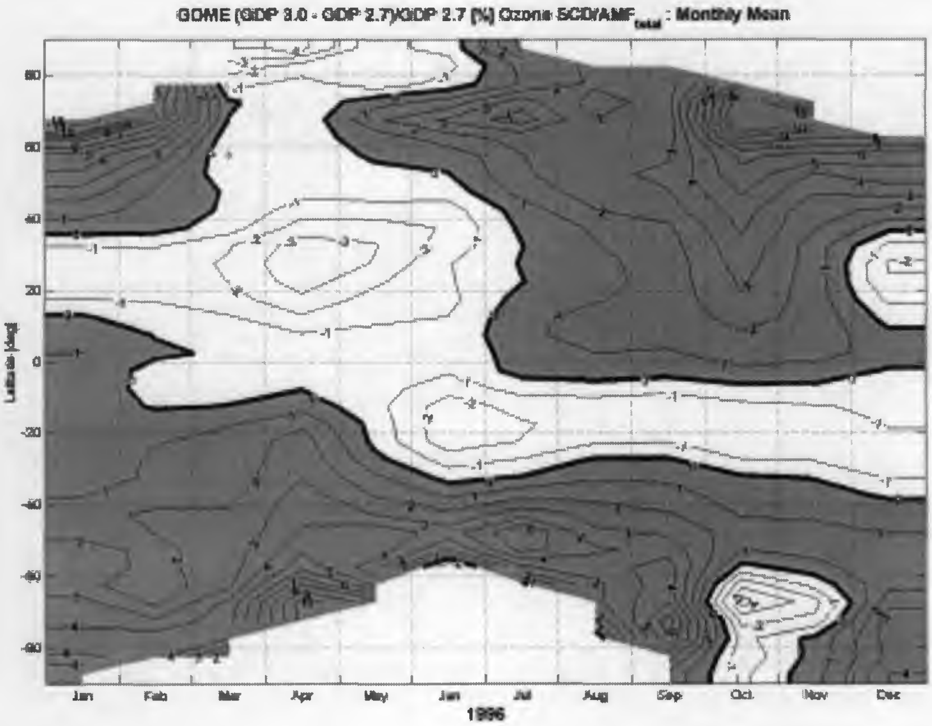

Figure 10 ***Latitude-month cross-section of the percentage relative difference between GDP 2.7 and 3.0 SCD/AMF$_{total}$. Shaded areas indicate an increase of the SCD/AMF$_{total}$ ratio from GDP 2.7 to GDP 3.0.***

IV.1.4.2 Ghost Vertical Column

The ghost vertical column is the total column hidden by clouds. As SCD and AMF, GVC is used in Equation 1 to calculate VCD. GDP 3.0 GVC is estimated using the same TOMS v7 climatological database of ozone profiles as used to calculate AMF, in stead of MPI 2D modelling results as previously used by GDP 2.7.

Figure 11 displays the absolute difference between GDP 2.7 and GDP 3.0 GVC in Dobson units (DU). GVC increases slightly (1 DU) around the ITCZ and decreases roughly (until -7 DU) at polar latitude during the late winter and the early spring, precisely when the polar regions are subject to high cloud coverage. We do not consider GVC without F because GVC contribution to VCD is weighted directly by F (Equation 1). If F value is high, SCD increases slightly and GVC decreases roughly, then new VCD must have lower values.

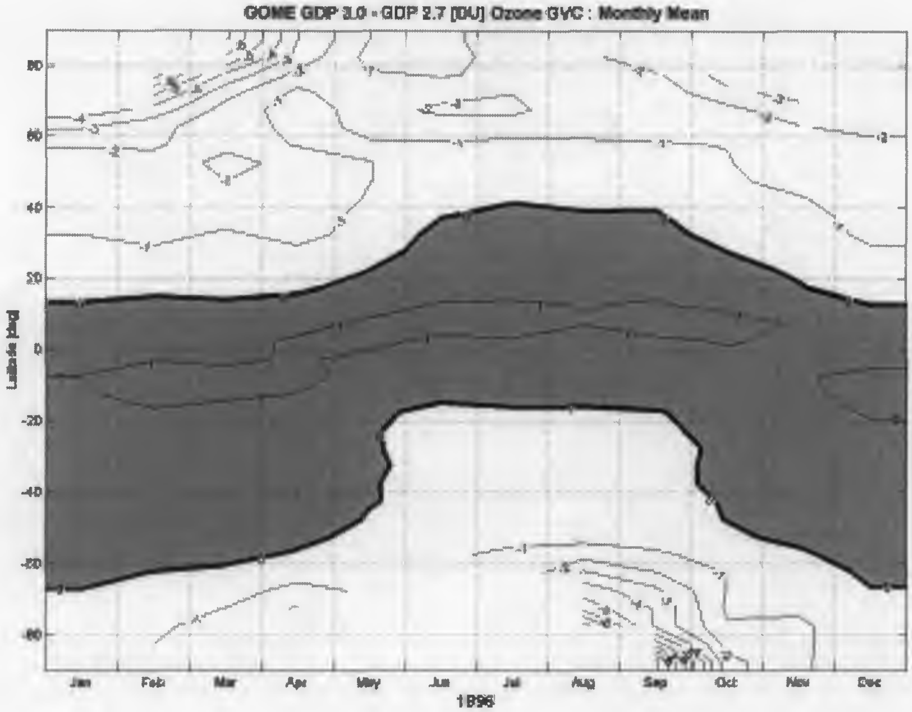

Figure 11 *Ozone ghost vertical column monthly mean and latitudinal absolute difference in Dobson units between GDP version 2.7 and 3.0. Shaded areas highlight positive evolution from GDP 2.7 to 3.0.*

Table 3 illustrates that this reasoning is valid for the late winter and early spring at polar latitudes. Indeed, for the selected latitudes and seasons, the decreases of VCD and GVC contribution in Equation 1 are in the same range order and correlate clearly, while the SCD contribution which always increases, has no correlation with VCD evolution.

Table 3 ***Comparison of the respective contribution of ghost vertical column (GVC) change and slant column density (SCD) change to the GDP total ozone (VCD) change, during late winter and early spring at the poles. The last three columns represent the monthly-zonal average evolution of values from GDP 2.7 to 3.0. Changes in VCD (4th column) calculated with Equation 1 correlate with changes due to GVC (5th column), decreasing similarly. The SCD contribution (6th column) always yields an increase of about 1 DU.***

Hemisphere	Month	Latitude [°]	Δ(VCD) [DU]	Δ(GVC.F.AMFc /AMFt) [DU]	Δ(SCD/AMFt) [DU]
North	March	85 to 90	-14.64	-6.32	0.97
		80 to 85	-8.25	-4.67	0.99
		75 to 80	-1.47	-3.50	1.00
South	August	-75 to -80	-12.05	-9.15	0.99
		-70 to -75	-5.51	-5.82	1.00
	September	-90 to -85	-8.95	-10.62	1.01
		-85 to 80	-4.67	-7.66	1.03

Figure 12 shows that in Antarctica the reduction of the F*GVC product from GDP 2.7 to GDP 3.0 always occurs during the late winter and the early spring, when the ozone vertical column is low, precisely in the "ozone hole" condition.

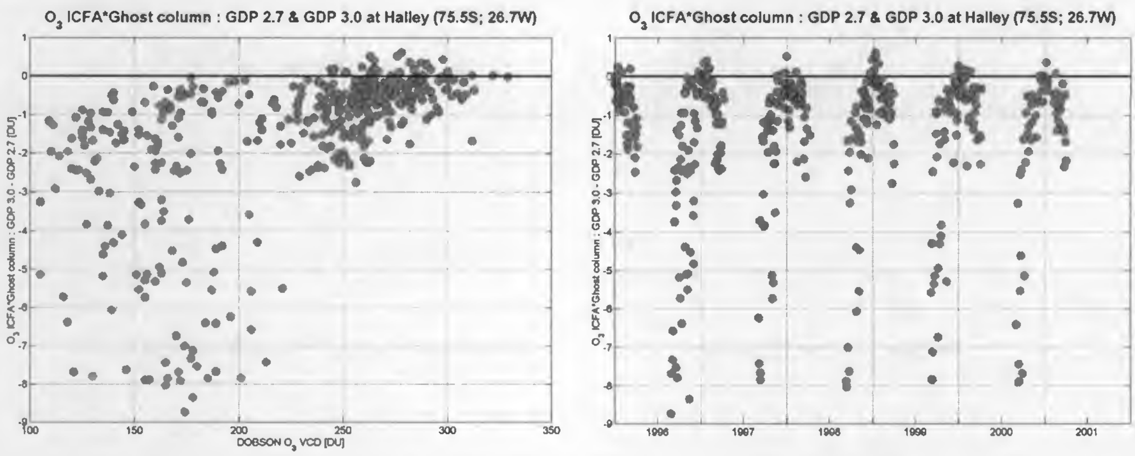

Figure 12 ***Absolute difference [DU] of the GDP 3.0 -GDP 2.7 product of cloud fraction and ghost vertical column at Halley, as a function of vertical column (left panel) and time (right panel). The reduction of this value always occurs during late winter and early spring in Antarctica when the vertical column is low.***

Despite the fact that GVC*F decreases from GDP 2.7 to GDP 3.0 at northern high latitudes during the same season, VCD is not proportionally affected by this evolution as much in the Arctic as in the Antarctic. It is probably due to the fact that northern total ozone does not decrease as much as in the Antarctic ozone hole, hence the GVC/VCD ratio is lower and less significant in the Arctic region.

IV.1.4.3 Budget of VCD Changes

In addition to the detailed studies described in previous subsections, we have estimated the impact of the different changes of GDP modules (SCD, AMF, GVC and ICFA) separately, using the GDP hybrid products described in Subsection IV.1.2.1. Figure 13 illustrates the evolution of GDP, representing for the same orbit: (a)VCD of GDP 2.7; (b to e) hybrid products; and (f) VCD of GDP 3.0. It shows clearly that in Antarctic ozone hole conditions, VCD decreases from one version to another due to the reduction of GVC. In fact, SCD does not change by more than 1% (see (b)). New AMF is the major responsible for changes in VCD values (compare (c) with (f)). However, if we calculate a new VCD based on GDP 3.0 SCD and AMF (preGDP_2, (d)), we still cannot explain why high latitude pixels (highlighted in red) is about 3% lower in the GDP 3.0 product (f) compared to that in preGDP_2. It can be understood when we have a look to the VCD ratio if only GVC and ICFA top of cloud pressure and cloud fraction are issued from GDP 3.0, which are about 3% lower at the concerned latitude. This confirms that globally VCD changes seem to be driven more by AMF modification.

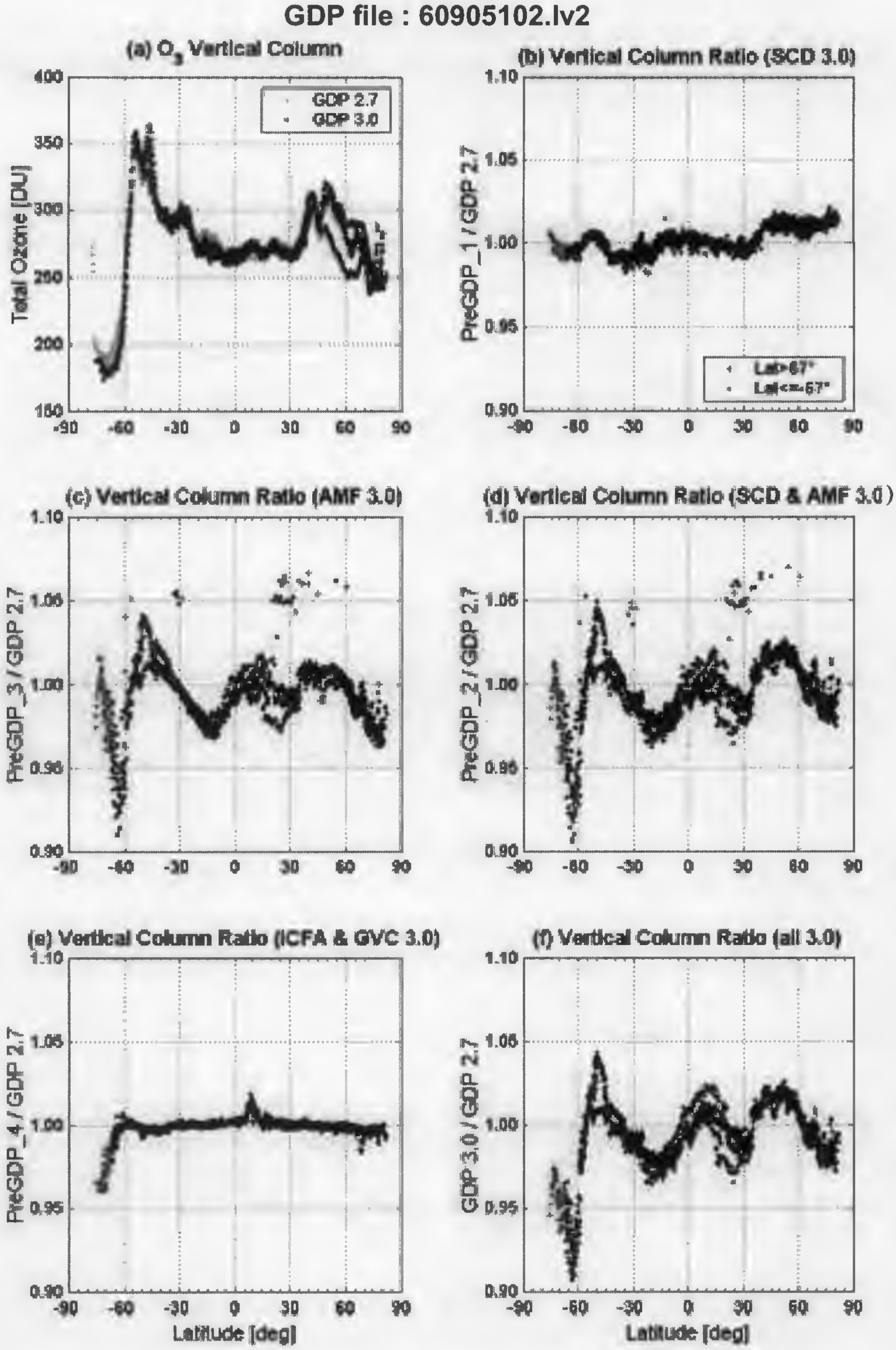

Figure 13 *Ozone vertical column and ratios obtained by GDP 2.7 and 3.0 and preGDP_x hybrid versions along one GOME orbit during the ozone hole season (5th September 1996). (a) GDP 2.7 (grey) and 3.0 (black) total ozone, then vertical amount ratio if: (b) only SCD comes from 3.0 version; (c) only AMF come from 3.0; (d) both SCD and AMF come from 3.0; (e) both ICFA top of cloud pressure and cloud fraction come from 3.0; and (f) all intermediate values come from GDP 3.0. Red dots highlight very high latitude (≤-67°) pixels which are reduced of 5% between two GDP versions due to the significant changes in GVC at those latitude and period of the year and not in SCD or AMF(see (e) compared to (b) and (d)).*

IV.1.5 Ozone Cross Section Temperature

It is well known that the depth of the differential absorption cross-sections of ozone in the Huggins bands vary with the temperature (Paur and Bass, 1984). This temperature dependence is illustrated in Figure 14 for the GOME Flight Model 98 cross-sections used in GDP. The differential structures of the absorption cross-sections decreases by about 3% for a temperature increase of 10K. Consequently, the retrieved slant column amount, which is inversely proportional to the depth of the differential cross-sections, should increase by 3% for a temperature increase of 10K.

Since the estimation of the absorption cross-section temperature and the fitting of ozone slant column density have been completely revisited in version 3.0, we propose in the present section to investigate how changes in the determination of the cross-sections temperature correlate with changes in retrieved SCD.

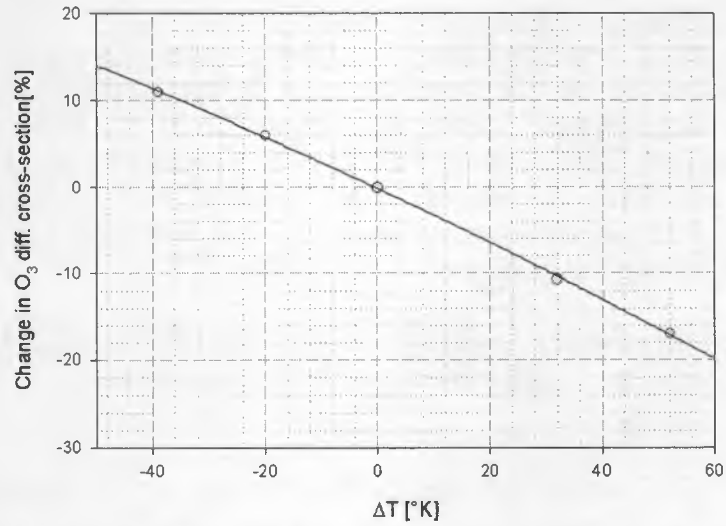

Figure 14 ***Temperature dependence of the ozone differential cross-section with respect to the ozone cross-section at 241°K in the 325-335 nm spectral band. Open circles are calculated values using GOME FM98 ozone cross-sections. The curve is a quadratic (quasi linear) equation fitting perfectly the cross-section/temperature dependence.***

IV.1.5.1 Data Sets

Five different types of cross-section temperature have been generated:

(a) IASB WinDOAS is a fitted temperature in the 325-335nm widow. In close collaboration with DLR, WinDOAS settings have been adjusted to match at best the GDP 3.0 temperature values (note that XST values are not provided in the DLR-IMF level-2 files).

(b) GDP 2.7 is the temperature at the ozone density maximum of MPI-2D modelling results.

(c) GOFAP 3.0 is the ECMWF temperature weighted by adequate Fortuin and Kelder (1998) climatological ozone profile, as done by the GOME fast delivery processor GOFAP.

(d) F&K Static is calculated by the same method as GOFAP 3.0, however the temperature is taken from a climatology combining ECMWF data in the troposphere (Trenberth, 1992) and CIRA in the stratosphere. Generally, the difference between GOFAP temperatures and F&K Static ones does not exceed a few Kelvin (see Figure 16).

(e) IASB UVSPEC is the effective temperature derived from an adapted version of the radiative transfer model UVSPEC, in which we entered as input the Fortuin and Kelder climatological ozone profiles. Calculation of the effective temperature is made at 325 nm, that is, the wavelength adopted for the calculation of GDP ozone AMFs.

IV.1.5.2 Comparison of Effective Temperatures

A total of 70 orbits (the first of each month from the validation data set) have been used to investigate along track effective temperature and SCD changes. In this subsection, we take the example of the orbits of the August 1, 1996, and December 1, 2000. These orbits represent well the general behaviour of the SCD and temperature changes. We tried to cross-correlate SCD and XST, but the task is perilous due to the fact that the effective temperature definition changes with each type of temperature. Behind the fact that effective absorption temperature is a pure geophysical concept that cannot be, once and for all, univocally defined, the philosophy of this value, and more practically, the method of calculation are absolutely different as well. Before making any cross-correlation, we must keep in mind that we might compare two different physical quantities.

Considering the remark made above, and assuming that WinDOAS and GDP 3.0 fitted temperatures match closely enough, it is still possible to make the following observations based on Figure 15 and 16:

- The four sets of XST seem to behave globally in the same way but the quantitative values can differ by 10%.
- GDP 3.0 has always the highest XST of the four compared values.
- GDP 2.7 has always the lowest XST of the four compared values.
- GDP 3.0 XST is approximately 20K above version 2.7.
- GDP 3.0 XST are sensitive to the South Atlantic Anomaly (SAA) due the fit made directly on spectra that are affected by the SAA as well.
- At high XST, GDP 3.0 is closer to the UVSPEC radiative transfer model value. It might be because the calculation is only made at 325nm in UVSPEC, whereas the fit is made in 325-335nm window in GDP 3.0. The more the effective temperature is high, the more the altitude of the ozone concentration maximum is high, and the absorption difference between a single wavelength and a 10 nm window should be smaller.
- GDP 2.7 XST in cold polar winter condition underestimate the values derived by the radiative transfer model.
- Even GOFAP underestimate the XST in cold polar winter condition compared to radiative transfer model results. The latter predict XST increasing at high SZA. This behaviour

might be explained by the fact that UV radiation at high SZA cannot reach the cold lower troposphere due to Rayleigh scattering. On the opposite, GOFAP 3.0 gives a similar weight to all altitudes.

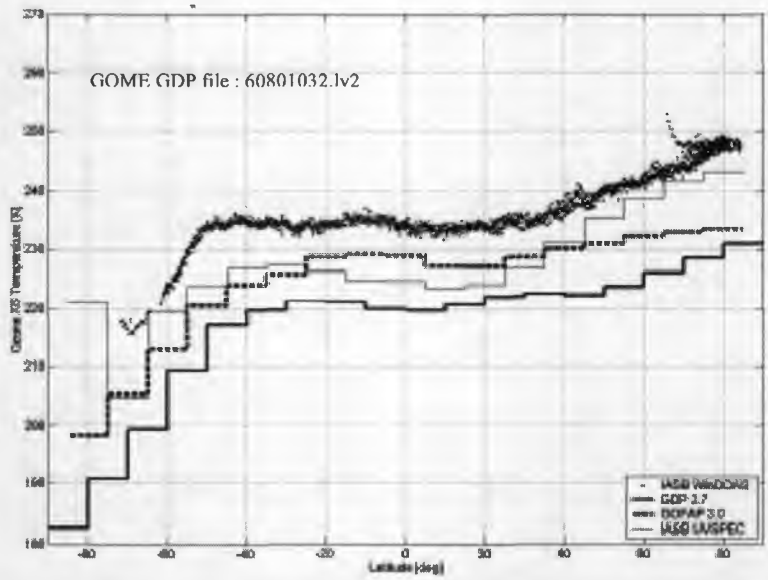

Figure 15 *Different ozone cross section temperatures along the GOME GDP file 60801032.lv2 of August 1, 1996. IASB WinDOAS (≈ GDP 3.0, dots), GDP 2.7 (continuous thick line), GOFAP 3.0 (dashed thick line) and IASB UVSPEC (continuous thin line).*

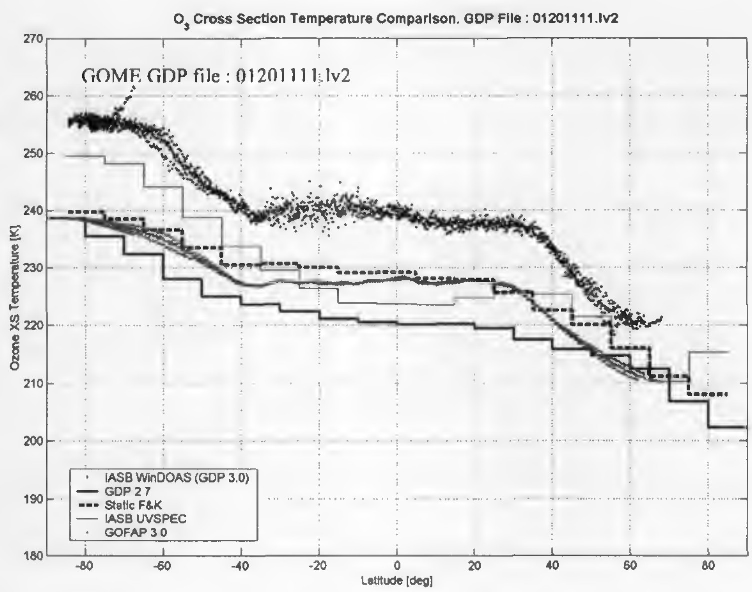

Figure 16 ***Same as Figure 15, along the GOME GDP file 01201111.lv2 of December 1, 2000***

IV.1.5.3 Effect on Retrieved Slant Columns

In general, the fitted XST is higher than the GDP 2.7 temperature by 20K. According to the proportional relation between temperature and SCD, this should lead to a general SCD increase of about 6% from GDP 2.7 to GDP 3.0. However, as illustrated in Figure 17, SCD changes between GDP 2.7 and GDP 3.0 fall within the ±2% range. In particular, GDP 3.0 SCD is even 1-2% lower than GDP 2.7 SCD at latitudes below 40°.
Figure 18 shows that, although not proportional, a linear relation exists between changes in temperature and changes in SCD, with the expected slope of about 3% by 10 K but also an unexpected offset. This phenomenon seems to be more visible if we study it by sorting the GOME pixels according to the latitude.

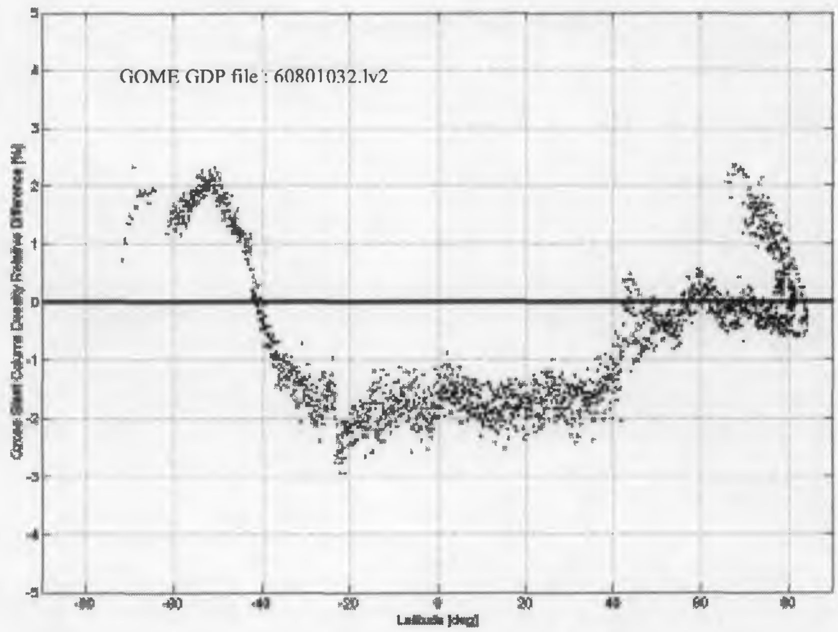

Figure 17 *GDP (3.0-2.7)/2.7 relative difference in slant column for the same orbit as in Figure 15.*

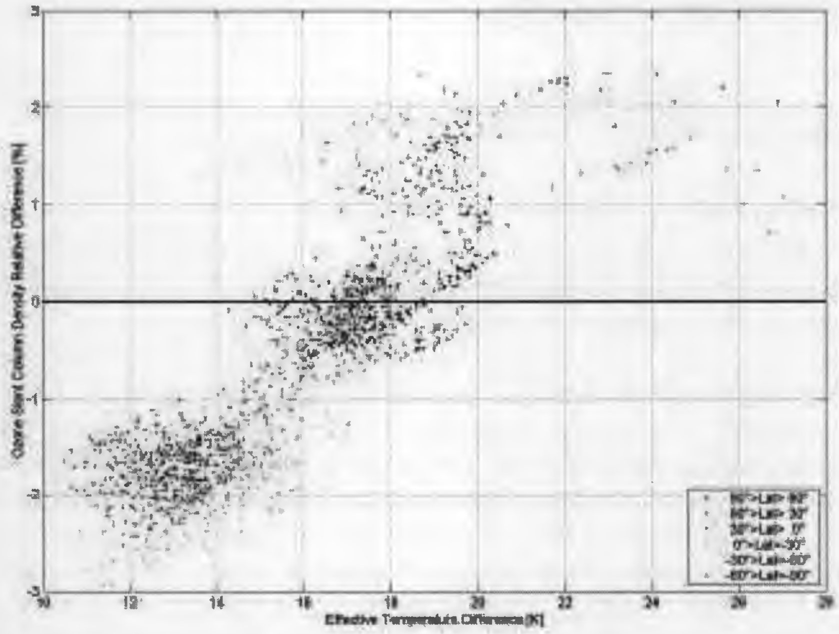

Figure 18 *GDP (3.0-2.7)/2.7 relative difference in slant column as a function of the GDP 3.0-2.7 effective temperature difference, for the same orbit as in Figure 15. Dots are sorted by latitude zone: black (60° to 90° North), red (30° to 60° North), blue (0° to 30° North), green (0° to 30° South), yellow (30° to 60° South), and pink (60° to 90° South).*

IV.1.5.4 Discussion and Conclusion

The cross-sections temperature fitting implemented in GDP 3.0 seems to work properly and yields consistent values with our current understanding of geophysics. It reports however systematically higher values than other methods do. It is not straightforward to understand precisely the cause of this overestimation and the consequences of the new ozone XST on the SCD, due to difference in concept of both the definition and the calculation method. Except this formal problem, in summary, we may confirm that SCD and XST changes from GDP 2.7 to GDP 3.0 are linked by a quasi-linear relation, the slope of this relation being consistent with the temperature dependence of the absorption cross-sections. Nevertheless, due to a systematic offset, the important temperature increase of about 20K between GDP 2.7 and 3.0 does not produce the expected 6% increase of the retrieved SCD, the latter varying hardly within ±2% from GDP 2.7 to 3.0. The offset might originate from other changes in the SCD retrieval such as the use of new Ring effect cross-sections and the new philosophy of the spectral fitting (see Chapters 2 and 6). A last remark concerns the fact that GDP 3.0 XST is now inferred directly from the GOME radiance measurement, instead of using modelling results. Besides the clear advantages of physically-based retrieval methods, GDP 3.0 XST has also disadvantages such as its sensitivity to the quality of the spectra. Consequently, the retrieved SCD is now sensitive to measurement perturbations such as those associated with the SAA.

IV.1.6 Correlative Study of Total Ozone

IV.1.6.1 General Consistency

IV.1.6.1.1 Cross-correlation of GDP ozone data along the orbit

Figures 19 and 20 depict GDP 2.7 and 3.0 ozone data along track for two individual orbits in February an August 1996. Similar results are obtained with the 30 orbits studied here. GDP 3.0 without any added mention means xcorr data.

Panel (c) of those figures shows that SCD has changed in a range of about ±2.5% at high latitude and can reach 7% of increase at southern very high latitude in August, but almost did not change 30° around the equator, where it has meanly increased slightly excepted in December to March where it decreases less than 1%. Cloudy and clear AMFs (panels (f) and (g)) can have a totally different evolution depending on latitude and season affecting the total AMF (panel (e)) independently. AMF change is limited at about ±2.5% below 60° of latitude but can reach 5 to 10% at higher one. Cloud fraction (panel (h)) globally slightly decreases in absolute difference for 0.01, but can be reduced by 0.02-0.03 at higher latitude. GVC which is taken into account in GDP processor, represented in panel (i) by its value weighted by cloud fraction difference between the two GDPs, has decreased at high latitude between 1 to 10 DU and has increased until 7.5 DU in the ITCZ.

Calibrated level-1 with the new method (xcorr) and the old method (no_xcorr), as illustrated in Figure 21, can have a level-2 VCD difference of ±1%, mostly no_xcorr is 0.5% higher than xcorr, mainly due to the same ratio of SCD, AMF excepting a few outsider pixels that can maximum be 0.5% different are exactly the same in the two products.

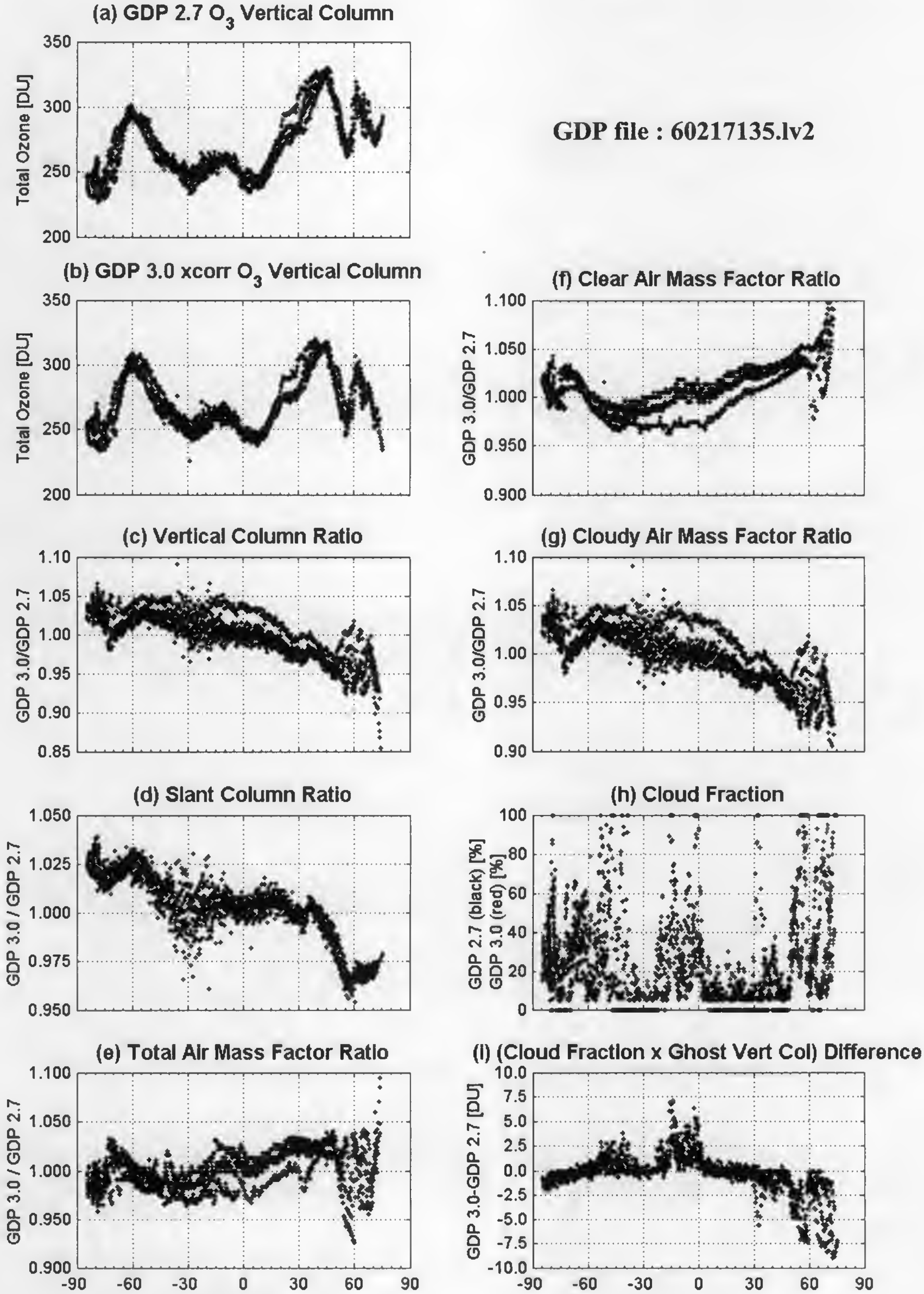

Figure 19 Along track (a) GDP 2.7 and (b) 3.0 total ozone for GOME orbit file 60217135 (February 17, 1996). (c) GDP 3.0/2.7 VCD ratio; (d) SCD ratio; (e) AMF_{total} ratio; (f) AMF_{clear} ratio; (g) AMF_{cloudy} ratio; (h) GDP 2.7 cloud fraction in black and 3.0 in red; and (i) F x GVC difference.

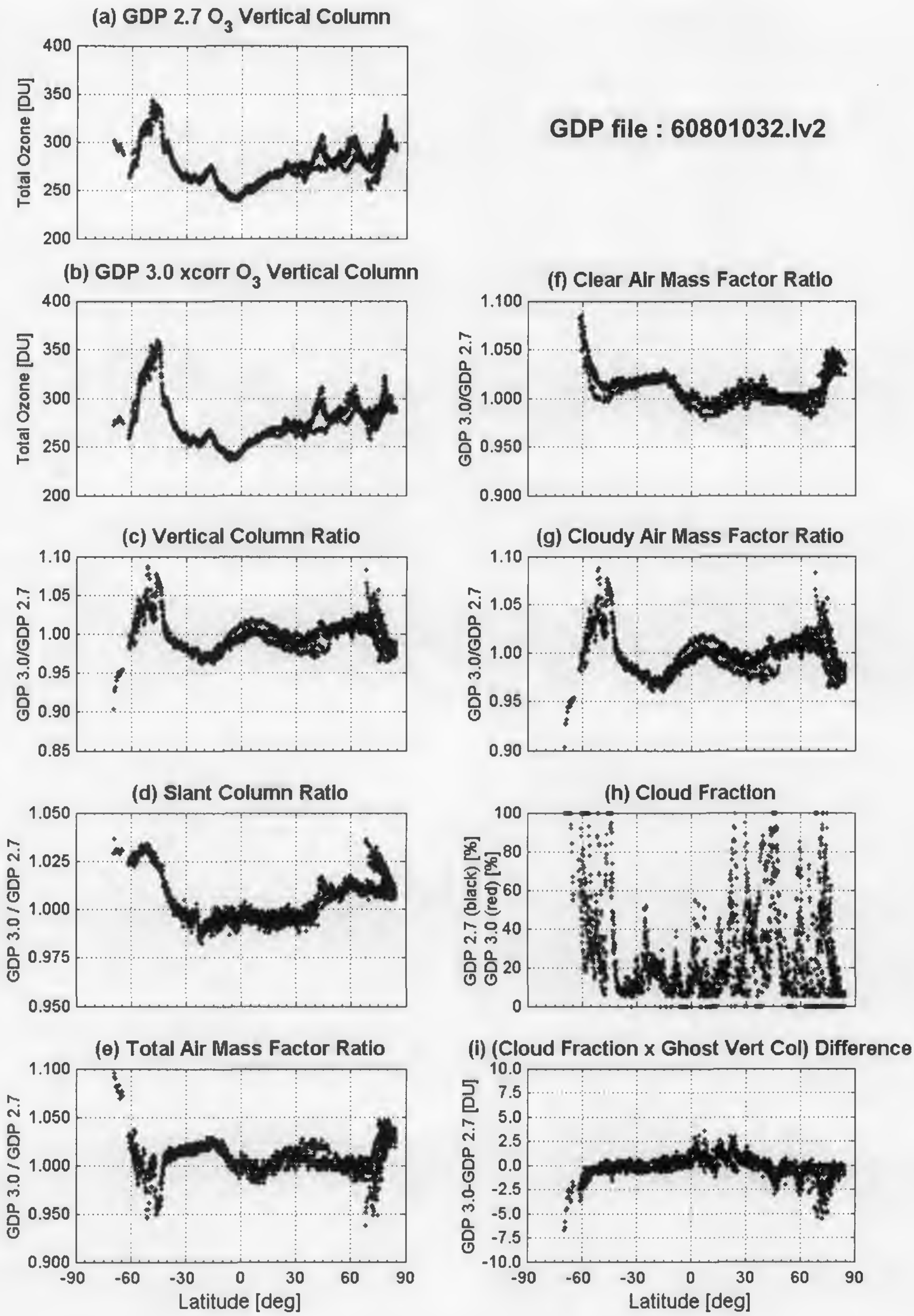

Figure 20 ***Same as Figure 19, but with GOME orbit file 60801032 (August 1, 1996).***

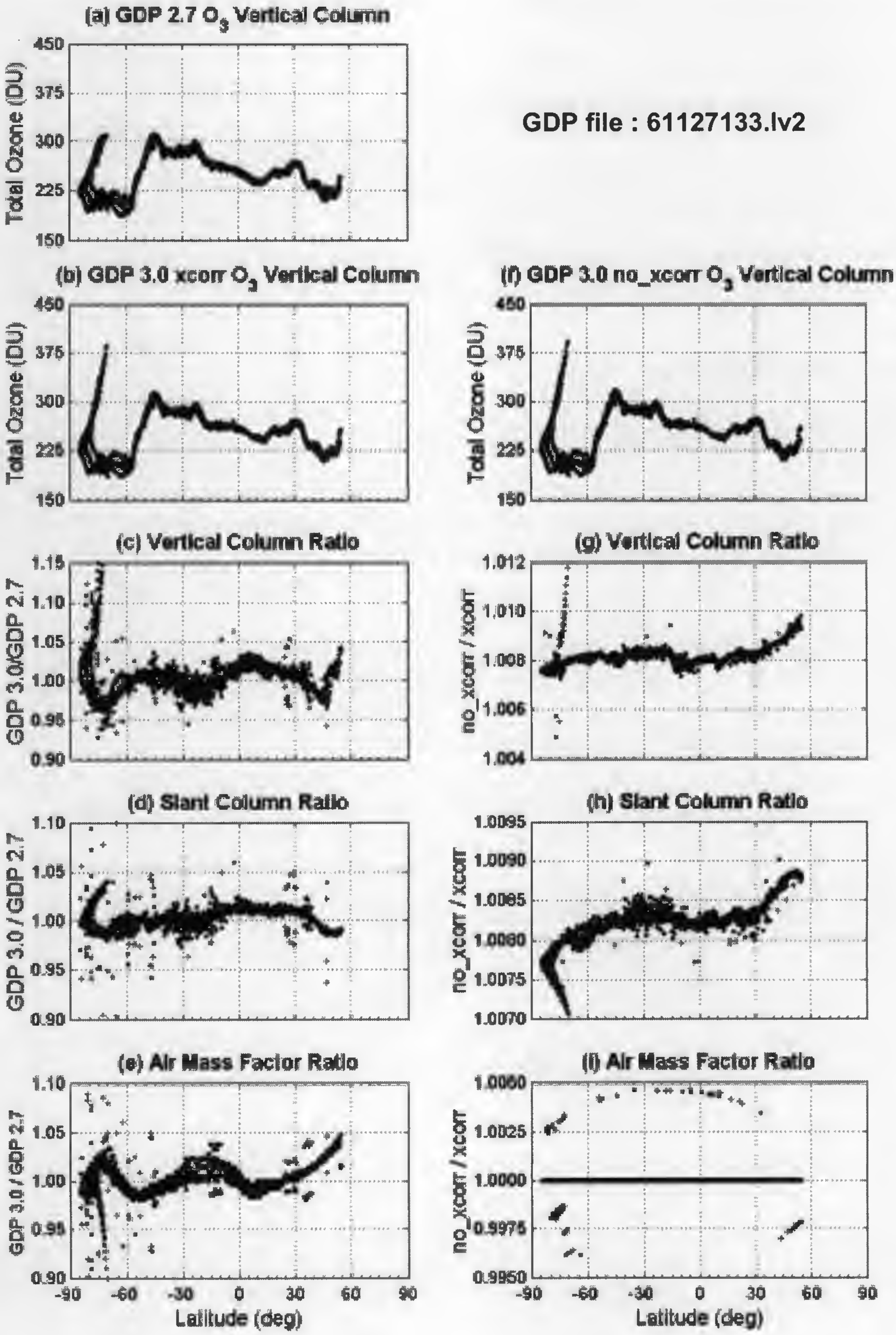

Figure 21 ***Same as Figures 19 and 20, but with GOME orbit file 61127133 (November 27, 1996).***

IV.1.6.1.2 Cross-correlation of GDP total ozone at NDSC stations

Figure 22 shows correlations between NDSC/GDP 2.7 and NDSC/GDP 3.0 relative differences at a few representative stations. The relative difference between GDP and NDSC is studied here in terms of amount of GOME pixels in better agreement in the new version. An average of about 60% of the GOME pixels are closer to NDSC than earlier. This value falls to 45% at equatorial stations, meaning that more than one of two pixels are more distant now than earlier. The best improvement is observed at southern mid-latitude stations like Lauder and Kerguelen, where 70% of GOME-NDSC relative difference have reduced.

IV.1.6.2 Cyclic Signatures

IV.1.6.2.1 Meridian and seasonal signatures

The seasonal variation of the GDP-NDSC discrepancy displayed hereafter (Figure 23 to Figure 26), is significantly reduced but still remaining. Globally, the reduction of the variation is about a factor 2, except in northern polar and mid-latitude stations where smaller improvements are observed. The main improvement in the northern hemisphere seems to be in fall (Figure 24 and Figure 26) with a reduction of 5% of the mean difference, although at Arosa for instance (Figure 24 right), there is improvement also in spring and winter by a reduction of 3% of the mean difference. In the southern hemisphere, the impact of GDP changes is more visible at every season (Figure 25 and Figure 26). Scatter of GDP 3.0 compared to ground-based values is still as high as in version 2.7.

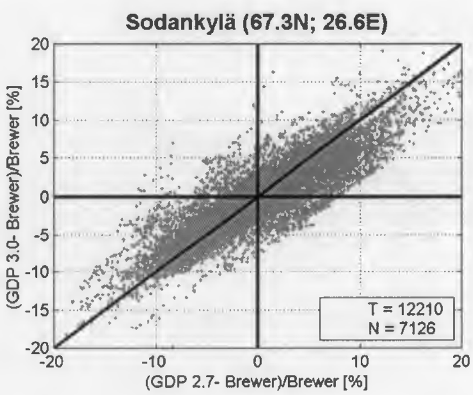

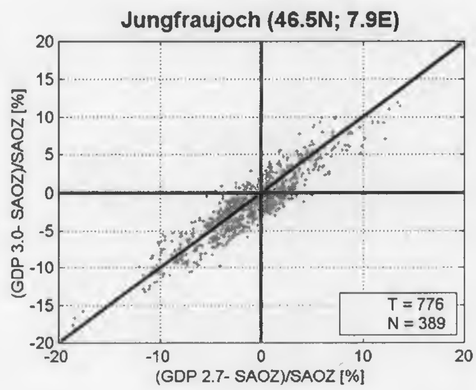

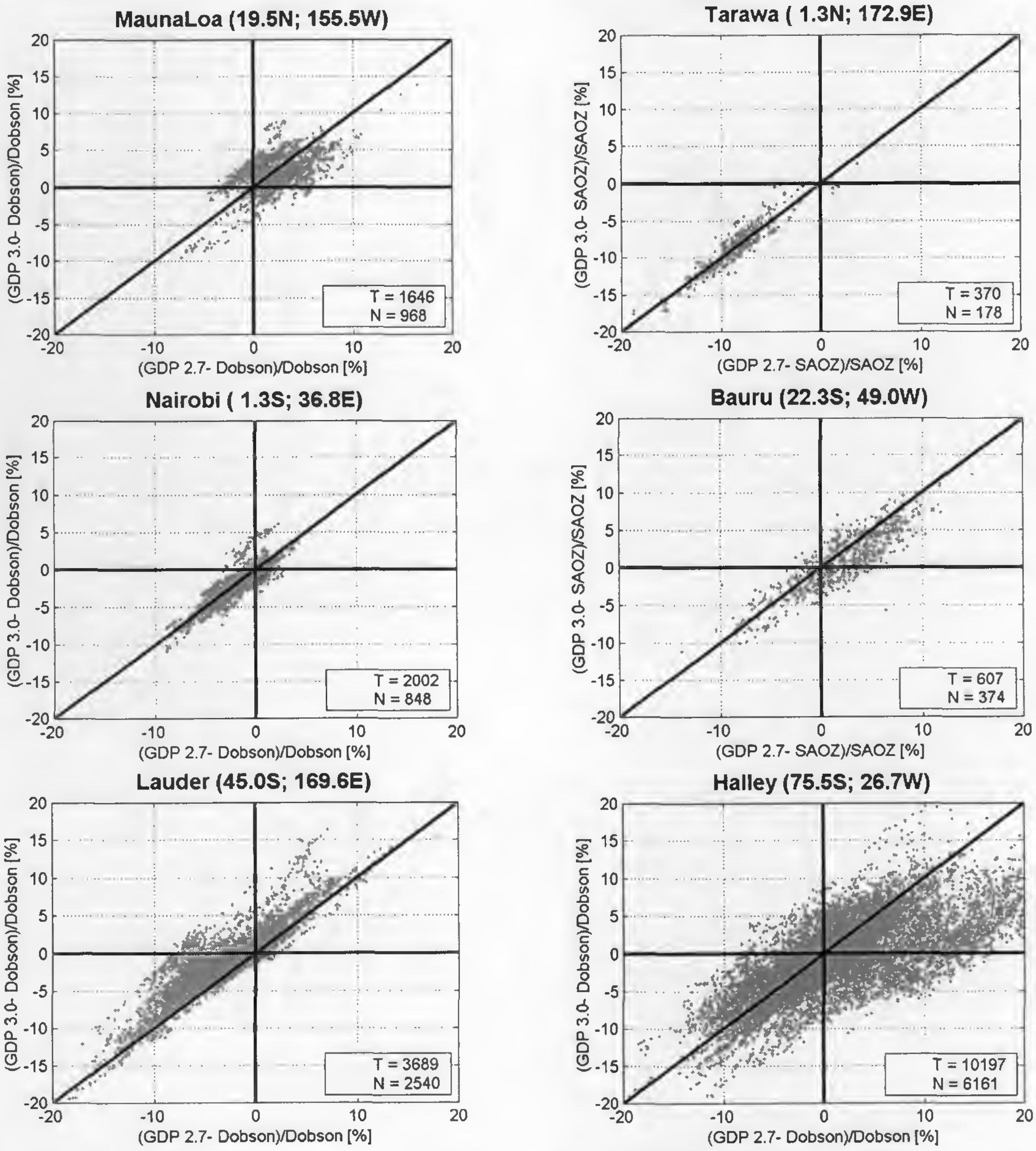

Figure 22 ***Change in the agreement between GDP 2.7/3.0 and NDSC total ozone: correlation of the relative difference at the NDSC stations of Sodankylä, Jungfraujoch, Mauna Loa, Tarawa, Nairobi, Bauru, Lauder, and Halley. N = amount of pixels in better agreement; T = total amount of pixels. N/T ratio is about 60% in average but only 45% at equatorial stations.***

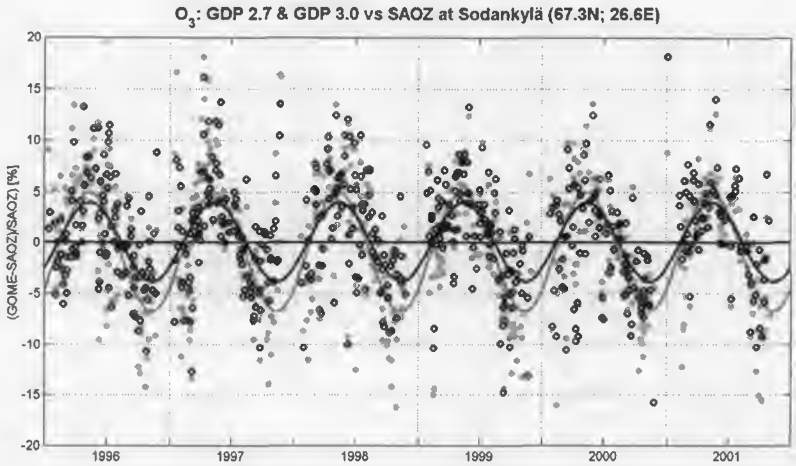

Figure 23-a ***Time series of relative difference between GDP 2.7 (grey dots) or 3.0 (black open circles) and SAOZ total ozone at the NDSC Arctic station of Sodankylä. Low-pass filtering of the time-series highlight seasonal cycles for GDP 2.7 (grey line) and GDP 3.0 (black line).***

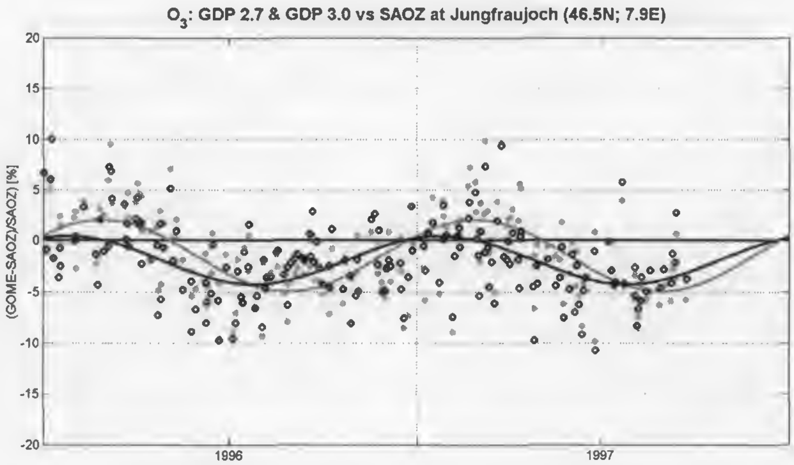

Figure 23-b ***Same as previous, but with SAOZ measurements at the NDSC Alpine station at the Jungfraujoch.***

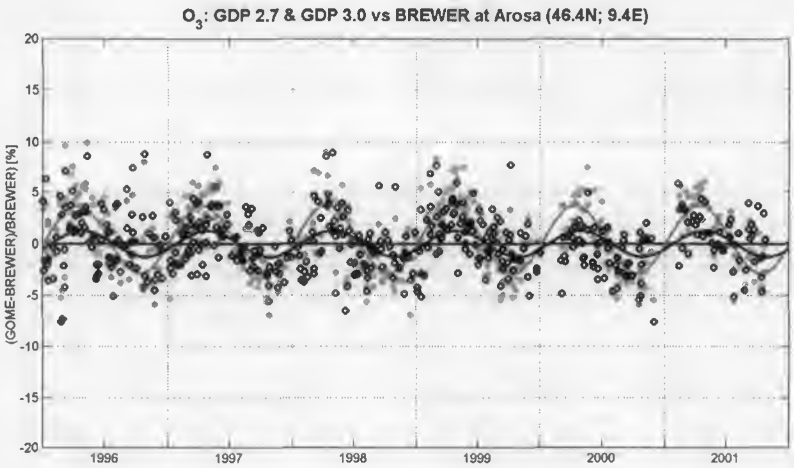

Figure 23-c ***Same as previous, but with Brewer measurements at the NDSC Alpine station of Arosa.***

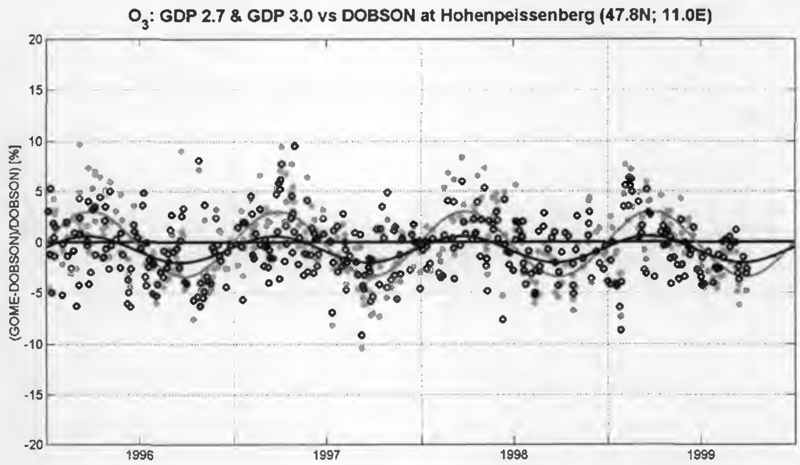

Figure 23-d ***Same as previous, but with Dobson measurements at the NDSC Alpine station of Hohenpeißenberg.***

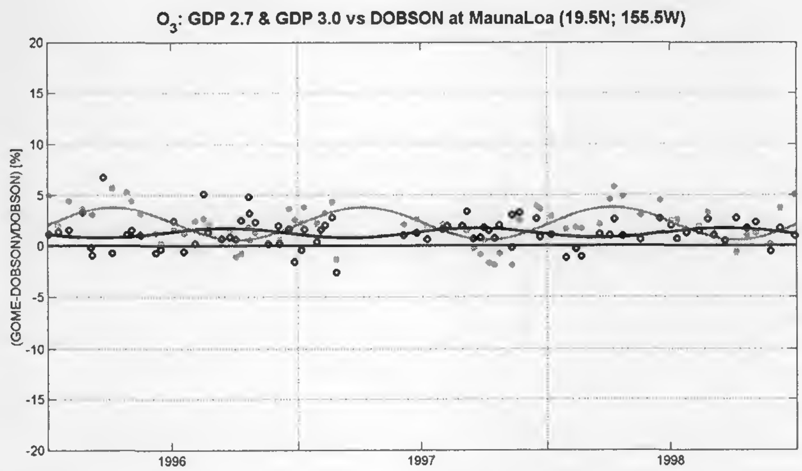

Figure 23-e ***Same as previous, but with Dobson measurements at the NDSC Hawaiian station of Mauna Loa.***

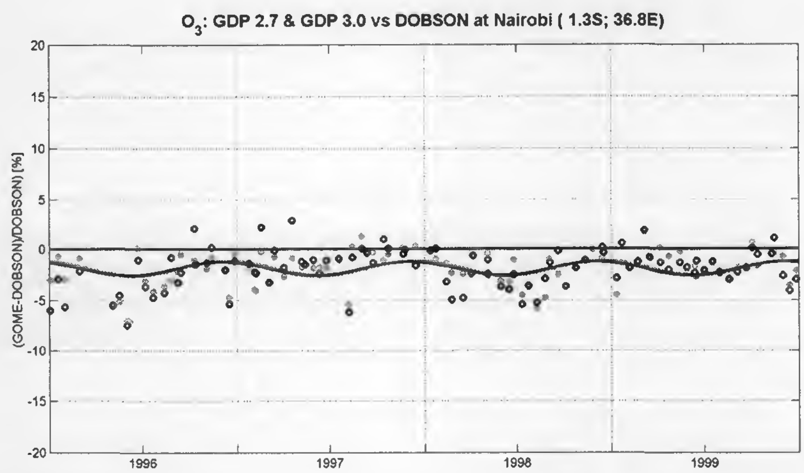

Figure 23-f *Same as previous, but with Dobson measurements at the equatorial station of Nairobi.*

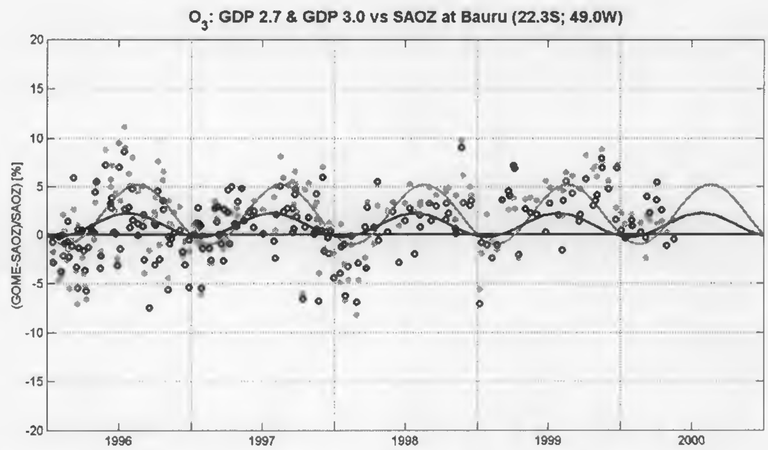

Figure 23-g ***Same as previous, but with SAOZ measurements at NDSC Brazilian station of Bauru.***

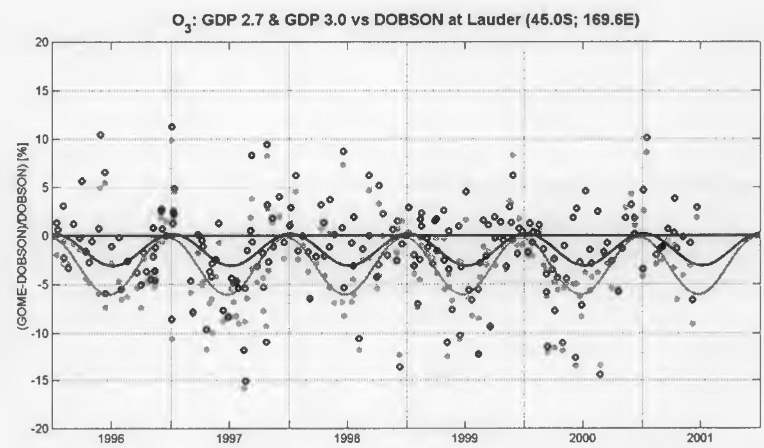

Figure 23-h ***Same as previous, but with Dobson measurements at NDSC New Zealand station of Lauder.***

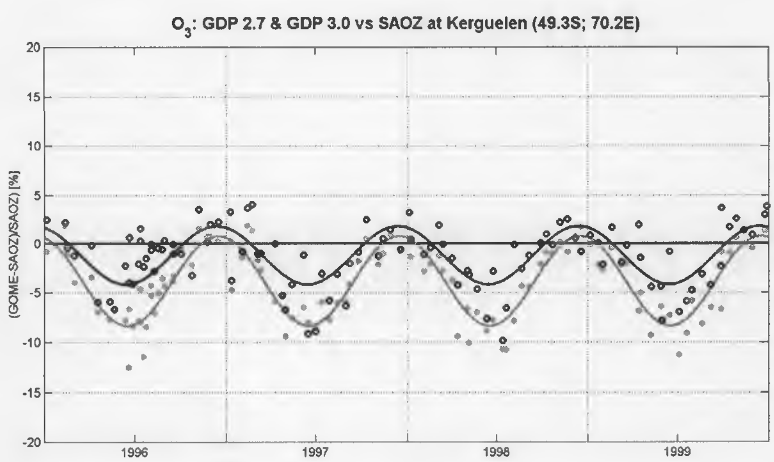

Figure 23-i *Same as previous, but with SAOZ measurements at the NDSC Indian Ocean station of Kerguelen.*

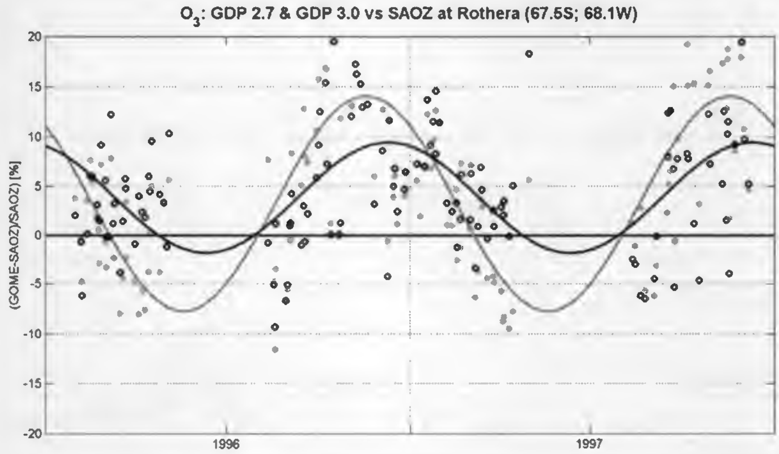

Figure 23-j ***Same as previous, but with SAOZ measurements at the NDSC Antarctic station of Rothera.***

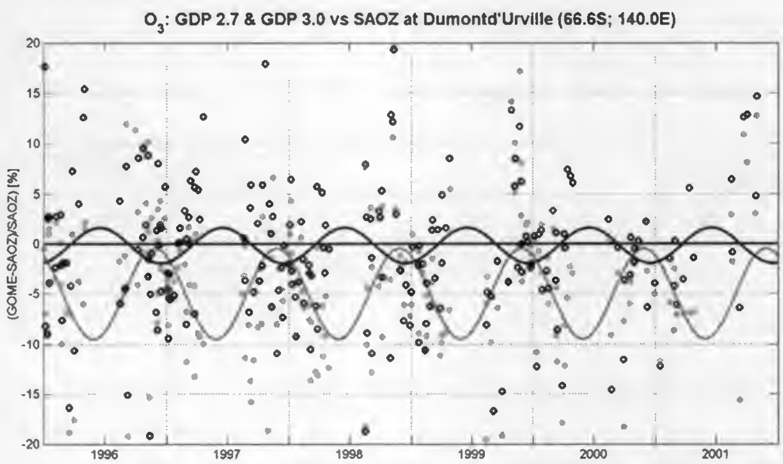

Figure 23-k ***Same as previous, but with SAOZ measurements at the NDSC Antarctic station of Dumont d'Urville.***

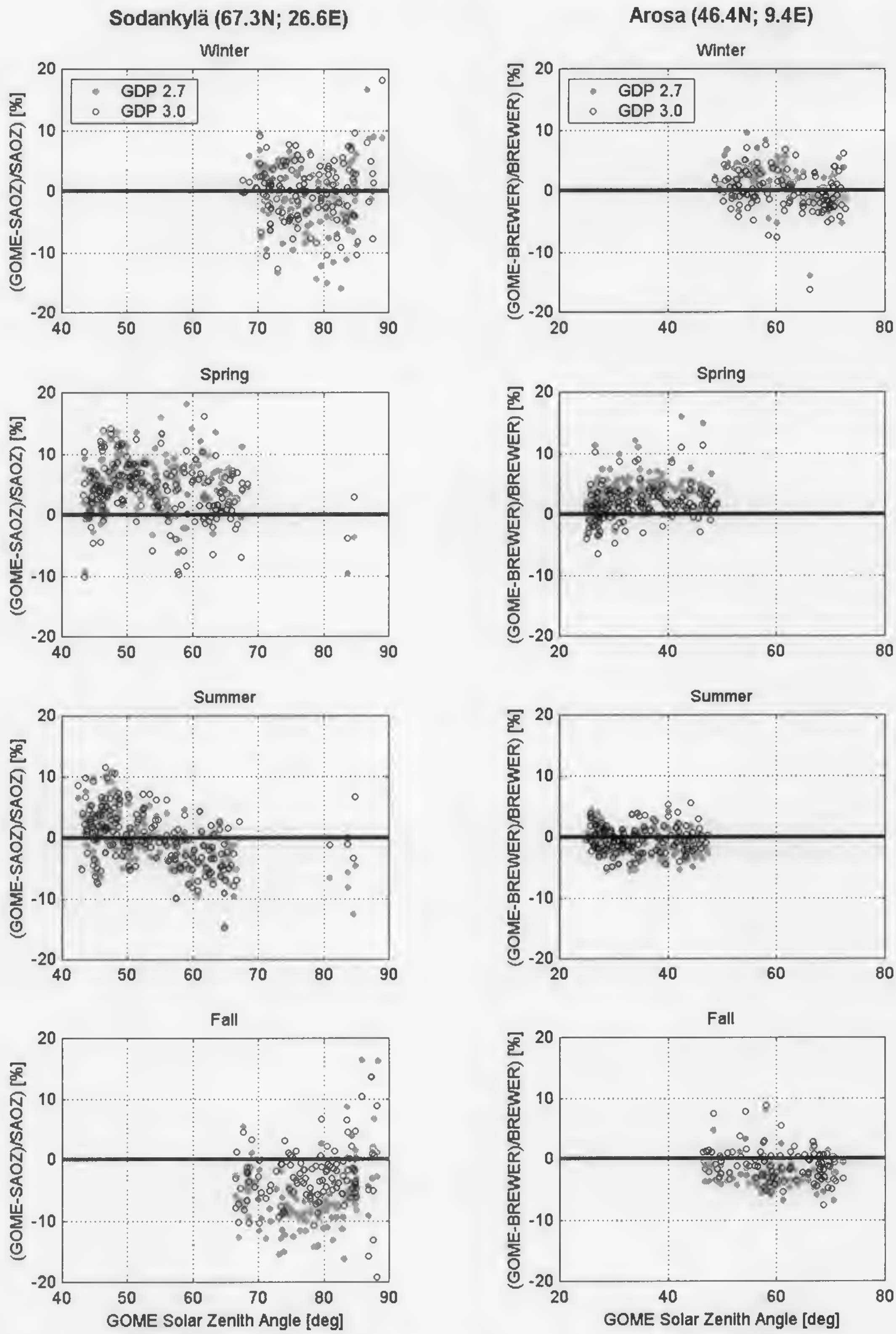

Figure 24 ***Seasonal variation (from top to bottom: winter-spring-summer-fall) of the relative difference in total ozone plotted as a function of the GOME solar zenith angle, between GDP 2.7 (grey plain dots), GDP 3.0 (black open circles) and Northern Hemisphere NDSC total ozone: SAOZ at Sodankylä and Brewer at Arosa.***

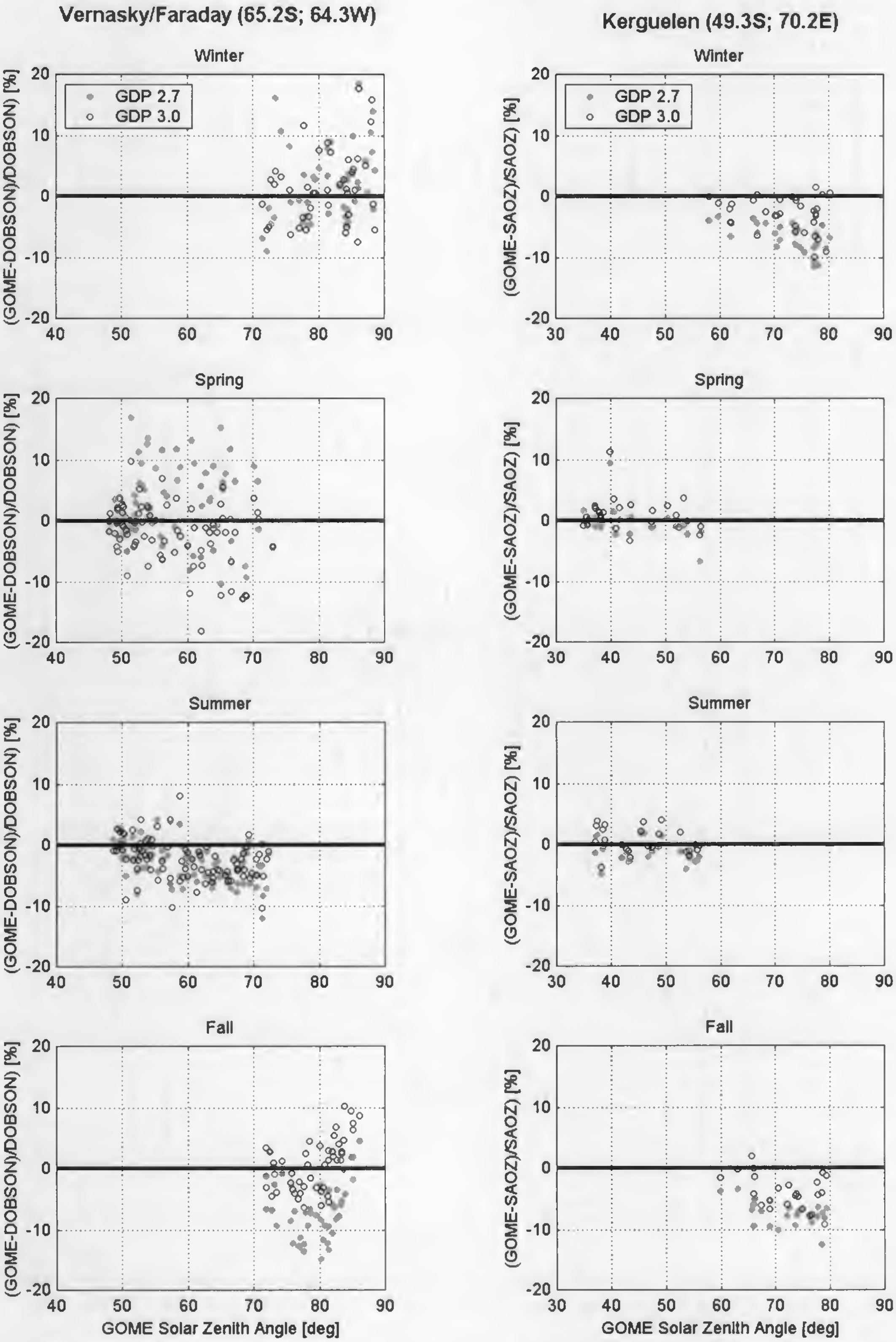

Figure 25 ***Same as Figure 24, but at two Southern Hemisphere NDSC stations: Dobson at Vernadsky/Faraday (left panel) and SAOZ at Kerguelen (right panel).***

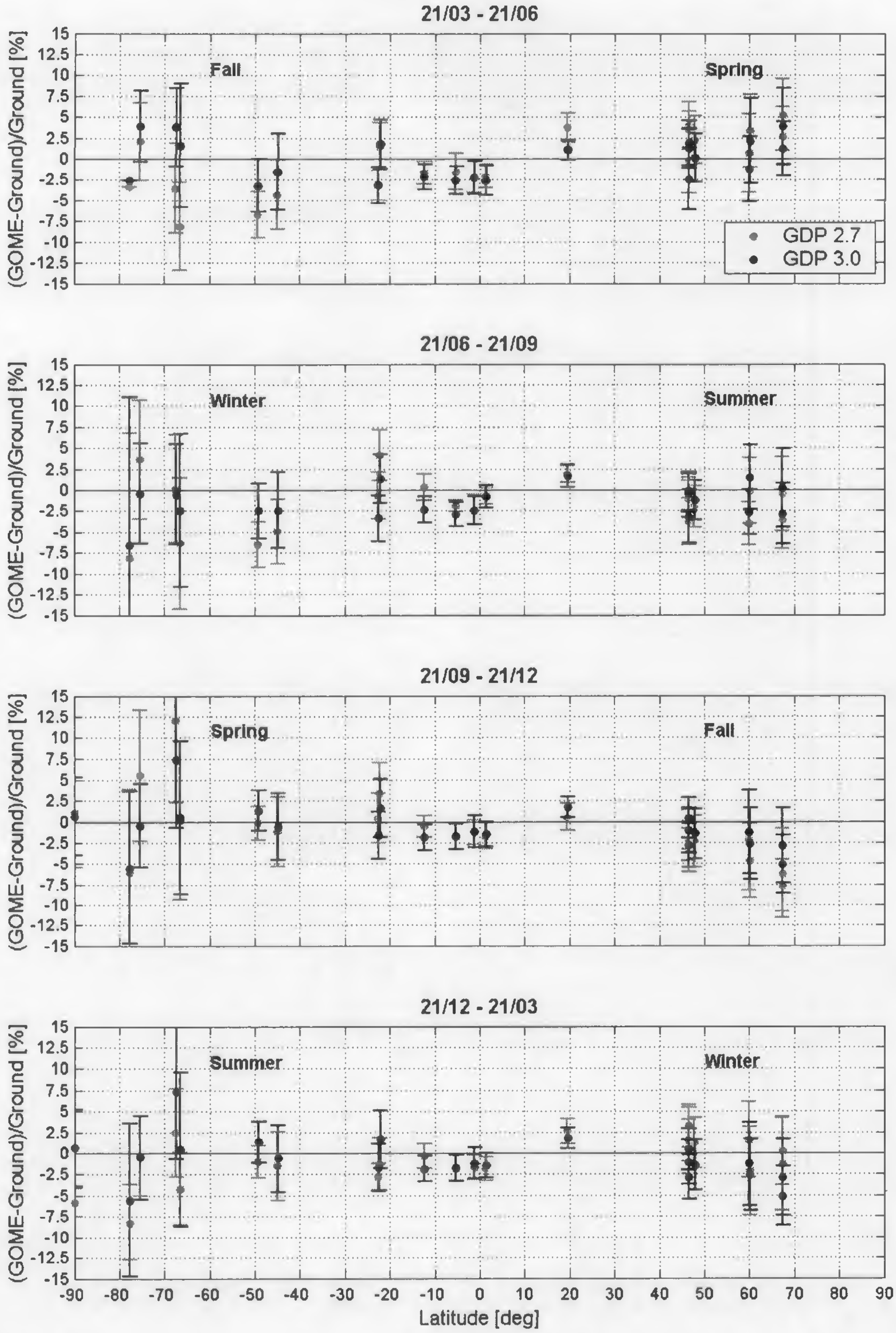

Figure 26 ***Meridian and seasonal variation of the percentage relative difference in total ozone between GDP 2.7 (grey) & 3.0 (red) and ground-based stations. Dots represent mean value and bars are the standard deviation (one sigma). Ground-based stations are, from North to South: Sodankylä (67°N, 2 instruments), Harestua (60°N), Oslo (60°N), Hohenpeißenberg (48°N), Jungfraujoch (47°N), Arosa (46°N, 2 intruments), Mauna Loa (20°N), Singapore (1°N), Nairobi (1°S), Natal (5°S), Darwin (12°S), Bauru (22°S), Cachoeira Paulista (23°S), Lauder (45°S), Kerguelen (49°S), Faraday/Vernadsky (65°S), Dumont d'Urville (66°S), Rothera (68°S), Halley (76°S), Arrival Heights (78°S), and Amundsen Scott (90°S).***

IV.1.6.3 Solar Zenith Angle Dependence

The solar zenith angle dependence of GOME total ozone has always been an issue and Figures 24 and 25 suggest that, despite some improvement, a SZA dependence persists with GDP 3.0. In this subsection, we highlight the impact of the GOME pixel population on SZA studies and we study further the SZA dependence at the Arctic station of Sodankylä.

Before making any statistical analysis from comparisons, it is crucial to make sure that the two studied populations are similar. Figure 27 shows that GDP 3.0 provides fewer data than GDP 2.7 at high and low SZA. Below 19° of SZA, there is about two times more data in GDP 2.7; between 19° and 85° the number of pixels are exactly the same; however, between 85° and 87° of SZA a slight number of pixels recognised by GDP 3.0 as being at those SZA are shifted from higher value in GDP 2.7; and above 87°, a large number of GOME pixels are not processed by GDP 3.0, as mentioned in Chapter 2 of the present issue. The ratio is about 7 to 8 times more pixels in GDP 2.7 at SZA around 90° and can reach 37 times between 93° and 94°. We have made carefully a selection of pixels from both GDP which have the same pixel number and the same SZA to prevent statistical differences due to sampling. Figure 28 shows an example of artefact that can be seen at high latitudes if this precaution is not taken. Indeed, between 85° and 90°, we should imagine that GDP evolved from 6% of the SAOZ overestimation to 2% of underestimation (Figure 28 top). However, limiting the study to the same set of pixels reduces the betterment from +3% to –2% (bottom of Figure 28).

Lower panel of Figure 28 shows a mean reduction of the SZA dependence with GDP 3.0 (from –2% to 4% of mean relative difference), and a more stable difference than version 2.7 along the SZA range (from –5% to 4% of mean relative difference). Nevertheless, the scatter around the mean difference does not seem to change, whatever the SZA class.

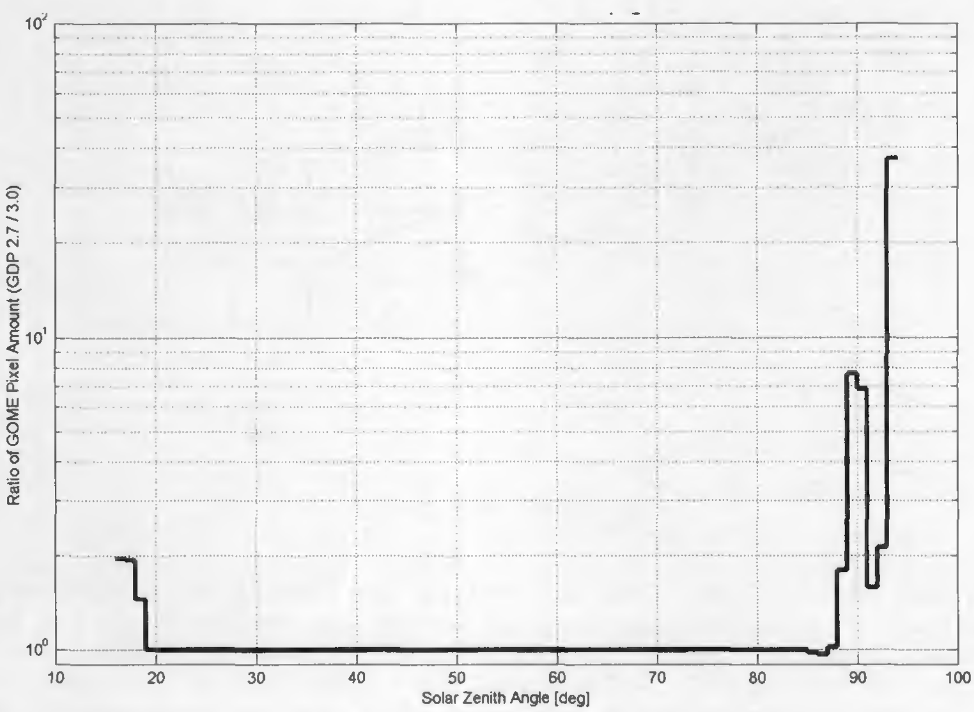

Figure 27 *Ratio of the amount of GOME pixels found in the available GDP 2.7 and 3.0 level-2 data sets, as a function of the GOME solar zenith angle.*

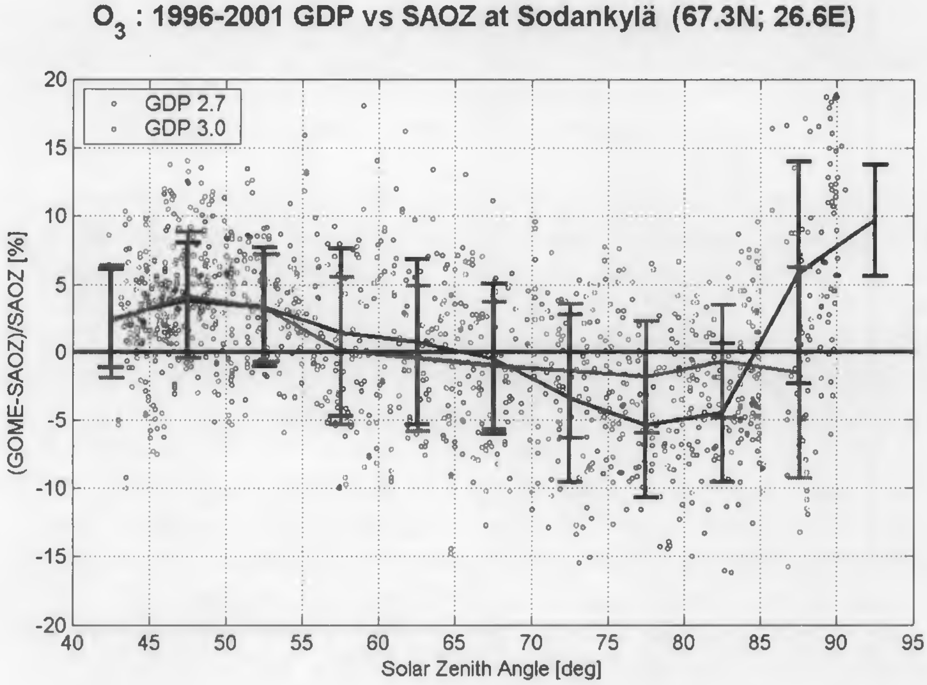

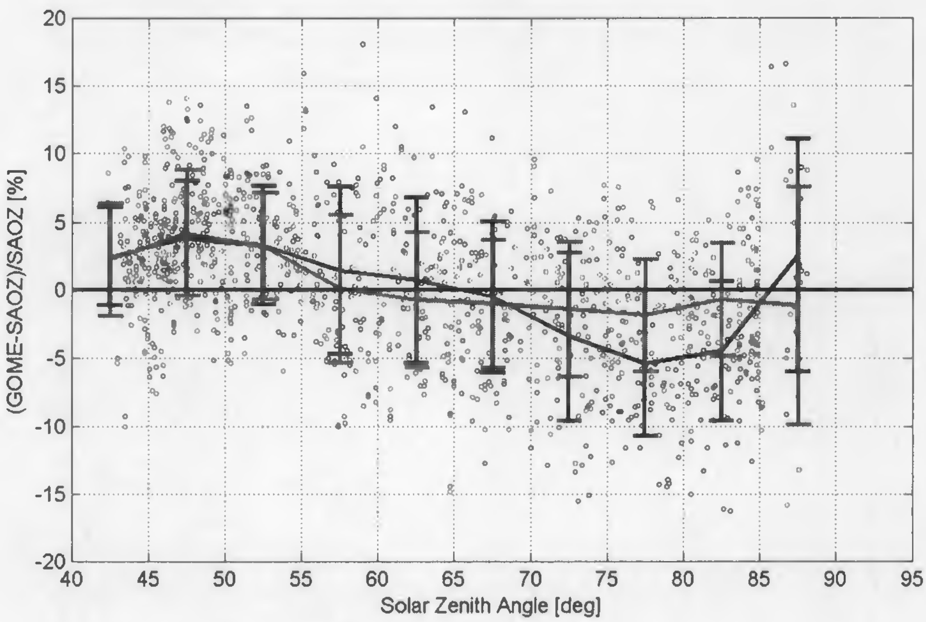

Figure 28 ***Relative difference between GOME and SAOZ total ozone at Sodankylä for GDP 2.7 (black) and 3.0 (grey), as a function of the GOME SZA, using delta validation orbits from 1996 through 2001. Dots are the individual differences, lines are the 5° SZA class average, and vertical bars the standard deviation within the SZA class. GDP 3.0 is closer to SAOZ than version 2.7. In the upper graphic all GDP overpasses have been used for statistics. In the lower graphic, only identical GOME pixels have been compared to ground-based data.***

Figure 29 displays the SZA dependence of the GDP-NDSC agreement at Sodankylä during polar summer (one month around summer solstice). Mid-morning and midnight sun pixels can be distinguished as low and high SZA data, respectively. The figure shows that Brewer and SAOZ data are in better agreement with GDP 3.0 mainly at high SZA.

Figures 30 and 31 compare the GDP-NDSC relative difference for both GDP 2.7 and GDP 3.0, as a function of SZA, season and latitude, respectively in the Northern and Southern hemispheres. A major observation is the general discontinuity between mean relative difference in different latitude zones, mostly the behaviour at middle and high latitudes during the southern summer. Another point is the clear improvement in northern summer (Figure 30). However, for instance northern fall has opposite trends depending on SZA if we consider polar circle and high latitude values, such that the mean value of those two curves should be almost constant with no discrepancy. These figures show that some improvements have been made but also that some problems persist.

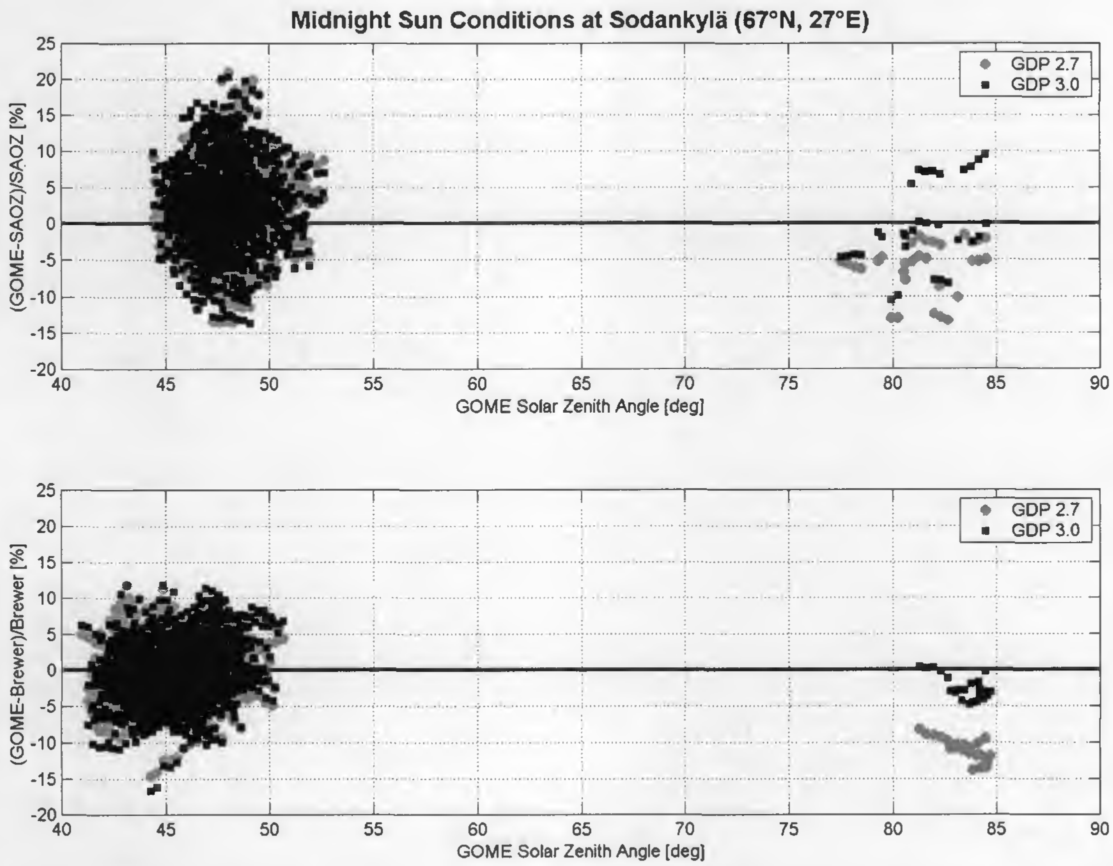

Figure 29 ***Relative difference in total ozone between GDP and Brewer data at Sodankylä during polar summer. Pixels are taken from 1996 to 2001, from the 21th of May to the 21th of July.***

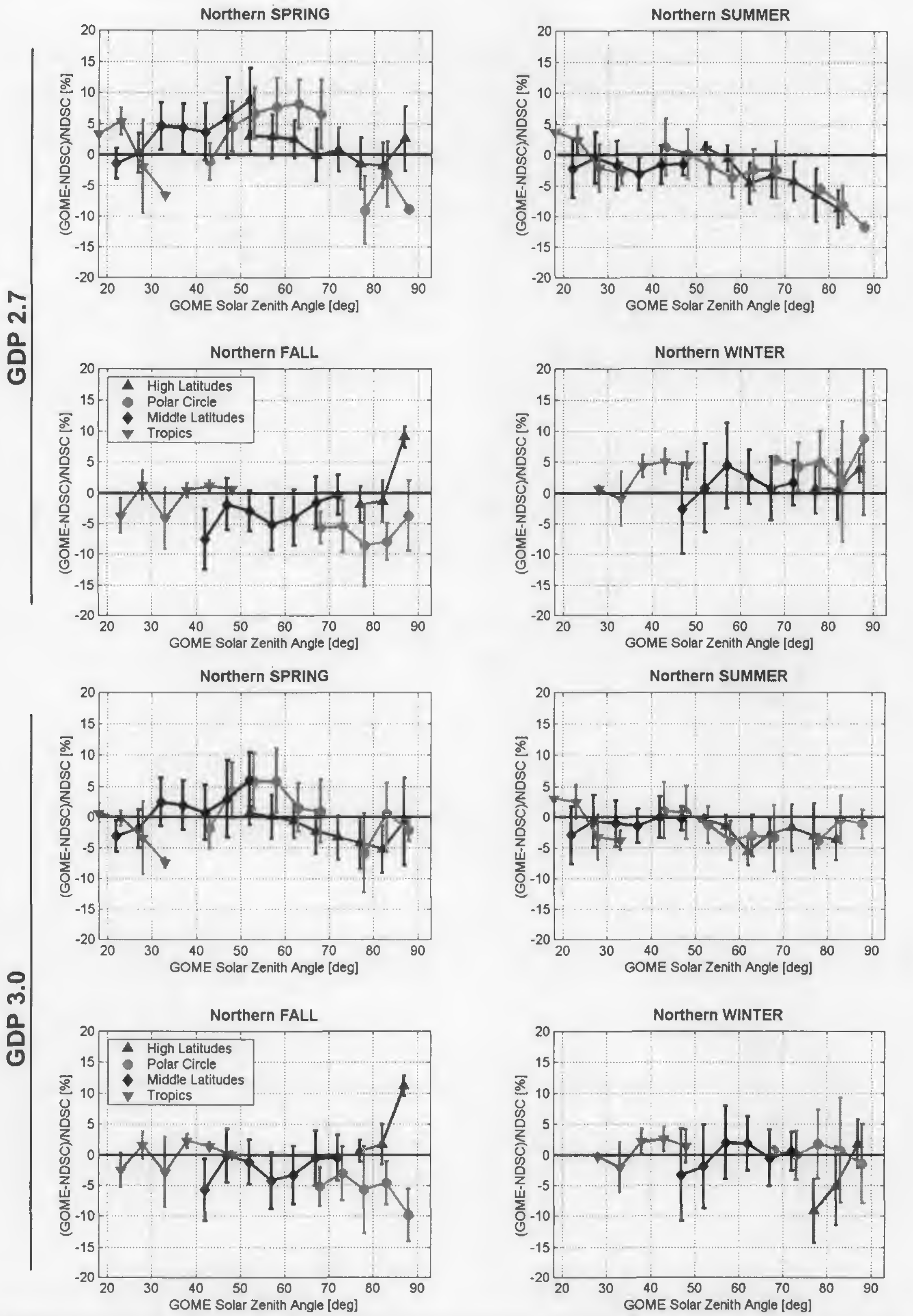

Figure 30 *Solar zenith angle dependence of the mean relative difference between total ozone retrieved with GDP 2.7 (upper) and GDP 3.0 (lower) and NDSC measurements in the Northern Hemisphere, and its seasonal variation. Symbols identify the latitude range. Vertical bars indicate one sigma standard deviation within 5 degree SZA class and latitude zone. Validation orbits of year1996 only were used for the comparison.*

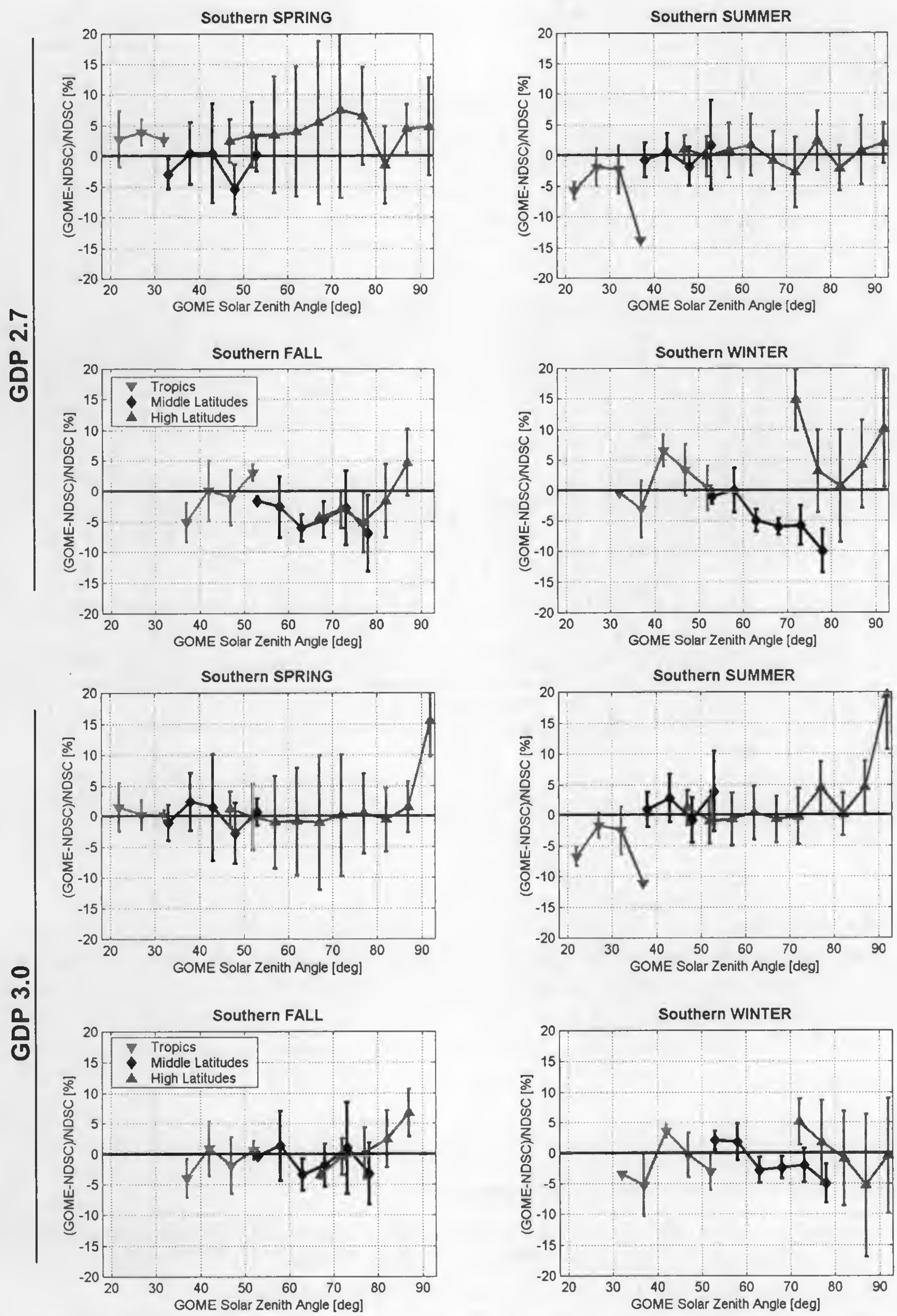

Figure 31 *Same as Figure 30 but for the Southern Hemisphere.*

IV.1.6.3.1 Ozone Column Dependence

Another important characteristic of the difference between GOME and ground-based total ozone is its column dependence. This effect is remarkable during springtime Antarctic ozone depletion, when the ozone column range is the widest. Figure 32 shows the column dependence of both version of GDP total ozone compared to ground-based Dobson data at the Antarctic station of Halley, under such ozone hole conditions. It appears that the systematic overestimation of ozone column values below 200 DU is significantly reduced with GDP 3.0, although persisting: about 5-10% of overestimation instead of 20-25%. The scatter is reduced as well. Similar results are observed at all ozone 'hole' stations.

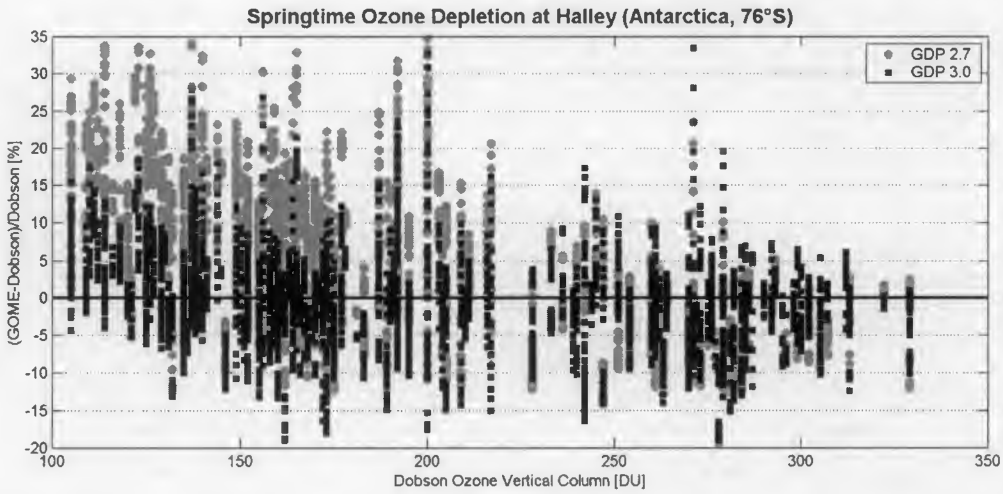

Figure 32 ***Column dependence of the GOME/Dobson total ozone difference at Halley (76°S) during the Antarctic ozone hole. The improvement with GDP 3.0 (black squares) appears clearly, compared to results with GDP 2.7 (grey circles). Data cover years from 1996 to 2001, from the 21st of August till the 21st of October.***

IV.1.6.4 Conclusion

Correlative studies between GDP 2.7 and 3.0 total ozone, slant column, air mass factor, cloud fraction, and ghost vertical column, confirm the consistency of the study and the conclusions drawn in previous sections. Most of cyclic signatures have decreased by about 30-50%. GDP 3.0 ozone hole observations are in better agreement with correlative NDSC data and dependences on the SZA and the vertical column reduce globally, although persisting.

IV.1.7 General Conclusion and Recommendations

Cross-correlation studies of GDP level-2 ozone data and comparisons with NDSC correlative measurements indicate that the present GDP upgrade from version 2.7 to 3.0 conducts globally to a better agreement of GOME with ground-based total ozone data. The improvement is mainly driven by air mass factor changes. Fitted cross-sections temperatures, much higher than the fixed temperatures used in GDP 2.7, affect slant column values with a slope complying with the theory (3% of SCD increase for a 10 K increase of temperature).

However, a negative offset hampers the expected SCD increase. The impact of the new effective temperature is difficult to estimate due to differences in temperature definition. New ghost vertical columns improve vertical columns during Antarctic springtime ozone depletion.

Ground-based comparisons show that seasonal and meridian dependences of the GOME-NDSC agreement reduce almost everywhere by about 30-50%. The well known total column and SZA dependences also reduce with the new GDP version. Globally, GDP improvements are more important and constant in the Southern than in the Northern Hemisphere.

Although significant improvements are observed, major issues remain. A list of DOAS–related errors affecting GDP 3.0 ozone retrievals are described in Chapter 6 of the present report. Another important issue relates to the way atmospheric databases are used for AMF and ghost vertical column calculation. The implementation of more adequate databases in GDP 3.0 is the first step in the good direction. Nevertheless, accurate ozone AMFs in the strong UV band of Huggins require knowledge on both the ozone profile shape and the total ozone amount. Better results gained by EP-TOMS in terms of seasonal and SZA dependence (Lambert *et al.*, 2000) are likely related to the fact that TOMS V7 algorithm retrieves both the profile shape and the ozone column range from the TOMS radiometric measurements in a first run before calculating its best total ozone estimate in a second run. Compared to GDP 2.7 where the ozone profile shape and total column are allowed to vary only with the season, GDP 3.0 is certainly an improvement since its neural network selects the AMF according to an ozone column estimate derived from the measurement. Further improvement of the GDP AMF module would consist in retrieving a profile shape estimate from the GOME spectra as well.

Acknowledgements

Contributing NDSC PIs and ground-based instrument operators (AWI, BAS, CAO, CNRS, DMI, DWD, ETH, FMI, IASB, IFE, KMI, KNMI, KTSU, NILU, SMI, U. Bordeaux, U. Reims, U. Réunion, U. Sao Paulo, U. Wales), DLR-IMF, science and Operation Teams are warmly thanked for data provision. Specials thanks to W. Thomas (DLR-IMF) and P. Valks (KNMI) for fruitful discussions. GOME level-2 data products were processed at DLR-IMF on behalf of ESA. The reported work has been supported by the ESRIN Contract No. 13554/99/I-DC/CCN-2 and by the Belgian Prime Minister Services – Scientific, Technical and Cultural Affairs through the PRODEX ERS-2 GOME Valorisation project.

References

Arlander, D.W., K.K. Tørnkvist, and G.O. Braathen, 1998: Ground-based UV-Vis Validation Measurements of Stratospheric Molecules above Spitsbergen, in *Proc. 24th Annual European Meeting on Atmospheric Studies by Optical Methods, Andenes 1997*, ISBN 82-994583-0-7, pp. 185-188.

Bass, A.M., and R. J. Paur, 1985 : The ultraviolet cross-sections of ozone: I. The measurements in Atmospheric ozone (Ed. C.S. Zerefos and A. Ghazi), Reidel, Dordrecht, Boston, Lancaster, pp. 606-610.

Bruhl, 1994: unpublished database.

Burrows, J.P., M. Weber, M. Buchwitz, V. Rozanov, A. Ladstaetter-Weissenmayer, A. Richter, and M. Eisinger, 1999: The Global Ozone Monitoring Experiment (GOME): Mission Concept and First Scientific Results, *J. Atm .Sci.*, **56**, 151-175.

Dahlback, A., and K. Stamnes, 1991: A new spherical model for computing the radiation field available for photolysis and heating at twilight, *Planet. Space Sci.*, **39**, pp. 671-683.

Delbouille, L., and G. Roland, 1995: High-resolution solar and atmospheric spectroscopy from the Jungfraujoch high-altitude station, *Optical Eng.*, **34**, pp. 2736-2739.

Denis, L., J. P. Pommereau, F. Goutail, T. Portafaix, P.V. Johnston, A. Matthews, and T.C. Clarkson, 1997: SAOZ total ozone and NO_2 at the southern tropics and equator, in *Atmospheric Ozone - Proc. 18th Quad. Ozone Symp., L'Aquila, Italy, 1996*, Ed. R.D. Bojkov and G. Visconti, Vol. I, pp. 29-32.

DLR, 2002, GOME Data Bases (Level 1 to 2 Processing), ER-TN-IFE-GO-0018, Iss./Rev. 3/A.

DLR, 2002, GOME Level 0 to 1 Algorithms Description, Technical Note, ER–TN–DLR–GO–0022, Iss./Rev. 5/B.

DLR, 2002, GOME Level 1 to 2 Algorithms Description, Technical Note, ER–TN–DLR–GO–0025, Iss./Rev. 3/A.

DLR, Product Specification Document of the GDP, ER-PS-DLR-GO-0016, Iss./Rev. 4/A, April 2002.

ESA, 1999: ERS-2 GOME Data Products Delta Characterisation Report 1999 / Validation Report for GOME Data Processor Upgrade: Level-0-to-1 Version 2.0 and Level-1-to-2 Version 2.7, J.-C. Lambert and P. Skarlas (Eds.), Issue 1, 103p.

Fayt, C., and M. Van Roozendael, 2001: WinDOAS 2.1 Software User Manual, available on http://www.oma.be/GOMEBrO/WinDOAS-SUM-210b.pdf, 91 pp.

Fortuin, J. P. F, and H. Kelder, 1998: An ozone climatology based on ozonesonde and satellite measurements, Journal of Geophysical Research, Vol. 103, p. 31,709-31,731

Hansen, G., A. Dahlback, F. Tønnessen, and T. Svenøe, 1999: Validation of GOME total ozone by means of the Norwegian ozone monitoring network, *Annales Geophysicae*, 17, pp. 430-436.

Koike, M., Y. Kondo, W.A. Matthews, P.V. Johnston, H. Nakajima, A. Kawaguchi, H. Nakane, I. Murata, A. Budiyono, M. Kanada, and N. Toriyama, 1999: Assessment of the uncertainties in the NO_2 and O_3 measurements by visible spectrometers, *J. Atm. Chem.*, **32**, pp. 121-145.

Kylling, A., 1995: UVSPEC: a program package for calculation of diffuse and direct UV and visible intensities and fluxes, available by anonymous ftp to kaja.gi.alaska.edu, cd pub/arve

Lambert, J.-C., and P.C. Simon, 1998: Geophysical Comparison of the GOME Data Processors GDP 2.0 and 2.3 by Means of Ground-based Networks, in *GOME Data Improvement Validation Report*, B. Greco (Eds.) - ESA/ESRIN APP/AEF/17/GB, 34-42.

Lambert, J.-C., M. Van Roozendael, M. De Mazière, P.C. Simon, J.-P. Pommereau, F. Goutail, A. Sarkissian, and J.F. Gleason, 1999a: Investigation of pole-to-pole performances of spaceborne atmospheric chemistry sensors with the NDSC, *J. Atmos. Sci.*, **56**, pp. 176-193.

Lambert, J.-C., M. Van Roozendael, P.C. Simon, J.-P. Pommereau, F. Goutail, J.F. Gleason, S.B. Andersen, D.W. Arlander, N.A. Bui Van, H. Claude, J. de La Noë, M. De Mazière, V. Dorokhov, P. Eriksen, A. Green, K. Karlsen Tørnkvist, B.A. Kåstad Høiskar, E. Kyrö, J. Leveau, M.-F. Merienne, G. Milinevsky, H.K. Roscoe, A. Sarkissian, J.D. Shanklin, J. Staehelin, C. Wahlstrøm Tellefsen, and G. Vaughan, 1999b: Combined characterisation of GOME and TOMS total ozone measurements from space using ground-based observations from the NDSC, *Advances in Space Research*, Vol. 26, pp. 1931-1940.

Lambert, J.-C., M. Van Roozendael, J. Granville, P. Gerard, P.C. Simon, J.-P. Pommereau, F. Goutail, and A. Sarkissian, 1999c: Geophysical validation of ERS-2 GOME ozone products by means of correlative observations from the NDSC, in *Proc. European Symposium on Atmospheric Measurements from Space (ESAMS), ESA/ESTEC, The Netherlands, 18-21 January 1999,* ESA WPP-161, Vol. 2, 595-601.

Lambert, J.-C., M. Van Roozendael, P.C. Simon, J.-P. Pommereau, F. Goutail, J.F. Gleason, S.B. Andersen, D.W. Arlander, N.A. Bui Van, H. Claude, J. de La Noë, M. De Mazière, V. Dorokhov, P. Eriksen, A. Green, K. Karlsen Tørnkvist, B. A. Kåstad Høiskar, E. Kyrö, J. Leveau, M.-F. Merienne, G. Milinevsky, H.K. Roscoe, A. Sarkissian, J.D. Shanklin, J. Staehelin, C. Wahlstrøm Tellefsen, and G. Vaughan, 2000: Combined characterisation of GOME and TOMS total ozone measurements from space using ground-based observations from the NDSC, Advances in Space Research, **26**, 1931-1940.

Lambert, J.-C., M. Van Roozendael, M. De Mazière, 2001: Development, Validation and Exploitation of ERS-2 GOME Satellite Data: Overview and Perspectives for ENVISAT, in *Space Scientific Research in Belgium,* Vol. III Part 3, Ed. by OSTC , 47-66.

Loyola D., 1999: Using Artificial Neural Networks for the Calculation of Air Mass Factors, ESAMS'99 - European Symposium on Atmospheric Measurements from Space.

Loyola D., 2000: Combining Artificial Neural Networks for Parameterization of Radiative Transfer Models, IEEE International Geoscience and Remote Sensing Symposium, IGARSS'2000.

Paur, R., and A. Bass, 1984: The ultraviolett cross sections of ozone: II. Results and temperature dependence. In *Proc. Quadrennial Ozone Symposium* (Halkidiki, Greece, 1984), pp. 611-616.

Pommereau, J.-P., and F. Goutail, 1988: Ground-based Measurements by Visible Spectrometry during Arctic Winter and Spring 1988, *Geophys. Res. Lett.*, **15**, pp. 891-894.

Richter, A., M. Eisinger, F. Wittrock, S. Schlieter, A. Ladstätter-Weißenmayer, and J. P. Burrows, 1998: Zenith sky and GOME DOAS measurements of atmospheric trace gases above Bremen, 53°N: 1994 - 1997, in *Polar Stratospheric Ozone - Proc. 4th European Workshop, Schliersee 1997*, N.R.P. Harris, I. Kilbane-Dawe, and G.T. Amanatidis (Eds.), Air Pollution Research Report 66 (CEC DG XII), pp. 482- 485.

Roscoe, H.K., P.V. Johnston, M. Van Roozendael, A. Richter, A. Sarkissian, J. Roscoe, K.E. Preston, J.-C. Lambert, C. Hermans, W. De Cuyper, S. Dzienus, T. Winterrath, J. Burrows, F. Goutail, J.-P. Pommereau, E. D'Almeida, J. Hottier, C. Coureul, D. Ramon, I. Pundt, L.M. Bartlett, C.T. McElroy, J.E. Kerr, A. Elokhov, G. Giovanelli, F. Ravegnani, M. Premuda, I. Kostadinov, F. Erle, T. Wagner, K. Pfeilsticker, M. Kenntner, L.C. Marquard, M. Gil, O. Puentedura, M. Yela, W. Arlander, B.A. Kåstad Høiskar, C.W. Tellefsen, K. Karlsen Tørnkvist, B. Heese, R.L. Jones, S.R. Aliwell, and R.A. Freshwater, 1999: Slant column measurements of O_3 and NO_2 during the NDSC intercomparison of zenith-sky UV-visible spectrometers in June 1996, *J. Atmos. Chem.*, **32**, pp. 281-314.

Tomas, W., and M. Van Roozendael, 2002: Private Communication.

Trenberth, K.E., Global analyses from ECMWF and Atlas of 1000 to 10 mb Circulation Statistics. Tech. Rep. NCAR/TN-373+STR, National Center for Atmospheric Research, Boulder, Colorado, 1992.

Van Roozendael, M., C. Hermans, Y. Kabbadj, J.-C. Lambert, A.-C. Vandaele, *et al.*, 1995: Ground-Based Measurements of Stratospheric OClO, NO_2 and O_3 at Harestua, Norway (60°N, 10°E) during SESAME, in *Proc. 12th ESA Symp. on European Rocket and Balloon Programmes & Related Research, Lillehamer 1995*, ESA SP-370, pp. 305-310.

Vaughan, G., H.K. Roscoe, L.M. Bartlett, F. O'Connor, A. Sarkissian, M. Van Roozendael, J.-C. Lambert, P.C. Simon, K. Karlsen, B.A. Kåstad Høiskar, D.J. Fish, R.L. Jones, R.A. Freshwater, J.-P. Pommereau, F. Goutail, S.B. Andersen, D.G. Drew, P.A. Hughes, D. Moore, J. Mellqvist, E.

Hegels, T. Klupfel, F. Erle, K. Pfeilsticker, and U. Platt, 1997 : An intercomparison of ground-based UV-Visible sensors of ozone and NO_2, *J. Geophys. Res.*, **102**, pp. 1411-1422.

Wellemeyer, C.G., S.L. Taylor, C.J. Seftor, R.D. McPeters, and P.K. Barthia, 1997 : A correction for total ozone mapping spectrometer profile shape errors at high latitude, *J. Geophys. Res.*,**102**, 9029-9038.

IV.2 RESULTS FROM NILU

By Georg H. Hansen

Contact: *G. H. Hansen*
Norwegian Institute for Air Research (NILU)
Polar Environment Centre
Tromsö, Norway
E-mail: georg.hansen at nilu.no

Delta characterisation and long-term geophysical validation of GOME total ozone

Georg H. Hansen

Norwegian Institute for Air Research (NILU), The Polar Environmental Centre
Tromsø, Norway

Abstract: Data records from the Norwegian ozone monitoring network have been used to validate at northern high latitudes the upgrade of GOME total ozone data product version 2.7 to 3.0, and perform long term validation of GOME total ozone.

IV.2.1 Introduction

In 2001, the off-line GOME Data Processor (GDP) at DLR was upgraded to its new version 3.0. Various parameters were modified compared to the previous version in the hope that problems with data at certain conditions, especially at large solar zenith angles, and the considerable seasonal variability of the deviations to ground-based measurements would be reduced.

The data obtained with the new algorithm version GDP 3.0 were validated in a comprehensive exercise in early 2002 (see this issue), with a contribution of NILU focussing on total ozone at high latitudes. The selected data set from GOME covers almost the complete life time of the instrument, namely January 1996 to October 2001.

IV.2.2 The ground-based data set

The tasks performed by NILU concentrated on total ozone data products. The ground-based data used are from three Norwegian stations, and three instrument types. These are listed in Table 1. The Norwegian stations cover a latitude range of 20 degrees, but due to the northern location only one of them (Oslo) can be used in the months November – January. In order to be able to make a statement on the SZA dependence of the GOME vs. ground-based data discrepancy also during these months, data from two other European stations (Arosa, Switzerland; Observatoire de Haute Provence, France) stored at the GOME validation database were included in the analysis.

Table 4 *List of contributing stations*

Station name	Geographical coordinates	Instruments
Ny-Ålesund	78.91°N, 11.88°E	Dobson, GUV
Tromsø (until 1999)	69.66°N, 18.97°E	Dobson, Brewer, GUV
Andøya (since 03/2000)	69.30°N, 16.02°E	Brewer, GUV
Oslo	59.91°N, 10.72°E	Dobson, Brewer, GUV
Arosa (until 02/99)	46.46°N, 9.40°E	Brewer
Observatoire de Haute Provence	43.55°N, 5.45°E	Dobson

The techniques used at the ground-based sites are mostly well-established. Measurements with the Dobson spectrometer in the AD direct-sun mode are a standard mode recognised by the WMO. Only such data are included here. The main disadvantage of the Dobson instrument is that it has to be run manually, i.e. the necessary manpower per measurement is considerable. Since the early 1990, the Brewer instrument has been set up at many Dobson stations, increasing the number of measurements considerably, since this instrument operates automatically. However, in its standard operation set-up, the Brewer has a similar problem as the Dobson: it has to be operated in different modes depending on weather conditions. Under clear-sky (or visible-sun) conditions, it is run in the direct-sun mode, while under overcast conditions, the zenith-sky mode is used. With respect to total ozone, there is a bias between the two modes, which only can be removed empirically (e.g., Svenøe, 2000).

Recently, a new method was developed at the University of Oslo to derive total ozone directly from the global irradiance measured with the instrument irrespective cloud conditions (Dahlback et al., 2002). The method has yielded a homogeneous ozone data series under almost all weather conditions and at solar zenith angles of up to 85°. All Brewer data from Oslo have been re-processed to derive ozone by this method, and an excellent agreement with direct-sun data was found in cases of simultaneous measurements (Dahlback, personal communication). Figure 1 shows a sequence of three days of Brewer and GUV data from Oslo, indicating a high data stability at solar zenith angles < 85°. The Brewer measurements in Tromsø (1994-1999) did not comprise the global irradiance mode, so that these measurements can not be re-evaluated. After the move of the instrument to Andøya in spring 2000, this mode was installed, but data are only available from the second half of 2001, and therefore not included in this project.

The GUV instrument is a 5-channel filter instrument with moderate bandwidth, developed primarily to monitor biologically effective UV radiation, from total ozone is derived in a similar way as for the Brewer global irradiance mode (Dahlback,1996). The instruments are placed at 8 locations in Norway, but only at three of them, parallel ozone measurements with other instruments, which allow regular comparisons, are performed. The instrument has been used in GOME validation projects before and shown to be well suited for such purposes (Hansen et al., 1999).

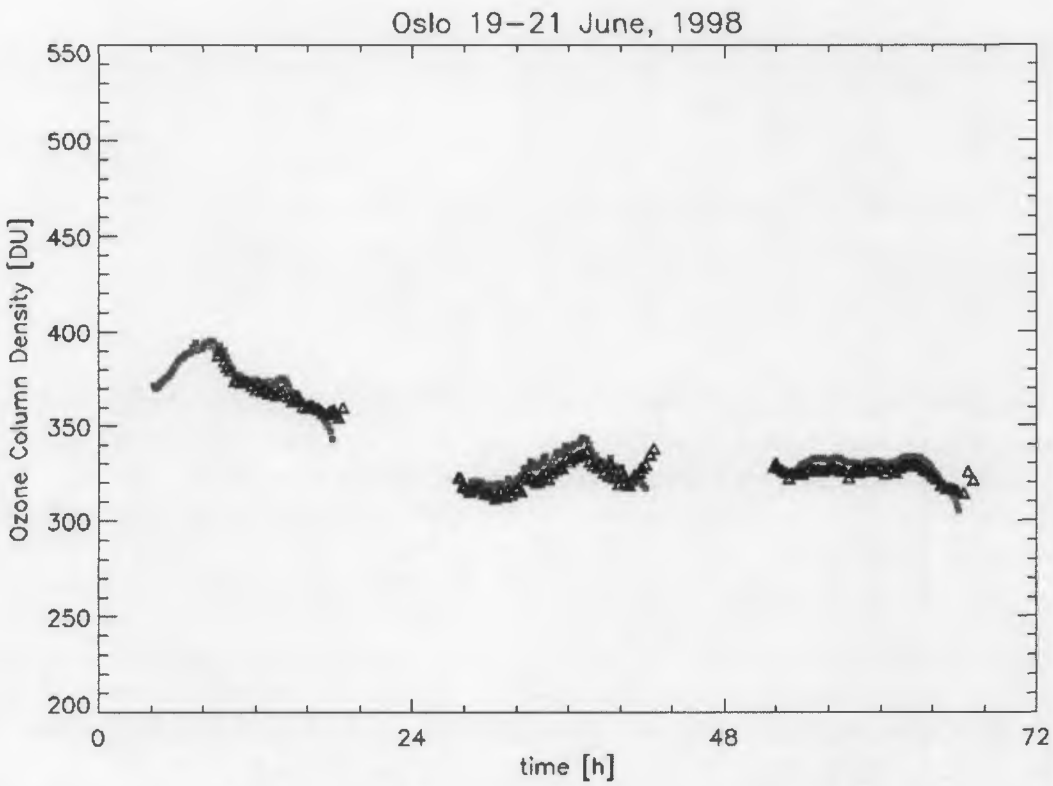

Figure 33 *Ground-based total ozone measurements taken with the Oslo Brewer instrument on June 19-21, 1998, in the global irradiance mode (blue triangles). For comparison, GUV data at the same site are shown (red squares).*

While a significant part of the Dobson measurements only contain one value per day, most of the GUV measurements have one measurement every 10 minutes. Figure 2 shows the comparison for May 1997, where the different instruments are marked with different colours: Green symbols denote comparison of GOME pixel values with Dobson measurements, blue marks denote comparison with Brewer, and red symbols comparison with GUV measurements. In this example, the Brewer and Dobson data with zenith angles of between 30 and 42° stem from the southern European stations Arosa and Haute Provençe. There is mostly a good agreement between the deviations of GOME and the various ground-based data sets (the variability bars overlap), i.e., the ground-based data are very consistent; this is found for a large majority of data sets. However, there are also several cases with systematic differences. These are mainly November and December data, when the deviations between GOME and the GUV in Oslo data are more positive (up to 10%) than the deviations between GOME and Brewer. This is very probably due to a negative bias in the GUV data at solar zenith angles > 80° under cloud-free conditions, which is not seen in the global irradiance Brewer data. There are also some examples of significant differences between (Arosa) Brewer and (Haute Provençe) Dobson data at small solar zenith angles, the source of which not known. There are, however, several publications on such inconsistencies between these two methods (e.g., Kerr et al., 1988; Staehelin et al., 1998), the reasons for which are under discussion.

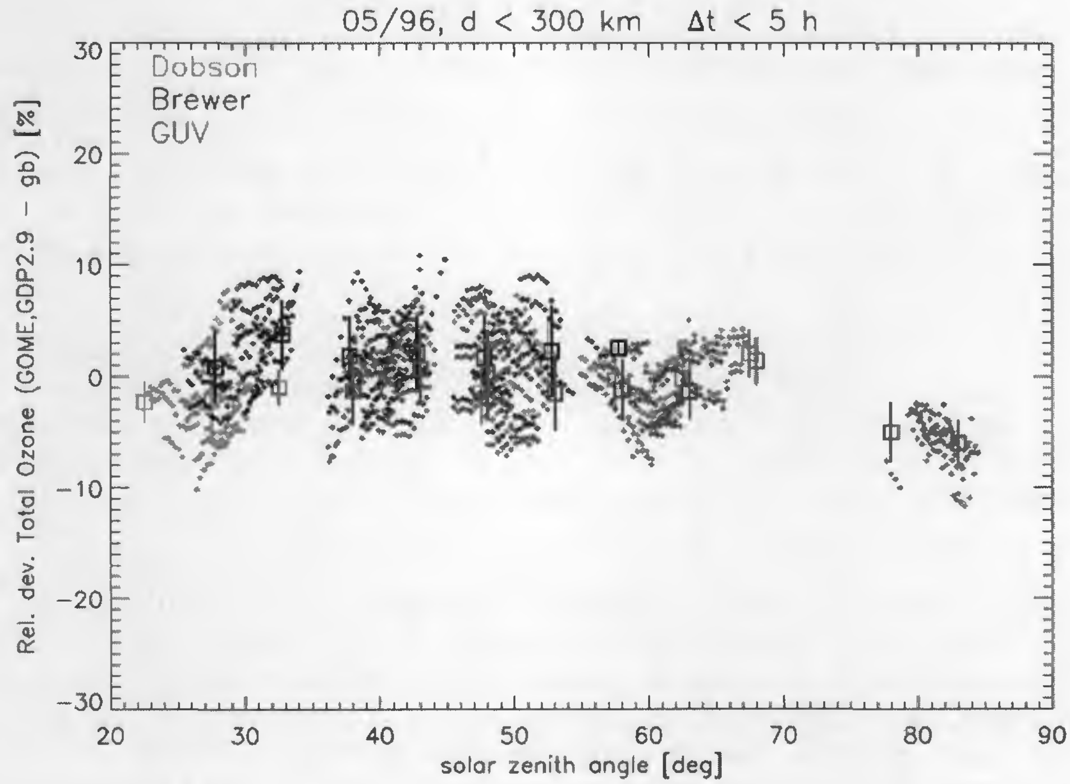

Figure 34 ***Relative deviations [%] between GOME total ozone and total ozone in May 1996, monitored with various ground-based instruments: Brewer (blue), Dobson (green), GUV (red). Only pixels closer than 300 km to the ground-based site and ground-based data recorded less than 5 hours from the satellite overpass are allowed. Squares with "error bars": monthly averages of deviations and standard deviation of the individual deviations for 5-degree solar zenith angle intervals.***

For this project, the following ground-based data records were used:

Station	Instrument	Time period
Ny-Ålesund	Dobson	4/96 – 9/99
Ny-Ålesund	Brewer	1/96 – 12/99
Ny-Ålesund	GUV	1/96 – 10/01
Tromsø	Dobson	5/96 – 4/97
Tromsø	Brewer	1/96 – 10/99
Tromsø	GUV	1/96 – 10/02
Andøya	Brewer	3/00 – 10/01

Andøya	GUV	3/00 – 10/01
Oslo	Dobson	6/96 – 4/97
Oslo	Brewer	1/96 – 12/99
Oslo	GUV	1/96 – 10/01
Arosa	Brewer	1/96 – 2/99
Haute Provence	Dobson	1/96 – 10/01

IV.2.3 Validation results

Despite the large set of data (400 orbits) used for the almost 6 year long validation period, it is only a small part of the total set of more than 30 000 orbits passed by ERS-2 since beginning of 1996. It is assumed that most of the orbits were selected to match the concentration of validation stations in the European sector, and in fact many coincidences with the ground-based stations during the main overpass of the satellite at noon are found. Unfortunately, this is not the case for the evening overpasses in the summer months at high latitudes which gave the unique opportunity to quality-assess GOME data measured at high solar zenith angles, while the ground-based data taken under these conditions could be quality-assessed against (more reliable) low-SZA measurements before and after these measurements.

In Figure 3, the average differences between GOME and ground-based measurements for the months of February, April, June, August, September and December are shown, including all data available from 1996 to 2001, separated according to ground-based instrument technique. The maximum allowed distance between the pixel centre and the ground-based site was set to 300 km, while the ground-based data were averaged over ±5 h relative to the GOME overpass time. The different months are colour-coded (see Figure caption), while the different years are marked with different symbols (see figure caption). The by far most comprehensive data set is that with the GUV ground-based data, covering 3 stations over 6 years, respectively, which is shown in the uppermost panel of Figure 3. In particular, this data set covers a considerable amount of data at large solar zenith angles. The large majority of monthly average deviations is between +2% and -5% with an increasing spreading towards larger zenith angles. It should be noted that most of the outliers, including those at the largest zenith angles, are based on small numbers of single comparisons included in the monthly average. Thus it cannot be excluded that the pattern would look quite different with a more comprehensive GOME data set at large solar zenith angles as used in previous validations efforts (e.g., Hansen et al. 1999). What seems to be a significant pattern, is the deviation "minimum" (most negative deviation) at 60-65° SZA of –3±2% and the change towards positive deviations with increasing SZA (+2±4% in the 75-80° SZA range).

This pattern is also seen in the much less comprehensive data set with Dobson measurements as ground-based reference, which is shown in the lowermost panel of Figure 3. Also in this case most outliers, e.g. those from April 2000 (dark blue triangles), originate from a small number of single pixel comparisons.

The Brewer data set, shown in the centre panel of Figure 3, at first glance reveals a significantly smaller scattering of the deviations than the Dobson and GUV data set at most solar zenith angles. However, as in the case of the GUV data set, the scattering of the deviations increases with increasing SZA, up to the SZA range 60-65°. At higher SZA values, the scattering is again very small, but also the number of months represented at these SZA values is reduced; the data are limited to February, October and December, while in the spring and summer months there are no Brewer data available that fulfil the selection criteria (mainly because of missing Brewer at Ny-Ålesund). In fact, when choosing the other six months of the year (January, March, May, July, September, November; not shown here), the scattering of the Brewer deviations at large SZA values approaches much more the GUV pattern.

Figure 4 shows the direct comparison of the deviations using the Brewer and the GUV data, of all data from the years 1996-1999. The months are colour-coded as in Figure 3. The lines show the same data as the symbols, but 3-point smoothed. It confirms the high stability of deviations of GOME from Brewer data (solid lines) where and when these are available, but cannot give information on the deviations at large SZA throughout all months. Most monthly average deviations are within ±3%. The deviations derived from GUV data show a slight negative offset of 1 to 2% compared to those derived from the Brewer data at solar zenith angles < 60°. At larger zenith angles the relation is less homogeneous, but in most cases, especially the winter months, the GUV-derived deviations are clearly more positive. The reason for this was indicated in the previous section (cosine response/SZA dependence of GUV data).

Finally, the difference between the GOME data with the new wavelength calibration algorithm based on cross-correlation (XCORR) and the set without this calibration (NO_XCORR) was investigated on the basis of the complete data set. As an example, the results for the year 1997 (February-April-June-August-October-December), using Brewer ground-based data are shown in Figure 5. These confirm the preliminary conclusions drawn from the much more limited data set in early 2002. The calibration leads only to a minor change of the GOME values, with less than 0.5% difference in the early months of the year and differences slightly larger than 1% in the second half of the year. A very similar result is found using other data sub-sets, e.g. GUV data in 1999.

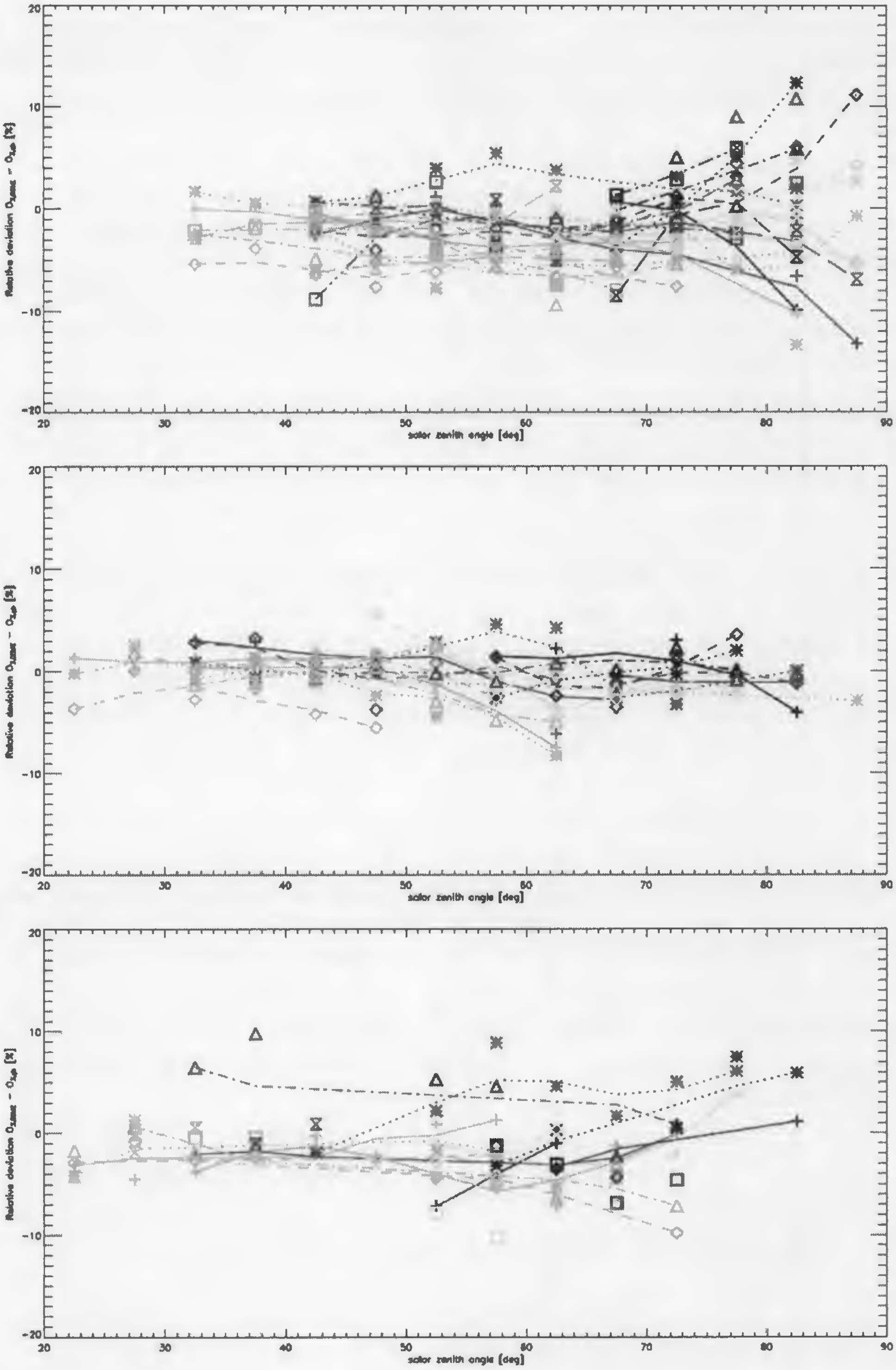

Figure 35 ***Monthly mean deviation between GOME and ground-based data from 1996 through 2001: GUV (upper panel), Brewer (centre panel), Dobson (lower panel) for February (violet), April (blue), June (turquoise), August (green), October (yellow-green) and December (red). Years are distinguished by symbol and line styles. 1996: crosses/solid line, 1997: asterisks/dotted, 1998: diamonds/dashed, 1999: triangles/dash-dotted, 2000: squares/dash-double-dotted, 2001:dashed-triple-dotted. Lines denote 3-point-smothed version of points.***

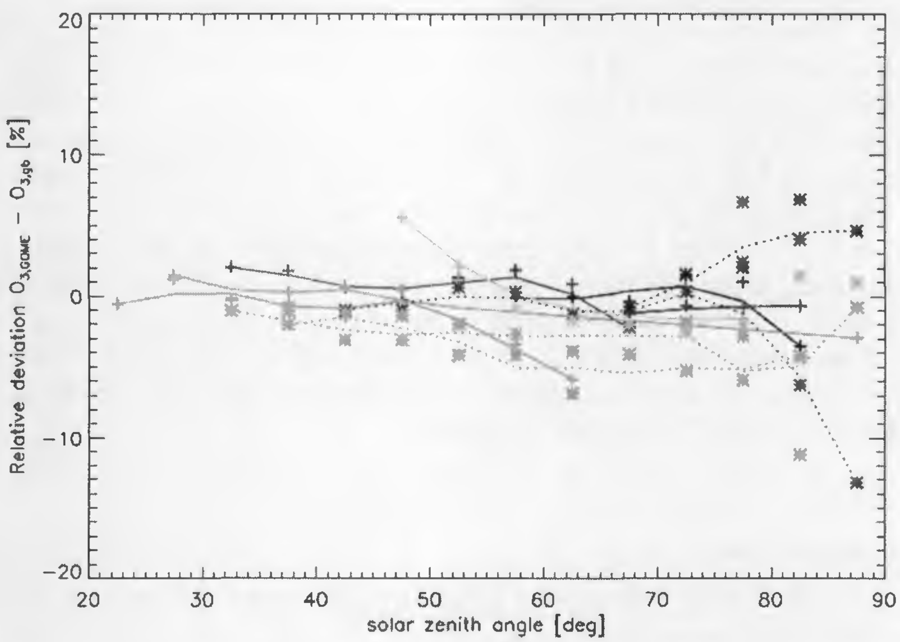

Figure 36 *Monthly mean deviations between GOME and Brewer data (solid lines/crosses), and GOME and GUV data (dotted lines/Asterisks), respectively, for the months of February, April, June, August, October and December, using all data from 1996 - 1999. Colour-coding as in Figure 3.*

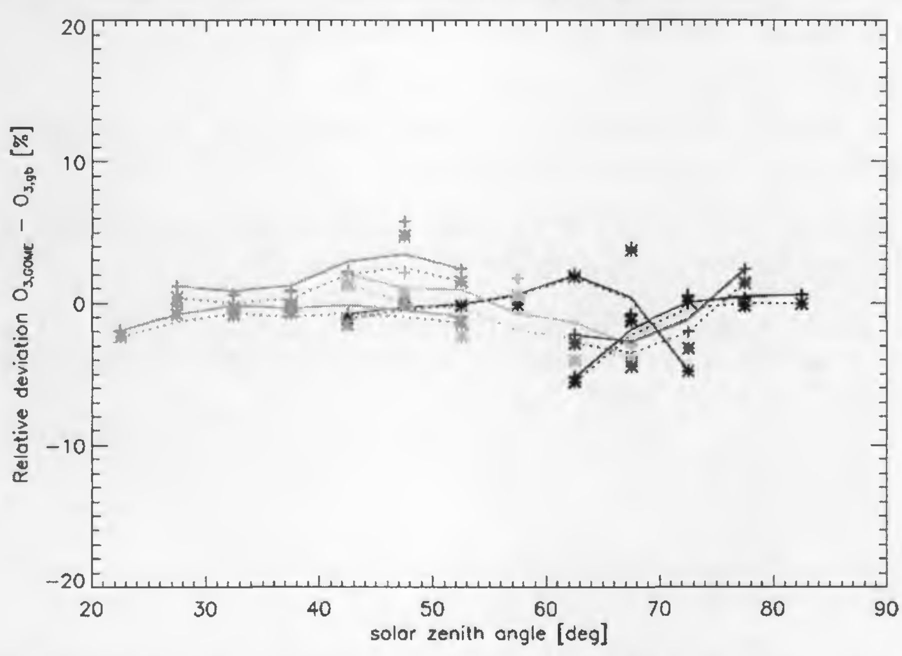

Figure 37 ***Monthly mean deviations between GOME and Brewer data in the XCORR mode (solid lines/ crosses) and in the NO_XCORR mode (dotted lines/asterisks). The months January, March, May, July, September and November in 1997 are used and colour-coded as the months February, ..., December in Figure 3.***

IV.2.4 Summary

A large set of GOME total ozone data calculated with the new GDP 3.0 algorithm version, covering almost the complete lifetime of GOME, has been compared with total ozone measured at several stations of the Norwegian ozone monitoring station (plus two central European stations) with different methods. The deviations between GOME and ground-based data still show a solar zenith angle dependence, especially at angles > 60°, which varies with the month of the year. From the most reliable ground-based data set, the Brewer measurements, the deviations are typically between +2 and –2% at solar zenith angles < 50°, while they reach –5 to +5% at 80°, depending on the season. Using the GUV data set (which has a significantly better statistics at large solar zenith angels), a spread of –8 to +7% is reached at 80° SZA. The increased spread can partially be due to a solar zenith angle dependence of the ground-based data themselves.

IV.2.5 Acknowledgments

Parts of this work have been funded by ESRIN (Contract 13554/99/I-DC/CCN-2), by the Norwegian Space Agency, and by PRODEX

IV.2.6 References

Dahlback, A., Measurements of biologically effective UV doses, total ozone abundances, and cloud effects with multichannel, moderate bandwidth filter instruments, *Appl. Optics*, 35, 33, 6514-6521, 1996.

Hansen, G., A. Dahlback, F. Tønnessen, and T. Svenøe, Validation of GOME total ozone by means of the Norwegian ozone monitoring network, *Ann. Geophys.*, 17, 430-436, 1999.

Kerr, J. B., Asbridge, I. A., and Evans, W.F.J., Intercomparison of total ozone measured by the Brewer and Dobson Spectrophotometers at Toronto, *J. Geophys. Res., 93,* 11,129-11,140, 1988.

Staehelin, J., Renaud, A., Bader, J., McPeters, R., Viatte, P., Högger, B., Bugnion, V., Giroud M., and Schill, H., Total ozone series of Arosa (Switzerland). Homogenization and data comparison, *J. Geophys. Res., 103,* 5827-5841, 1998.

IV.3 RESULTS FROM UNIVERSITY OF THESSALONIKI

By Dimitris Balis and Cristos Zerefos

Contact: *D. Balis*
Laboratory of Atmospheric Physics
Aristotle University of Thessaloniki
Box 149, 54124 Thessaloniki, Greece
E-mail: balis at auth.gr

Validation of GOME total ozone v3.0 using the WMO-network stations

D. Balis[1] and C. Zerefos[2]

[1] *Laboratory of Atmospheric Physics, Aristotle University of Thessaloniki, Greece*
[2] *Laboratory of Climatology, Department of Geology, University of Athens, Greece*

IV.4 ABSTRACT

Several versions of GOME total ozone have been compared with WMO's World Ozone and UV Data Center (WOUDC) total ozone data records. About 140 Dobson, Brewer and M-124 ground-based stations have been used to investigate seasonal, sun zenith angle (SZA) and column dependences of GOME total ozone retrieved with (i) version 2.7 of the off-line GOME Data Processor (GDP) operated at DLR, (ii) version 3.0 of the GOME fast-delivery processor (GOFAP) operated at KNMI, and (iii-iv) the upgraded version 3.0 of GDP with and without new cross-correlation spectral calibration technique, respectively. The study concludes that the upgrade to GDP 3.0 results in a better agreement with WMO's quasi-global network data. GDP 3.0 data sets obtained with the old and new calibration approach yield similar results, although biased by about 0.3%. Seasonal and SZA dependences have been reduced with the new GDP but they still remain, with differences in phase and amplitude. Best agreement is obtained with the new calibration method. Small differences of WMO-based global validation results with respect to global results obtained with NDSC data can be explained by differences in the sampling of geographical regions and atmospheric conditions. E.g., WMO includes stations influenced by desert aerosols while NDSC consists mainly of clean-air stations. The study does not allow to conclude at very high SZA due to the limitation of direct sun ground-based measurements at low sun elevation..

IV.5 RESULTS FROM NASA/GSFC

By James F. Gleason and Gordon Labow

Contact: *J. F. Gleason*
NASA Goddard Space Flight Center
Code 916
Greenbelt, Maryland (USA)
E-mail: gleason at redwind.gsfc.nasa.gov

GOME GDP 3.0 Validation With EPTOMS and Dobson Comparisons

J. F. Gleason[1] and G. Labow[2]

[1] *NASA Goddard Space Flight Center, Greenbelt, MD, USA*
[2] *Science Systems & Applications, Inc. (SSAI), NASA Goddard Space Flight Center, Greenbelt, MD, USA*

Abstract : The upgrade of GOME Data Processor (GDP) total ozone from version 2.7 to 3.0 has been studied with respect to correlative data from EP-TOMS V7 satellite and WMO/Dobson ground-based network. Comparison results are presented as time-filtered zonal mean time-series. A preliminary remark is that the subset of validation orbits reprocessed with GDP 3.0, selected to meet the needs of ground-based network studies, do not offer sufficiently global coverage needed by GOME/TOMS studies. Nevertheless, comparisons of the two GDP versions with EP-TOMS and Dobson network data conclude to a better agreement with GDP 3.0 and a reduction of the amplitude of seasonal differences in both the Northern and Southern middle latitudes. In the Tropics, differences of about 1% in total ozone can be observed between the lamp calibration and cross-correlation calibration methods

V TOTAL NITROGEN DIOXIDE

By Jean-Christopher Lambert, José Granville, Vincent Soebijanta,
and Michel Van Roozendael

Contact: *J-C. Lambert*
Space Aeronomy Institute of Belgium (BIRA-IASB)
Avenue Circulaire 3, B-1180 Brussels, Belgium
E-mail: j-c.lambert at iasb.be

Geophysical Validation of GOME GDP 3.0 Total NO_2

J.-C. Lambert, J. Granville, V. Soebijanta, and M. Van Roozendael

Space Aeronomy Institute of Belgium (IASB-BIRA)
Avenue Circulaire 3, B-1180 Brussels, Belgium

Abstract : Following the upgrade of GOME Data Processor (GDP) from version 2.7 to 3.0, a delta validation campaign was organised in 2002 to verify the correctness of changes and to assess the geophysical quality of the upgraded data products. This report summarises delta validation results of the new total nitrogen dioxide data product. The study relies on quasi-global comparisons of GOME data with ground-based measurements from the Network for the Detection of Stratospheric Change (NDSC), satellite data from UARS Halogen Occultation Experiment (HALOE), SPOT-3 Polar Ozone and Aerosol Measurement (POAM-II) and SPOT-4 POAM-III, and chemical-transport modelling results. A first assessment of the quantitative agreement between GOME and NDSC total NO_2 is presented.

V.1 INTRODUCTION

At the end of 2001, the level-1b-to-2 segment of the off-line GOME Data Processor (GDP) established at DLR-IMF on behalf of ESA, was upgraded from version 2.7 to version 3.0 [DLR, 2002a-c]. Consequently, a delta validation campaign took place in 2002 to verify the correctness of changes and to assess the geophysical quality of the upgraded data products. The present document reports on such delta validation studies of the nitrogen dioxide data product upgrade to version 3.0.

Studies reported hereafter rely on the confrontation of a representative subset of the GOME data record, with correlative ground-based measurements associated with the international WMO/GAW Network for the Detection of Stratospheric Change (NDSC) [Lambert *et al.*, 1999a]. GOME data have also been compared to stratospheric columns derived from satellite measurements by UARS Halogen Occultation Experiment (HALOE) [Russell *et al.*, 1993], SPOT-3 Polar Ozone and Aerosol Measurement II (POAM-II) [Randall *et al.*, 1998] and its successor SPOT-4 POAM-III [Lumpe *et al.*, 2002]. Chemical-transport modelling of the global troposphere has been used to support the interpretation of the comparisons.

Section 2 describes the adopted methodology and available data sets. Before investigating the new GDP data product, previous validation results of GDP 2.7 are summarised in Section 3. Correlative studies between GDP 2.7 and 3.0, NDSC, HALOE and POAM NO_2 data are outlined in Section 4. The report ends with general conclusions and recommendations for further improvement.

V.2 DATA SETS AND METHODOLOGY

V.2.1 GOME Validation Orbits

Starting from the list of 399 orbits used for the delta validation of GDP upgrade to version 2.7 [Lambert *et al.*, 1999b], we have selected an additional list of 1858 validation orbits with the twofold objective to optimise validation studies relying on ground-based network data and to allow long-term verification. The resulting list of 2257 validation orbits is a good compromise between minimum processing time and maximum representativeness.

The selection of orbits is based on histograms of GOME/NDSC comparisons performed with the GDP 2.7 data record since January 1996. Orbits have been selected when leading to closest values to the median value of the relative difference in total ozone. Assuming that ozone is a tracer, using ozone differences instead of nitrogen dioxide differences is expected to reduce uncertainties associated to atmospheric variability and to the diurnal cycle of NO_2.

The selection has been constrained in such a way that the sampling of the NO_2 column range and of its cyclic variations (with season, latitude, and solar illumination) complies with both Nyquist and Central Limit theorems. Most of data records have been limited to the period of 1996-1997, that is, limited in terms of instrumental degradation. For long-term verification purposes, data records have been extended from 1996 through 2001 at a few representative stations.

Practically, the new set of validation orbits allows:

- Validation at about 15 total NO_2 monitoring stations from the Arctic to the Antarctic;
- Accurate investigation of major stratospheric features: seasonal variation, meridian structure, winter-spring polar photochemistry, midnight sun conditions;
- Only limited information on day-to-day variability and zonal structures;
- Comparison between polluted and unpolluted areas;
- Long-term verification from 1996 through 2001.

V.2.2 Correlative Data

Studies reported hereafter are based on comparisons with high quality, well controlled correlative measurements of atmospheric nitrogen dioxide performed by several independent sensors. The backbone of the correlative database consists of pole-to-pole observations of total NO_2 at sunrise and sunset collected from a network of UV-visible spectrometers associated with the NDSC [Vaughan *et al.*, 1997; Roscoe *et al.*, 1999; Lambert *et al.*, 1999a], listed in Table 1. Due to their twilight measurement geometry, they are mostly sensitive to the stratospheric contribution to the vertical column. Contributing sensors consist in: (a) scanning instruments developed by NIWA since the late 1970s [McKenzie and Johnston, 1982]; (b) SAOZ grating instruments (Système d'Analyse par Observation Zénithale) developed by CNRS and performing automated network operation since the late 1980s [Pommereau and Goutail, 1988]; and 3 spectrometers of a similar design developed at (c) IASB [Van Roozendael *et al.*, 1995], (d) IFE [Richter *et al.*, 1998], and (e) NILU [Arlander *et al.*, 1998], respectively. NO_2 vertical column is inferred from recorded zenith-scattered spectra using a two-step approach of the Differential Absorption Optical Spectroscopy (DOAS) technique similar to that used in the GOME processing chain: apparent slant columns are retrieved from a spectral analysis and then converted into vertical columns by means of a geometrical enhancement factor, or air mass factor (AMF). All contributing UV-visible sensors have been certified for the NDSC after fruitful participation to major intercomparison campaigns organised through the NDSC and/or the EC Environment Programme. During such campaigns, the agreement between the various instruments generally falls within the 5% to 10% range [e.g., Hofmann *et al.*, 1995; Vaughan *et al.*, 1997; Roscoe *et al.*, 1999]. Long-term comparisons of nearly co-located instruments conclude to a mean agreement of 3% in summer and 9% in winter [e.g., Koike *et al.*, 1999]. The figure is consistent with an estimated 5-10% accuracy of the retrieved slant column amount taking into account the 5% uncertainty of the NO_2 absorption cross-sections [Merienne *et al.*, 1995], their temperature dependence [Harwood and Jones, 1994; Coquart *et al.*, 1995], and the average 1.5% one sigma confidence level of the least-squares spectral fit. The zenith-sky NO_2 AMF exhibits periodic signatures related to seasonal, latitudinal, and sunrise/sunset change of the vertical distribution of atmospheric constituents [Lambert *et al.*, 1999c]. Not taken into account in the ground-based data processing yet, those features generate in the resulting vertical columns fictitious cyclic signatures of a few percent, superimposed on the real total NO_2 variations observed by the instrument. As shown in an NDSC-based study of GOME NO_2 data [Lambert *et al.*, 1999c], those cyclic biases should not affect current GOME validation studies.

Table 1 - Characteristics of NDSC NO_2 UV-visible instruments contributing to the present study: station name, geographical location, coordinates, type of instrument, and responsible institute.

Station	Location	Lat.	Long.	Instrument	Institute
Ny-Ålesund	Spitsbergen	79°N	12°E	SAOZ	NILU
				DOAS	IFE/IUP
Longyearbyen	Spitsbergen	78°N	16°E	DOAS	NILU
Thule	Western Greenland	77°N	69°W	SAOZ	DMI
Scoresbysund	Eastern Greenland	70°N	22°W	SAOZ	CNRS/DMI
Sodankylä	Finland	67°N	27°E	SAOZ	CNRS/FMI
Zhigansk	Eastern Siberia	67°N	123°E	SAOZ	CNRS/CAO
Salekhard	Western Siberia	67°N	67°E	SAOZ	CNRS/CAO

Harestua	Norway	60°N	11°E	DOAS	IASB
Aberystwyth	Wales	52°N	4°W	SAOZ	U. Wales
Jungfraujoch	Swiss Alps	47°N	8°E	SAOZ	IASB
Obs. Haute Provence	French Alps	44°N	6°E	SAOZ	CNRS
Mauna Loa	Hawaii	20°N	156°W	NIWA	NIWA
Tarawa	Kiribati	1°N	172°E	SAOZ	CNRS
				NIWA	NIWA
Saint Denis	Reunion Island	21°S	55°E	SAOZ	CNRS/U. Réunion
Bauru	Brazil	22°S	48°W	SAOZ	CNRS/UNESP
Lauder	New Zealand	45°S	170°E	NIWA	NIWA
Kerguelen	Kerguelen Islands	49°S	70°E	SAOZ	CNRS
Macquarie	New Zealand	54°S	159°E	NIWA	NIWA
Faraday	Antarctic Peninsula	65°S	64°W	SAOZ	BAS
Rothera	Antarctic Peninsula	68°S	68°W	SAOZ	BAS
Arrival Heights	Antarctica	78°S	167°E	NIWA	NIWA

Complementarily, sunrise and sunset NO_2 stratospheric columns have also been derived from stratospheric profiles measured by UARS Halogen Occultation Experiment (HALOE) [Russell *et al.*, 1993; Gordley *et al.*, 1996], by SPOT-3 Polar Ozone and Aerosol Measurement II (POAM-II) [Randall *et al.*, 1998] and by SPOT-4 POAM-III [Lumpe *et al.*, 2002]. HALOE NO_2 data cover altitudes spanning from above the stratopause down to 20 km, while POAM data cover altitudes from 40 km down to 20 km. POAM and HALOE NO_2 profile data generally agree to better than 10-15% from 20 to 40 km, that is, at altitudes where the stratospheric column is the most sensitive to.

To be comparable to GOME total column data, integrated stratospheric profiles from HALOE and POAM have been completed at each NDSC site with a tropospheric column at noon, representative of an unpolluted troposphere for the site. This tropospheric column has been estimated using the three-dimensional chemical-transport model of the global troposphere, named Intermediate Model of Global Evolution of Species (IMAGES) [Müller and Brasseur, 1995]. IMAGES NO_x modelling results are found to be in reasonable agreement with correlative airborne *in situ* measurements.

V.2.3 Methodology

To fulfil the twofold objective of verifying the correctness of changes and assessing the geophysical consistency of the upgraded data product, the reported study combines a cross correlation of the two GDP versions followed by comparisons with independent measurements of stratospheric NO_2.

According to the description of current GDP upgrade, no important change is to date in the total NO_2 retrieval chain itself (see Chapter 2 of the present issue). Nevertheless, a new level-1b product based on cross-calibration (hereafter referred to as "xcorr") of the lamp spectral features has been generated by DLR. Therefore the study also includes comparisons of NO_2 data retrieved with the two different calibration methods (hereafter "xcorr" and "no-xcorr") in order to qualify and quantify the impact of this new calibration scheme on the level-2 product.

The interpretation of the comparisons follows a methodology described elsewhere, which takes into account various aspects linked to the remote-sensing and geophysical nature of the data. Among them, the difference in sampled air mass [Lambert *et al.*, 1997], the error budget of the ground-based instrumentation [Vaughan *et al.*, 1997, Roscoe *et al.*, 1999, Lambert *et al.*, 1999c, Koike *et al.*, 1999], and the diurnal cycle of stratospheric NO_2 [Roscoe and Pyle, 1987; Lambert *et al.*, 2002]. The latter effect, driven by the daytime photolysis of NO_2 into NO and its night-time conversion into N_2O_5, is particularly important for a proper interpretation of the comparisons.

V.3 GEOPHYSICAL CONSISTENCY OF GDP 2.7 NO_2

Based on a subset of 399 orbits, a preliminary quality assessment of GDP 2.7 total NO_2 was drawn during its delta validation with respect to GDP 2.4 [Lambert *et al.*, 1999d; Timofeyev *et al.*, 1999; Richter *et al.*, 1999; Wagner *et al.*, 1999]. Comparisons with NDSC ground-based network data were extended to the entire GOME data record. GDP data were also compared with global data from UARS HALOE and SPOT POAM satellite sensors and from PSCBOX/SLIMCAT coupled modelling results [Lambert *et al.*, 2001]. Compared to GDP 2.4, GDP 2.7 provides a much more consistent NO_2 data product. The inclusion in the fitting NO_2 window (425-450 nm) of the absorptions of H_2O and O_4, coupled with a number of software improvements [Loyola *et al.*, 1999], results in a clear amelioration. The agreement with ground-based and satellite measurements has improved especially in the inter-tropical region. Figure 1 demonstrates this improvement at the equatorial station of Tarawa in the Central Pacific Ocean, where low NO_2 values combine with small optical path making GOME NO_2 measurement particularly difficult.

Major stratospheric features (seasonal variation, day-to-day fluctuations, meridian structures, episodes of polar denoxification etc.) are captured similarly by the satellites and the ground-based networks. Over regions with high tropospheric NO_x amounts, the NO_2 enhancement observed by GOME generally is consistent with the enhancement predicted by tropospheric models. Although it is difficult to evaluate precisely the accuracy of this product due to various problems such as the diurnal variation of NO_2 and the profile shape effect on the Air Mass Factor (AMF), the overall accuracy in areas of low tropospheric NO_2 is estimated to fall within the 5% to 20% range. GDP 2.7 total NO_2 is affected by larger uncertainties under particular circumstances, e.g., over polluted areas, in the South Atlantic Anomaly, and during midnight sun conditions.

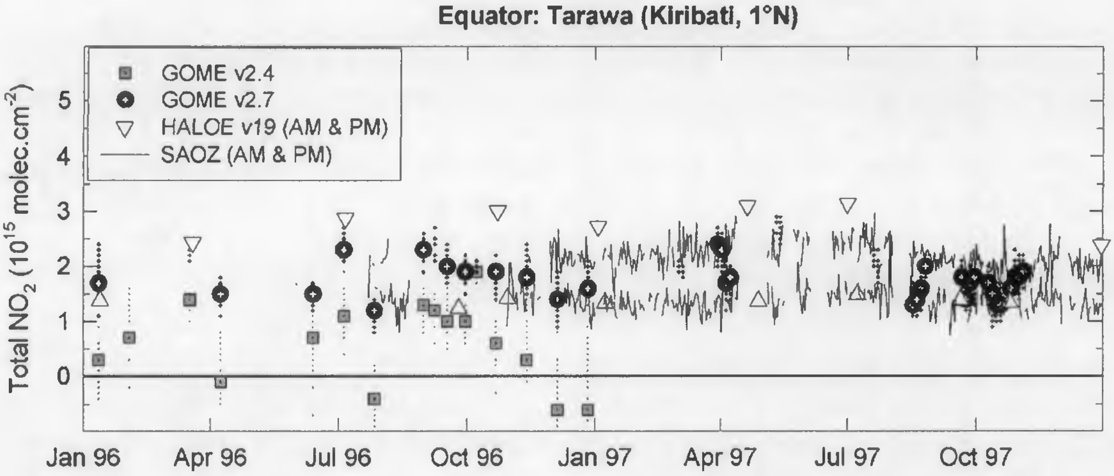

Figure 38 - **Improvement of GDP 2.7 NO_2 data compared to GDP 2.4: comparison of GDP total NO_2 with NDSC/SAOZ ground-based columns and integrated HALOE v19 satellite profiles at Tarawa (from Lambert et al., 1999d).**

V.4 CORRELATIVE STUDY OF GDP 3.0 NO_2

V.4.1 GDP 2.7/3.0 Cross-correlation

Figures 2 to 4 compare GDP 2.7 and 3.0 NO_2 data along three individual orbits in February 1996 (60215135.lv2 data file), June 1996 (60607153.lv2), and September 1997 (70908204.lv2), respectively. Those three orbits contain most of the interesting features observed in about 25 orbits studied here. GDP 3.0 without any added information means that the data are based on the new "xcorr" level-1b calibration.

Small changes in the vertical column that do not affect the spatial structures along track appear in all orbits. Globally, total NO_2 column decreases by an average of 2.5% at high NO_2 values and to 15% at low NO_2 values. Converted in absolute value, this decrease ranges from about 0.5 10^{14} molec.cm^{-2} at the poles to 3-4 10^{14} molec.cm^{-2} at low latitudes. This general case is illustrated in Figure 2 and 3. More rarely, it happens that total NO_2 increases by 1-3.10^{14} molec.cm^{-2} along the entire orbit except at high latitudes. Such an exceptional event is illustrated in Figure 4. A larger scatter is observed around 30° south in the GDP 3.0/2.7 ratio in Figure 2 but not in other Figures. It results from measurement perturbations where ERS-2 flies within the South Atlantic Anomaly (SAA).

Changes in the vertical column are driven directly by the evolution of the slant column. E.g., the similarity is obvious between the GDP 3.0/2.7 vertical column ratios (panel (c) of Figures 2-4) and the corresponding slant column ratios (panel (d) of Figures 2-4). The air mass factor is found to increase slightly by a maximum of 2.5% in regions of low solar elevation and 1% elsewhere. Those results comply with the description of GDP differences [DLR, 2002c] between versions 2.7 and 3.0.

In general, the effect of the new spectral calibration method on the NO_2 level-2 product is relatively small. Compared to the previous level-1 product (no-xcorr), recalibrated level-1 spectra (xcorr data set) yield differences in total NO_2 falling to below 1%, as shown in the orbit of February in Figure 2. However, exceptions happen, such as in the orbits of June 1996 and September 1997: at low latitudes the recalibration is associated with a decrease of 7% and an increase of 20% of the NO_2 vertical column, respectively (panel (g) of Fig. 3 and 4). As expected, differences in the calibration method impact only the slant column values (panel (h) of Fig. 2-4). Air mass factors are absolutely not affected by the new spectrum calibration (panel (i) of Fig. 2-4).

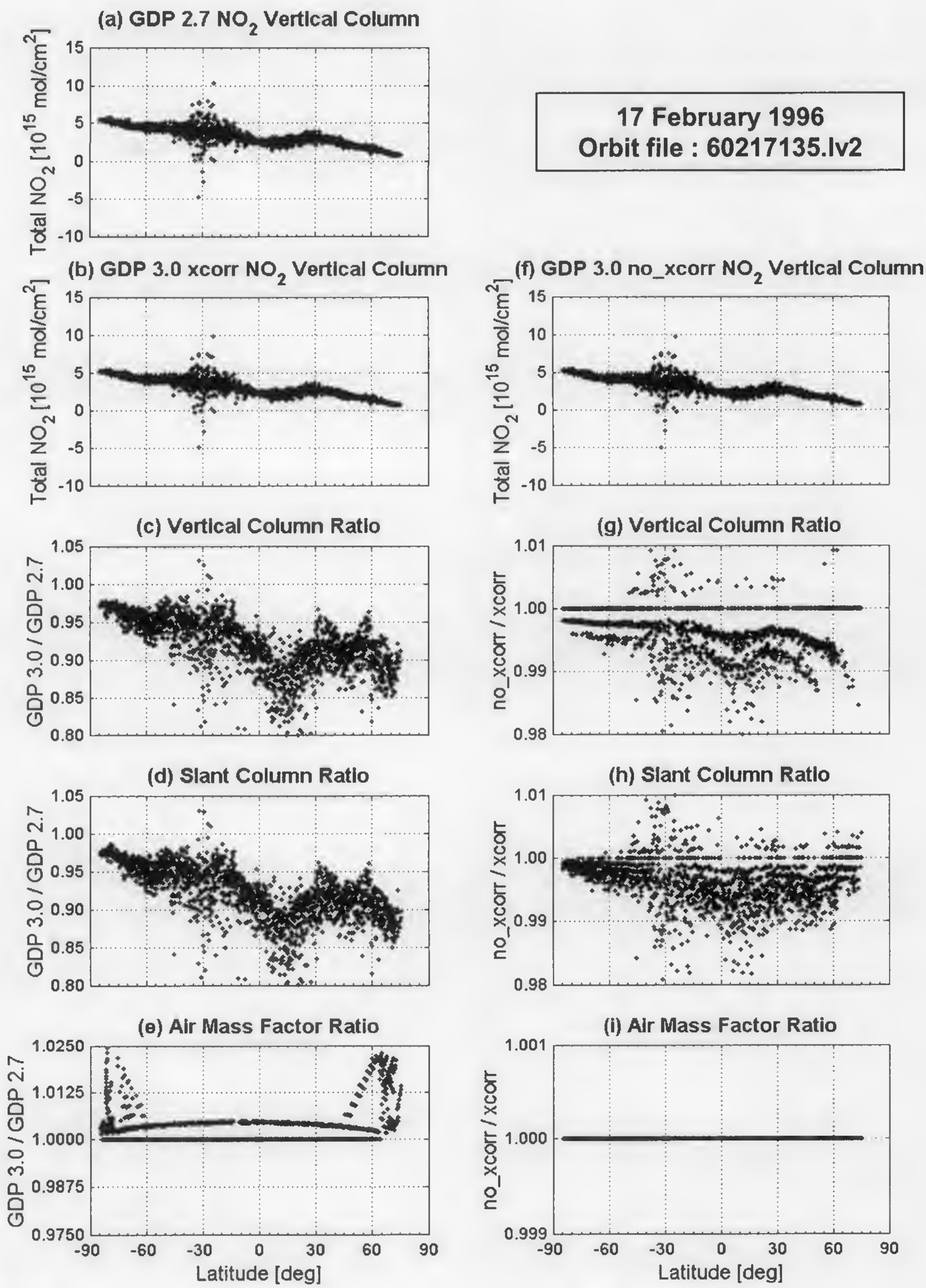

Figure 39 - **Comparison of GOME NO_2 data for orbit file 60217135.lv2 (February 17, 1996). Left part: GDP 3.0 compared to GDP 2.7; right part: GDP 3.0 no-xcorr compared to GDP 3.0 xcorr. From top to bottom: Total NO_2 derived with (a) GDP 2.7, (b) GDP 3.0 xcorr and (f) GDP 3.0 no-xcorr; and ratio of (c, g) vertical columns, (d, h) slant columns, and (e, i) air mass factors.**

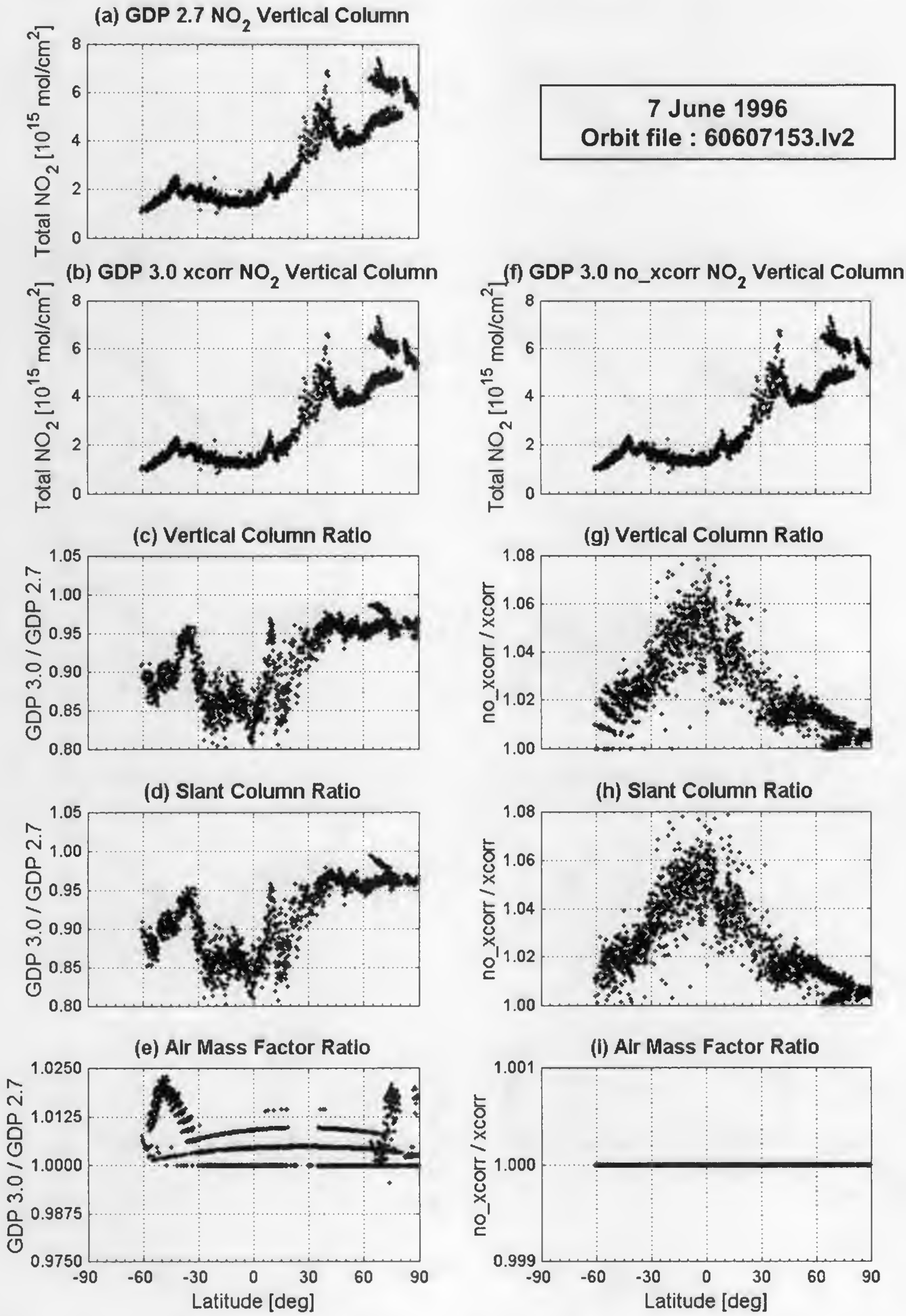

Figure 40 - **Same as Figure 2 but for orbit file 60607153.lv2 (June 7, 1996).**

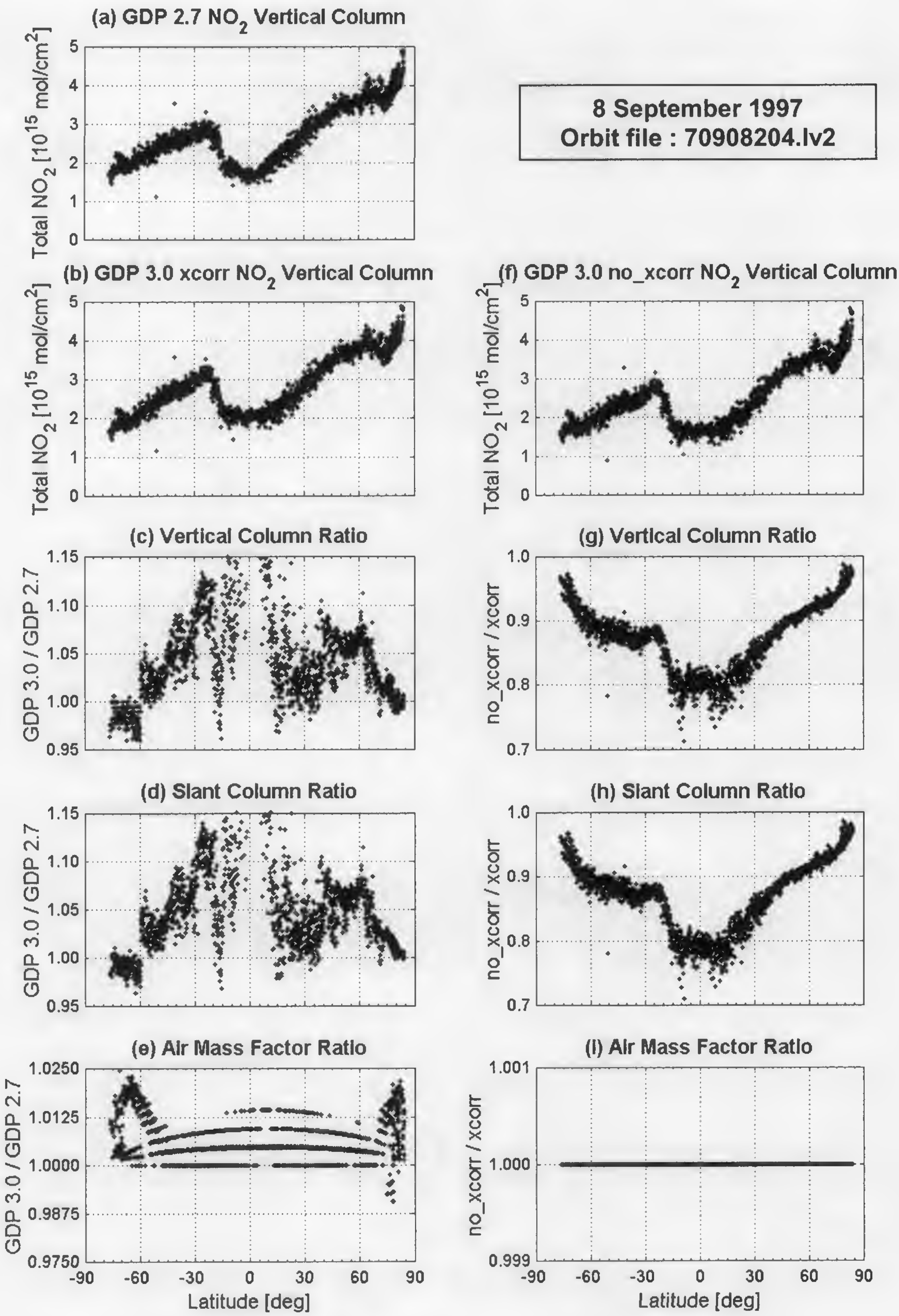

Figure 41 - **Same as Figures 2 and 3 but for orbit file 70908204.lv2 (September 8, 1997).**

V.4.2 Temporal Behaviour of GDP Changes

After the study of meridian structures of GDP changes presented in the previous subsection, the present subsection describes temporal features. Ratios of GDP quantities have been studied as a function of time at a variety of NDSC stations, including the 21 sites listed in Table 1. Main characteristics are illustrated in Figures 5 and 6. Figure 5 displays changes in vertical column amount typical of low and middle latitude stations. At such latitudes, changes result in a systematic decrease of about 5% with a seasonal variation depending on the latitude and the hemisphere, the largest variation being observed at austral latitudes.

In polar regions, wintertime data are affected by a larger decrease, reaching sometimes 25% near the spring terminator. This is illustrated in Figure 6 for an Antarctic station. Figure 6 gives also details of the changes of GDP quantities, confirming that changes in NO_2 vertical column are driven by changes in NO_2 slant column. Changes due to the air mass factor (lower panel of Figure 6) are not significant, even in winter-spring when air mass factors can change by a few percent Finally, it is worth mentioning that meridian structures as identified in the previous subsection are confirmed when integrating the results at individual stations.

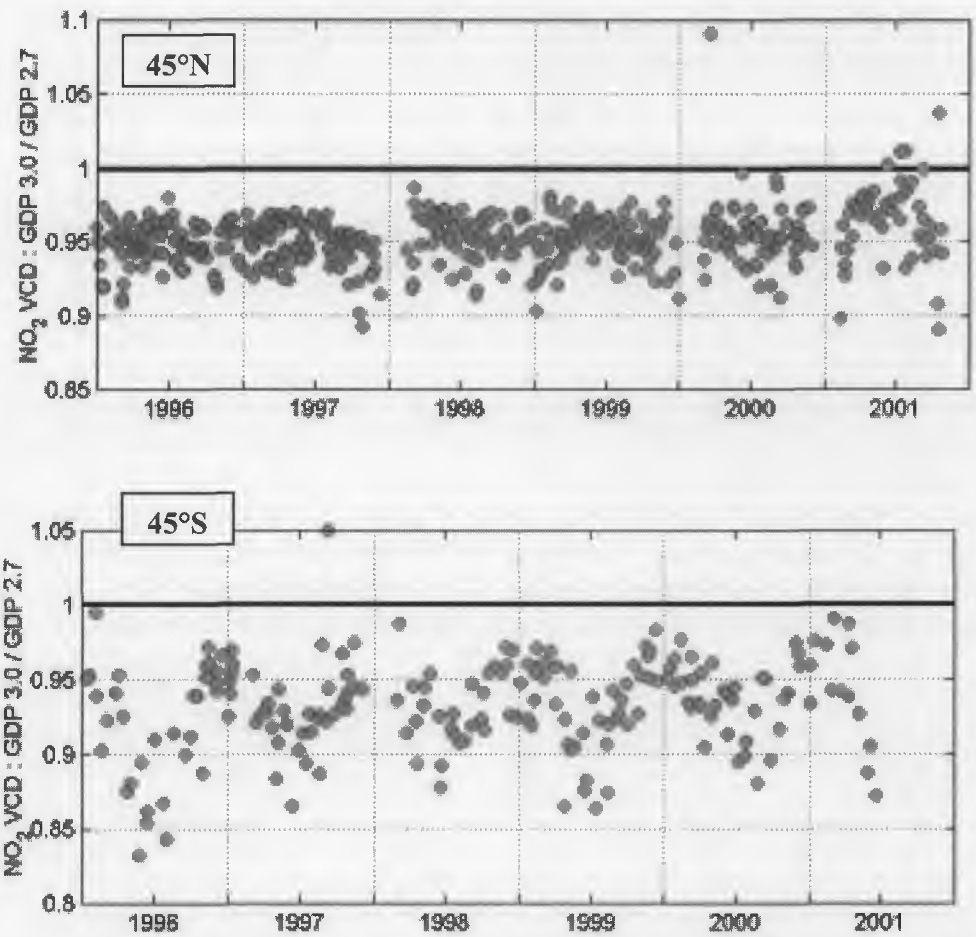

Figure 42 - **Ratio of GDP 3.0 to 2.7 NO_2 vertical columns (VCD) at northern (upper panel) and southern (lower panel) middle latitudes. New GDP 3.0 reports lower total NO_2 by about 5%, with a seasonal variation depending on the latitude and the hemisphere.**

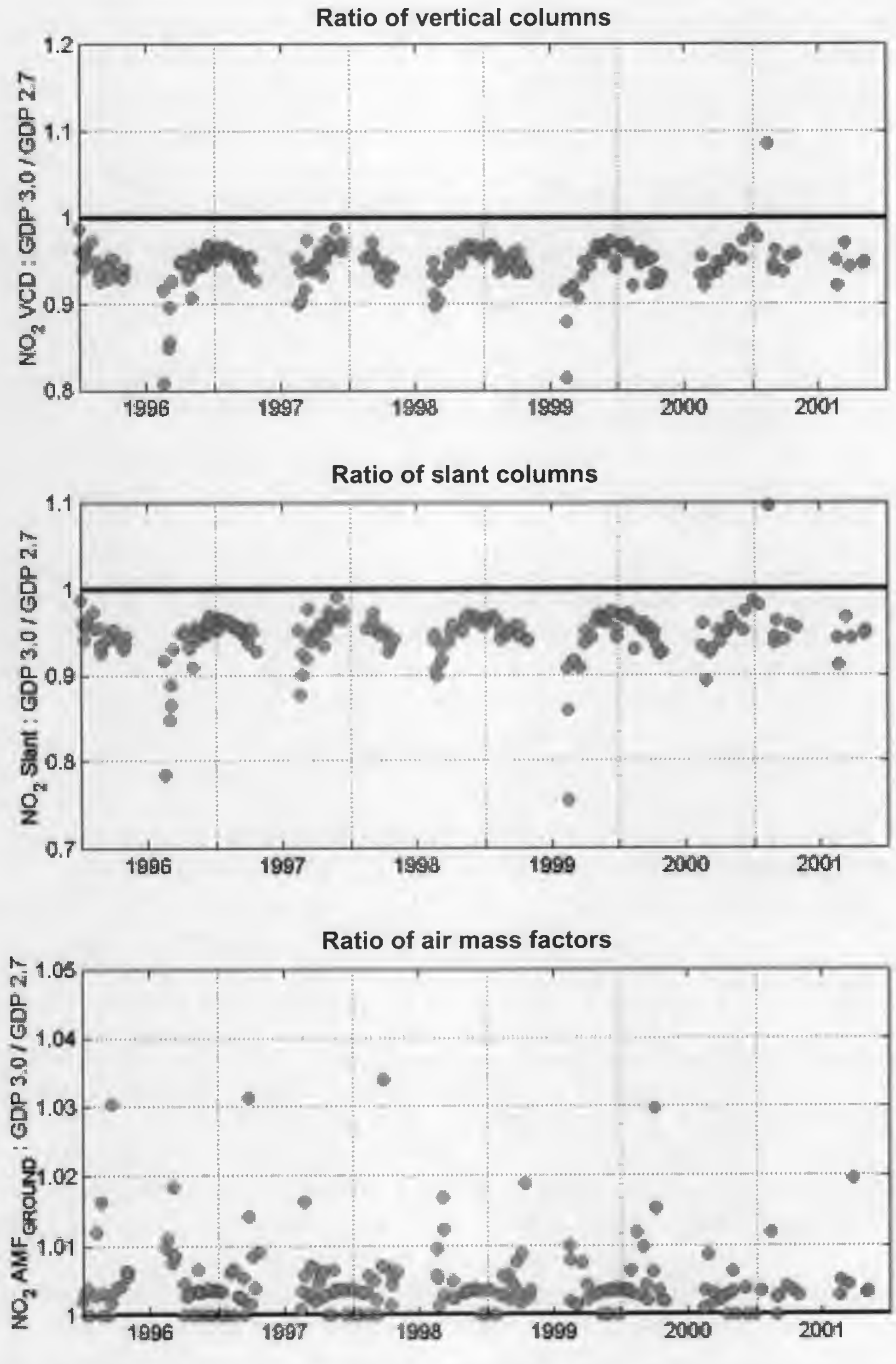

Figure 43 - Ratio of GDP 3.0 to 2.7 NO_2 data from 1996 through 2001 over the Antarctic station of Dumont d'Urville (67°S, 140°E). The ratio of vertical columns (upper panel) shows a similar behaviour as that observed at middle latitudes, except near the winter terminator where larger deviations may occur. Changes in vertical columns are directly driven by changes in slant columns, as shown in the middle panel. Changes due to the air mass factor (lower panel) are not significant.

V.4.3 Geophysical Confrontation with Correlative Measurements

At every station listed in Table 1, correlative data records have been compared to GOME NO_2 validation data sets generated (i) with both GDP 2.7 and 3.0 and (ii) with both level-1 calibration techniques. As expected, the small decrease of NO_2 values pointed out in previous sections does not affect the qualitative agreement with correlative data.

From pole to pole, GOME and other observing systems report similarly major stratospheric features such as seasonal cycles, meridian structures and day-to-day variability. This is illustrated at Figures 7 and 8 for extreme conditions in terms of NO_2 remote sensing. Figure 7 shows total NO_2 time-series at Arctic and Antarctic stations, gathering periods of optimal signal-to-noise ratio with low variability (polar summer), of weak signal-to-noise ratio (e.g., wintertime denoxification), of high variability (e.g., vortex edge overpass), of strong deviations from the climatological temperature used in the retrieval (cold polar vortex), of low sun elevation (winter terminator or summer midnight sun) and associated photochemical change along the line of sight. Figure 8 shows total NO_2 at low latitudes, with weak short-term variability but also low signal-to-noise ratio, strong spectral interference with the high water vapour content, intense tropospheric pollution events (e.g., sugar cane burning in Brazil), and perturbations related to the South Atlantic Anomaly (again in Brazil).

Compared to ground-based data, GOME time-series are more scattered during polar summer. Modelling results suggest that this scatter could be partly attributed to the different photochemical states observed by GOME during one day, ERS-2 satellite flying over polar stations several times a day. Systematic biases observed in summer (GOME underestimates ground-based values) and winter (GOME overestimates ground-based values) might also be attributed to the photochemical cycle of NO_2. Indeed, the diurnal cycle varies with the season as a consequence of seasonal cycles of atmospheric temperature, NO_y partitioning, and aerosols [Lambert *et al.*, 2002]. In summertime, as the N_2O_5 reservoir vanishes due to the permanent illumination of the pole, the complete day/night cycle moves to its polar day regime where the diurnal cycle is limited to NO/NO_2 partitioning driven directly by solar elevation. With this particular regime, it is logical that GOME measurements acquired in the mid-morning – that is, when a higher sun photolyses more NO_2 – yield lower NO_2 values than NDSC/UV-visible data acquired near midnight sun where photolysis is at its minimum.

Over clean sites, sporadic pollution episodes as reported by GOME– e.g. peaks at Sodankylä in Figure 7 – correlate quite well with ground-based observations, at least qualitatively. In regions of more permanent tropospheric pollution, its higher sensitivity to the troposphere makes GOME reporting higher and more scattered total NO_2 values than NDSC, HALOE and POAM. Although the difference between GOME and those pure stratospheric measurements follows the seasonal evolution predicted by IMAGES tropospheric modelling results, GOME GDP NO_2 data over polluted areas are significantly biased due to remaining uncertainties in the determination of the air mass factor and of the cross-section temperature. Several studies have shown that NO_2 AMFs and effective absorption temperatures are strongly affected by variations in the profile shape of the NO_2 vertical distribution, especially for high pollution conditions. Atmospheric parameters used by GDP introduce fictitious meridian/seasonal variations of a few percent superimposed on the geophysical variations in stratospheric NO_2 and a larger bias in case of enhanced tropospheric NO_2 [Lambert et al., 1999c].

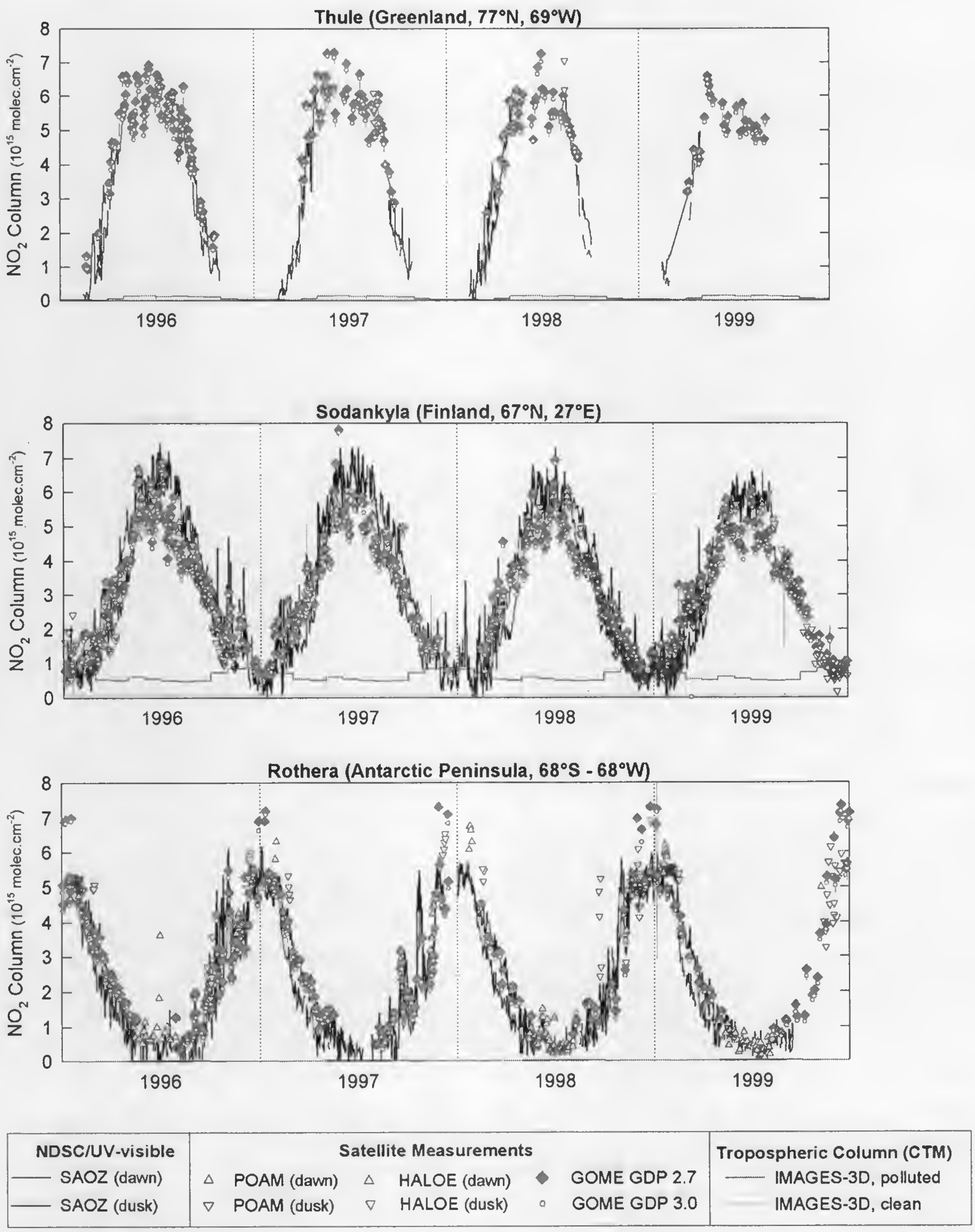

Figure 44 - **Total NO_2 at Arctic (Thule and Sodankylä) and Antarctic (Rothera) sites as measured by NDSC/SAOZ UV-visible instruments, HALOE and POAM satellites, and as derived from GOME spectra with GDP 2.7 and 3.0. For GOME, large symbols stand for the closest ground pixel while vertical lines indicate standard deviation of total NO_2 over five closest pixels.**

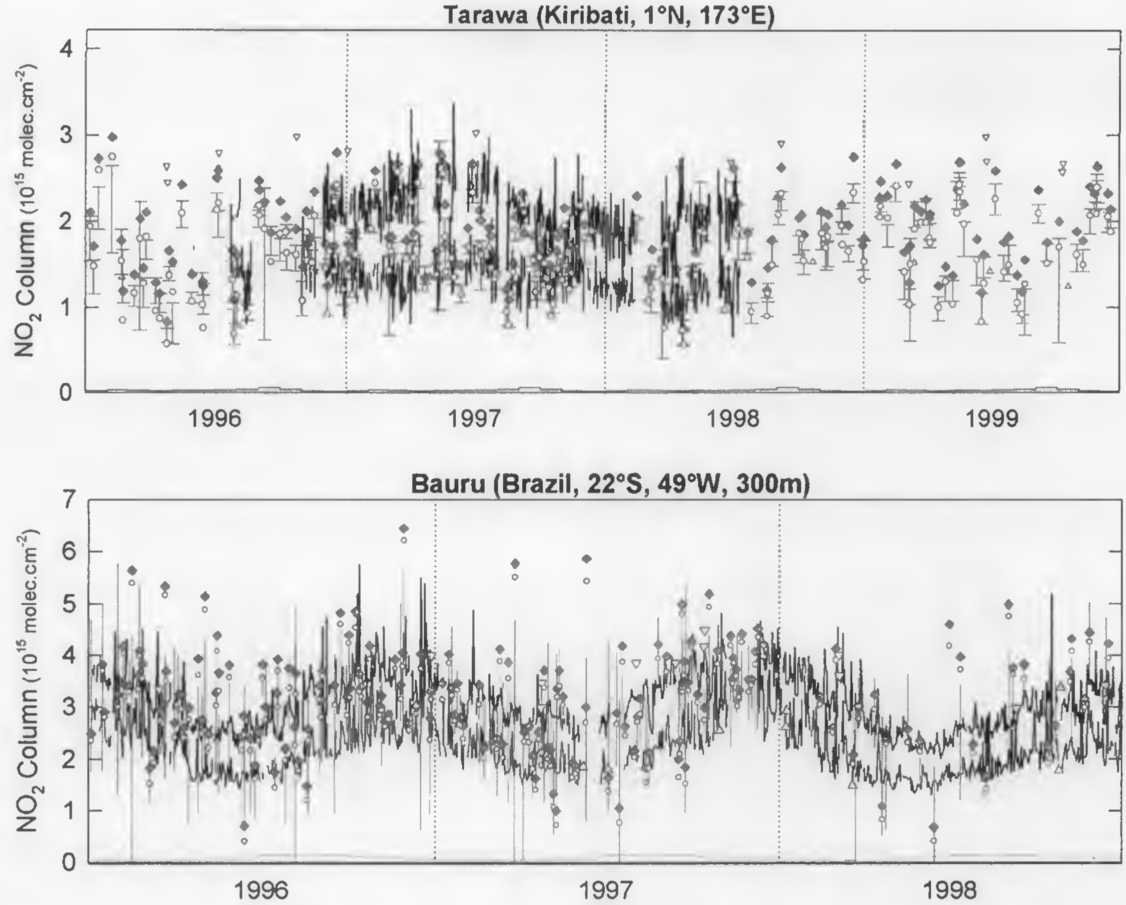

Figure 45 - Same as Figure 7 but at the equatorial station of Tarawa and the tropical station of Bauru.

V.4.4 Quantitative Assessment of GOME/NDSC Agreement

The diurnal cycle of nitrogen dioxide constitutes the main obstacle to qualitative comparisons between GOME and twilight data. The difference in photochemical state between correlative data acquired during sunset and GOME data acquired in the morning varies with the season, the latitude and the aerosol loading. It can exceed 1.5 10^{15} molec.cm^{-2} under special circumstances, e.g. during polar day. Fortunately, chemical-modelling results suggest that mid-morning GOME data might be sufficiently close to the sunrise values reported by ground-based UV-visible spectrometers, the residual photochemical difference ranging from 1 10^{14} to 5 10^{14} molec.cm^{-2}. This simple comparison method is valid world-wide, unless polar winter heterogeneous processes or polar day photochemistry are activated. In the latter case, a photochemical adjustment factor can be applied. This factor is a simple function of the solar zenith angle of the GOME measurement [Lambert *et al.*, 2002].

Using this comparison method and the photochemical adjustment for polar day conditions, the quantitative agreement between GOME and NDSC values falls to within ± 5 10^{14} molec.cm^{-2} for stratospheric NO_2 observations and ± 8 10^{14} molec.cm^{-2} at very low slant column. In many cases, the small reduction of NO_2 values from GDP 2.7 to 3.0 improves slightly the situation, GOME mid-morning NO_2 being now closer to sunrise NDSC measurements. The quantitative agreement varies from one station to another, as illustrated in Figures 9-11. Best results are observed over remote stations of the middle latitudes and in the tropics when the signal-to-noise ratio is sufficiently high. Such cases are illustrated in Figure 9 at three stations characterised by a clean troposphere. At the mid-latitude site of Lauder, New Zealand, the average absolute difference in total NO_2 does not exceed a few 10^{14} molec.cm^{-2} with a slight seasonal variation. The scatter is also limited to a few 10^{14} molec.cm^{-2}. At the tropical site of Mauna Loa, where the troposphere is almost clean, similar results are obtained, though the agreement is systematically better in winter. Although the mean agreement remains good, the scatter increases drastically at the equatorial site of Tarawa where GOME NO_2 measurements are difficult due to low signal-to-noise ratio and high water vapour content.

Lauder (New Zealand, 45°S, 170°E)

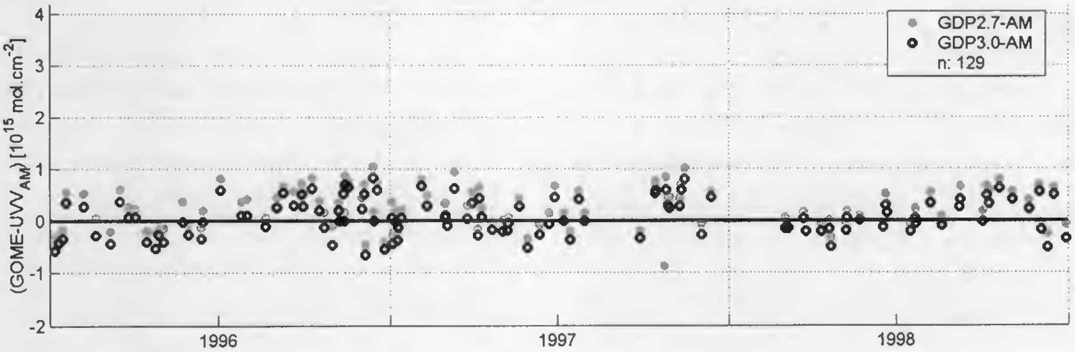

Mauna Loa (Hawaii, 20°N, 155°W)

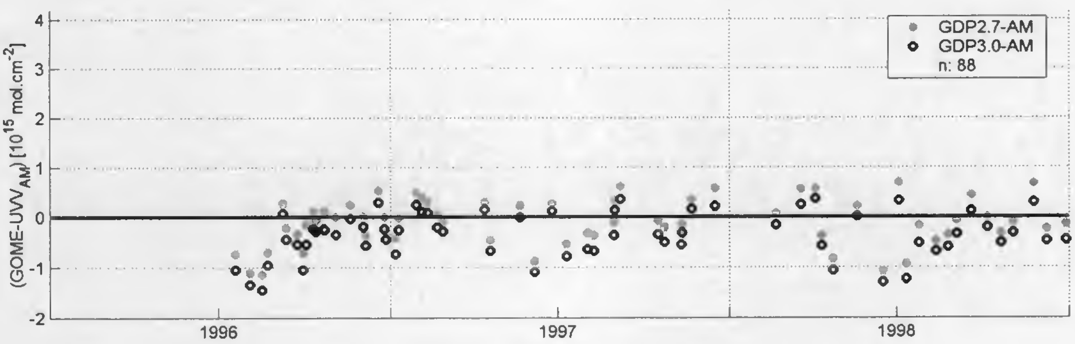

Tarawa (Kiribati, 1°N, 173°E)

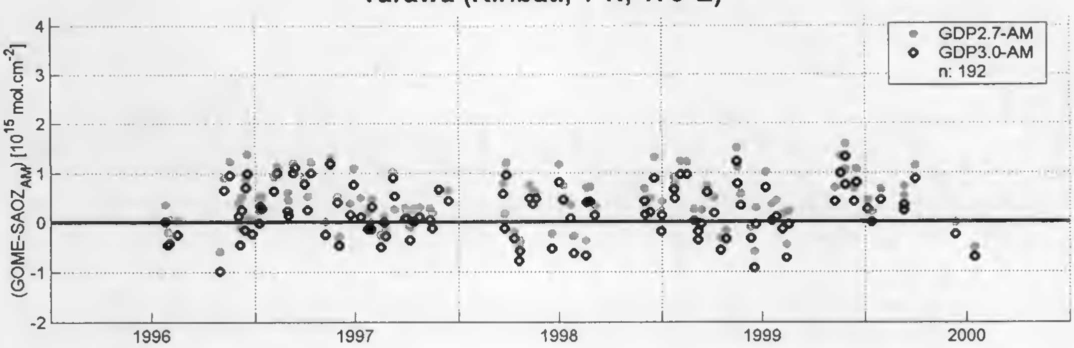

Figure 46 - **Absolute difference, as a function of time, between GOME (mid-morning) and NDSC/UV-visible (sunrise) total NO_2 at three clean stations presented by decreasing latitude: Lauder (New Zealand), Mauna Loa (Tropical Pacific), and Tarawa (Equatorial Pacific).**

Absolute differences increase largely over polluted areas, as illustrated in Figure 10. In the Alps, where both relatively clean and heavily polluted conditions might coexist with a permanent background of tropospheric NO_2, the GOME/NDSC agreement exhibits a strong seasonal variation of 1-2 10^{15} molec.cm^{-2} with a scatter twice as large as that observed in Lauder. The best agreement and lower scatter are observed in summer, corresponding to the lowest tropospheric background and the highest stratospheric NO_2 content. The bias and the scatter are larger in winter-spring when both the tropospheric background and the tropospheric variability reach their maximum. At the Brazilian station of Bauru, the situation is even worse due to lower slant columns, high water vapour content, and measurement perturbations related to South Atlantic Anomaly.

Finally, Figure 11 shows GOME/NDSC agreement at the Arctic station of Sodankylä, typical of the results in polar regions. The agreement is characterised by an average difference of 1-6 10^{14} molec.cm^{-2} and an seasonal variation of about 1 10^{15} molec.cm^{-2} from peak to peak. The best agreement appears in fall. The scatter is comparable to the scatter reported at clean mid-latitude stations, e.g. Lauder in Figure 9, except in springtime and around summer solstice when it increases. Part of this behaviour correlates with residual photochemical differences between GOME and NDSC measurement times. However, other effects related to the retrieval or the instrument can certainly not be ruled out. Figure 11 also illustrates the obvious improvement gained by using the adjustment factor for polar summer photochemistry.

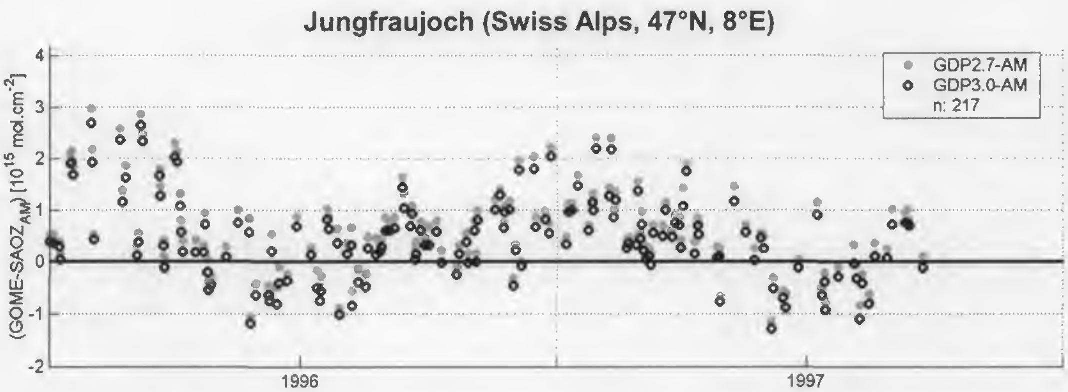

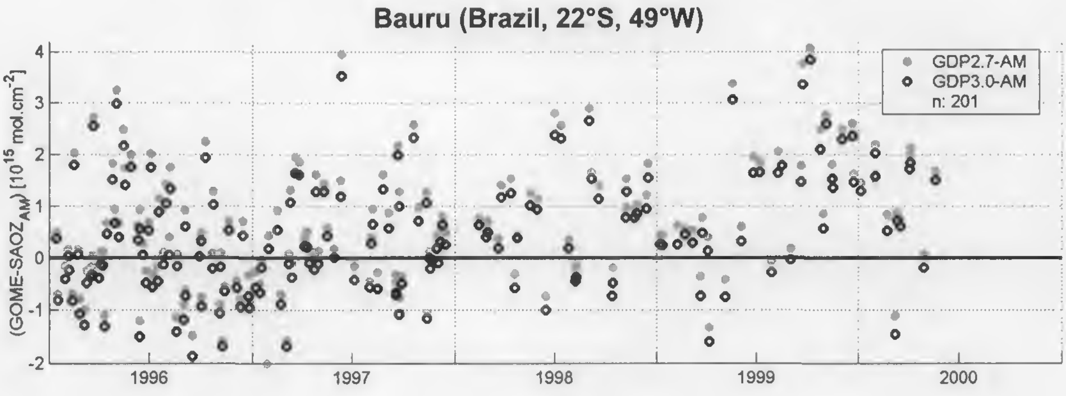

Figure 47 - **Same as Figure 9, but at the Alpine station of the Jungfraujoch (upper panel) and the tropical site of Bauru in Brazil (lower panel).**

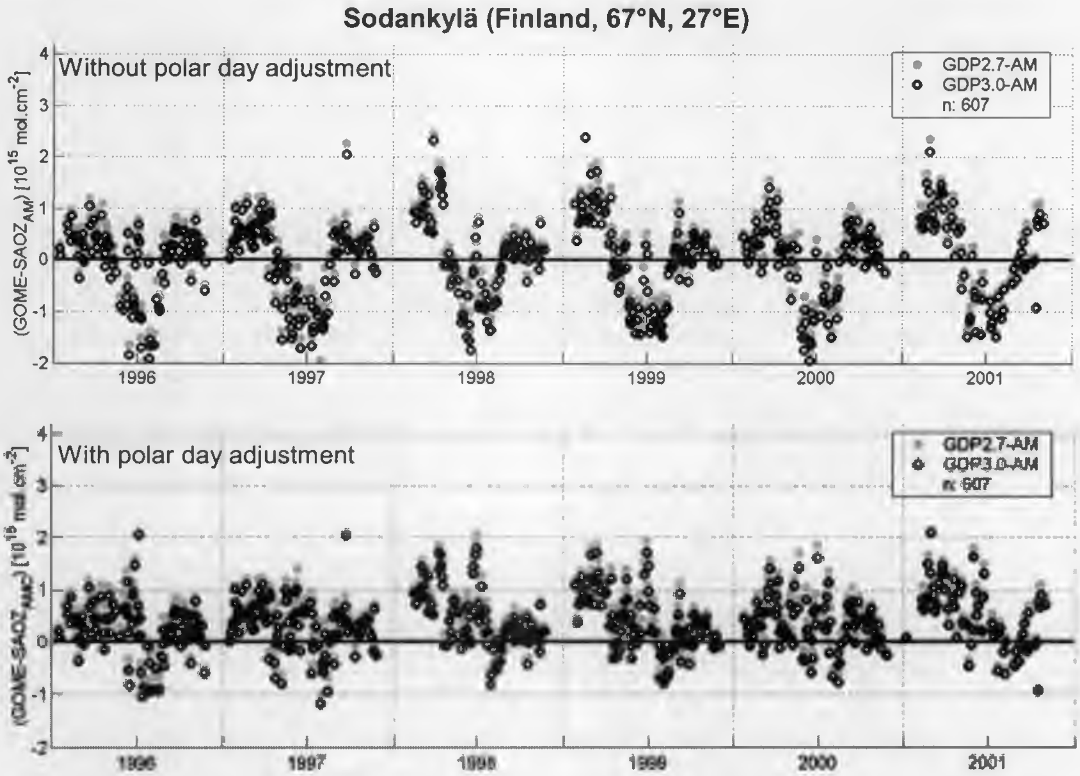

Figure 48 - **Same as Figures 9 and 10, but at the station of Sodankylä on the Arctic Polar Circle, without (upper panel) and with (lower panel) adjustment for polar day photochemistry.**

V.5 CONCLUSION

According to this study, changes between GDP 2.7 and GDP 3.0 total NO_2 data products are not significant, as expected from the minor changes in the NO_2 segment of the GDP level-1-to-2 processor described in Chapter 2 of the present report.

Total NO_2 data sets derived from level-1 radiometric data calibrated with the calibration lamp method (no-xcorr) and the cross-correlation technique (xcorr) are mutually consistent within 1%. However, a few sporadic events where relative differences can reach 7 to 20% at low latitudes have been identified.

Comparisons of GOME with various independent sensors operating from the ground (NDSC network of UV-visible spectrometers) and from space (HALOE, POAM-II and POAM-III), conclude to a good qualitative agreement among all sensors. Major stratospheric characteristics are captured similarly. Particular features found in GOME data over polluted areas correlate reasonably with tropospheric features predicted by chemical-transport modelling.

The quantitative agreement between GOME and NDSC/UV-visible total NO_2 data records is within a few 10^{14} molec.cm^{-2} for clean-troposphere stations from the tropics to the middle latitudes, and within 1-1.5 10^{15} molec.cm^{-2} at the poles during springtime. Over polluted areas, the difference can exceed 1-2 10^{15} molec.cm^{-2} and exhibits a seasonal variation of the same order of magnitude, correlating with seasonal cycles predicted by tropospheric modelling. The scatter of the difference falls to within a few 10^{14} molec.cm^{-2} for clean-troposphere stations but it increases dramatically over polluted areas and, to a less extent, at very low slant column.

GOME GDP total NO_2 data are found in good agreement with independent data records where the tropospheric NO_2 content is negligible. However, several issues remain to be addressed in order to improve the quality of the data products. Among those issues, the accuracy of the air mass factor and of the effective absorption temperature are certainly important. To improve the AMF and effective temperature under clean conditions, it is recommended to use an atmospheric profile database with seasonal/latitudinal stratospheric features and a consistent tropospheric background. Accurate evaluation of the AMF and temperature under polluted conditions remains a real matter of concern, as well as the quality of GOME NO_2 data in the South Atlantic Anomaly.

Acknowledgements

Contributing NDSC PIs and ground-based instrument operators (BAS, CAO, CNRS/SA, DMI, IASB, IFE, FMI, NILU, NIWA, UNESP, and U. Wales), DLR-IMF, and the HALOE and the POAM Science and Processing Teams are warmly thanked for data provision and fruitful discussions. The support provided by F. Hendrick (IASB) for photochemical modelling and J-F. Müller (IASB) for tropospheric modelling is greatly appreciated. All GOME level-2 data products were processed at DLR on behalf of ESA. Published in ESA Technical Note ERSE-DTEX-EOAD-TN-02-0006, the reported work has been funded by ESRIN (Contract 13554/99/I-DC/CCN-2) and by the Belgian Prime Minister's Services – Office for Science, Technical and Cultural Affairs through grant MO/35/006 and PRODEX ERS.AO3.356/GOME Valorisation project.

References

Arlander, D.W., K.K. Tørnkvist, and G.O. Braathen, 1998: Ground-based UV-Vis Validation Measurements of Stratospheric Molecules above Spitsbergen, in *Proc. 24th Ann. Europ. Meeting on Atmospheric Studies by Optical Methods, Andenes 1997*, ISBN 82-994583-0-7, 185-188.

Coquart, B., A. Jenouvrier, and M.-F. Merienne, 1995: The NO_2 Absorption Spectrum II. Absorption Cross-Sections at Low Temperature in the 400-500 nm Region, *J. Atm. Chem.*, **21**, 251-261.

DLR, 2002a: Product Specification Document of the GDP, Technical Note ER-PS-DLR-GO-0016, Iss./Rev. 4/A, April 2002.

DLR, 2002b: GOME Level 0 to 1 Algorithms Description, Technical Note ER–TN–DLR–GO–0022, Iss./Rev. 5/B, July 31, 2002.

DLR, 2002c: GOME Level 1 to 2 Algorithms Description, Technical Note ER–TN–DLR–GO–0025, Iss./Rev. 3/A, July 31, 2002.

Gordley, L.L., J.M. Russell, L.J. Mickley, J.E. Frederick, J.H. Park, K.A. Stone, G.M. Beaver, J.M. McInerney, L.E. Deaver, G.C. Toon, F.J. Murcray, R.D. Blatherwick, M.R. Gunson, J.P.D. Abbatt, R.L. Mauldin, G.H. Mount, B. Sen, and J.-F. Blavier, 1996: Validation of nitric oxide and nitrogen dioxide measurements made by the Halogen Occultation Experiment for UARS platform, *J. Geophys. Res.*, **101**, 10 241-10 266.

Harwood, M. H., and R. L. Jones, 1994: Temperature Dependent Ultraviolet Cross-sections of NO_2 and N_2O_4: Low Temperature Measurements of the Equilibrium Constant $2NO_2$ <--> N_2O_4, *J. Geophys. Res.*, **99**, 22 955-22 964.

Hofmann, D., J., P. Bonasoni, M. De Mazière, F. Evangelisti, A. Sarkissian, G. Giovanelli, A. Goldman, F. Goutail, J. Harder, R. Jakoubek, P. Johnston, J. Kerr, T. McElroy, R. McKenzie, G. Mount, J. P. Pommereau, P. Simon, S. Solomon, J. Stutz, A. Thomas, M. Van Roozendael, E. Wu, Intercomparison of UV/Visible Spectrometers for Measurements of Stratospheric NO_2 for the Network for the Detection of Stratospheric Change, *J. Geophys. Res.*, pp. 16 765-16 791, 1995.

Koike, M., Y. Kondo, W.A. Matthews, P.V. Johnston, H. Nakajima, A. Kawaguchi, H. Nakane, I. Murata, A. Budiyono, M. Kanada, and N. Toriyama, 1999: Assessment of the uncertainties in the NO_2 and O_3 measurements by visible spectrometers, *J. Atm. Chem.*, 32, pp. 121-145.

Lambert, J.-C., M. Van Roozendael, J. Granville, P. Peeters, P.C. Simon, H. Claude and J. Staehelin, 1997: Comparison of the GOME ozone and NO_2 total amounts at mid-latitude with ground-based zenith-sky measurements, in *Atmospheric Ozone - Proc. 18th Quad. Ozone Symp., L'Aquila, Italy, 1996*, Ed. R.D. Bojkov and G. Visconti, Vol. I, pp. 301-304.

Lambert, J.-C., M. Van Roozendael, M. De Mazière, P.C. Simon, J.-P. Pommereau, F. Goutail, A. Sarkissian, and J.F. Gleason, 1999a: Investigation of pole-to-pole performances of spaceborne atmospheric chemistry sensors with the NDSC, *J. Atmos. Sci.*, **56**, 176-193.

Lambert, J.-C., P. Peeters, A. Richter, N. A. J. Schutgens, Y. M. Timofeyev, T. Wagner, J. P. Burrows, N. F. Elansky, A. S. Elokhov, P. Gerard, J. Granville, A. M. Gruzdev, D. V. Ionov, V. V. Ionov, R. B. A. Koelemeijer, A. Ladstätter-Weißenmayer, C. Leue, D. Loyola, U. Platt, O. V. Postylyakov, A. M. Shalamiansky, P. C. Simon, P. Stammes, W. Thomas, M. Van Roozendael, M. Wenig, and F. Wittrock, 1999b: ERS-2 GOME Data Products Delta Characterisation Report 1999 – Validation Report for GOME Data Processor Upgrade: Level-0-to-1 Version 2.0 and Level-1-to-2 Version 2.7, Ed. by J.-C. Lambert and P. Skarlas (IASB), 104 pp., 10-12.

Lambert, J.-C., J. Granville, M. Van Roozendael, J.-F. Müller, J.-P. Pommereau, F. Goutail, and A. Sarkissian, 1999c: A pseudo-global correlative study of ERS-2 GOME NO_2 data with ground-, balloon-, and space-based observations, in *Proc. European Symposium on Atmospheric Measurements from Space (ESAMS), ESA/ESTEC, The Netherlands, 18-21 January 1999*, ESA WPP-161, Vol. 1, 217-224.

Lambert, J.-C., P. Gerard, J. Granville, and M. Van Roozendael, 1999d: Delta characterisation of GOME level-2 data products version 2.7 using NDSC and HALOE correlative measurements, in *ERS-2 GOME Data Products Delta Characterisation Report 1999*, J.-C. Lambert and P. Skarlas (Eds.), 104 pp., 34-60.

Lambert, J.-C., J. Granville, F. Hendrick, M. P. Chipperfield, P. Gerard, F. Goutail, J.-F. Müller, J.-P. Pommereau, and M. Van Roozendael, 2001: Geophysical Consistency of Multi-Platform Global Measurements of Atmospheric Nitrogen Dioxide, *NDSC 2001 Symposium, Arcachon, France, 24-27 September 2001*, Paper 6-14, Abstract Book p. 166.

Lambert, J.-C, J. Granville, F. Hendrick, M. P. Chipperfield, and M. Van Roozendael, 2002: Diurnal cycle of stratospheric NO_2 and its effects on the interpretation of multi-platform measurements, to be submitted to *Adv. Space Res.*, 2002.

Loyola, D., S. Slijkhuis, and W. Thomas, 1999: New GDP settings for the spectral fitting of NO_2, Report to the GOME Science Advisory Group (March 1999).

Lumpe, J. D., C. E. Randall, D. W. Rusch, R. M. Bevilacqua, E. P. Shettle, L.L. Gordley, E. Thompson, H. K. Roscoe, and J. Slusser, 2002: Validation of POAM II Nitrogen Dioxide Data, *J. Geophys. Res.* (*in press*).

McKenzie, R.L., and P.V. Johnston, 1982: Seasonal variations in stratospheric NO_2 at 45°S, *Geophys. Res. Lett.*, **9**, 1255-1258.

Müller, J.-F., and G.P. Brasseur, 1995: IMAGES: A three-dimensional chemical transport model of the global troposphere, *J. Geophys. Res.*, **100**, 16 445-16 490.

Pommereau, J.-P., and F. Goutail, 1988: Ground-based Measurements by Visible Spectrometry during Arctic Winter and Spring 1988, *Geophys. Res. Lett.*, **15**, 891-894.

Randall, C.E., D.W. Rusch, R.M. Bevilacqua, K.W. Hoppel, and J.D. Lumpe, 1998: Polar Ozone and Aerosol Measurement (POAM) II stratospheric NO_2, 1993-1996, *J. Geophys. Res.*, **103**, 28361-28371.

Richter, A., M. Eisinger, F. Wittrock, S. Schlieter, A. Ladstätter-Weißenmayer, and J. P. Burrows, 1998: Zenith sky and GOME DOAS measurements of atmospheric trace gases above Bremen, 53°N: 1994 - 1997, in *Polar Stratospheric Ozone - Proc. 4th European Workshop, Schliersee 1997*, N.R.P. Harris, I. Kilbane-Dawe, and G.T. Amanatidis (Eds.), Air Pollution Research Report 66 (CEC DG XII), 482- 485.

Richter, A., A. Ladstätter-Weißenmayer, F. Wittrock, and J. P. Burrows, 1999: Delta characterisation of GOME data products – Detailed verification report, in *ERS-2 GOME Data Products Delta Characterisation Report 1999*, J.-C. Lambert and P. Skarlas (Eds.), 104 pp., 77-86.

Roscoe, H. K., and J. A. Pyle, 1987: Measurements of Solar Occultation: the Error in a Naïve Retrieval if the Constituent's Concentration Changes, *J. Atm. Chem.*, **5**, 323-341.

Roscoe, H.K., P.V. Johnston, M. Van Roozendael, A. Richter, A. Sarkissian, J. Roscoe, K.E. Preston, J.-C. Lambert, C. Hermans, W. De Cuyper, S. Dzienus, T. Winterrath, J. Burrows, F. Goutail, J.-P. Pommereau, E. D'Almeida, J. Hottier, C. Coureul, D. Ramon, I. Pundt, L.M. Bartlett, C.T. McElroy, J.E. Kerr, A. Elokhov, G. Giovanelli, F. Ravegnani, M. Premuda, I. Kostadinov, F. Erle, T. Wagner, K. Pfeilsticker, M. Kenntner, L.C. Marquard, M. Gil, O. Puentedura, M. Yela, W. Arlander, B.A. Kåstad Høiskar, C.W. Tellefsen, K. Karlsen Tørnkvist, B. Heese, R.L. Jones, S.R. Aliwell, and R.A. Freshwater, 1999: Slant column measurements of O_3 and NO_2 during the NDSC intercomparison of zenith-sky UV-visible spectrometers in June 1996, *J. Atmos. Chem.*, **32**, 281-314.

Russell, J.M. III, L.L. Gordley, J.H. Park, S.R. Drayson, W.D. Hesketh, *et al.*, 1993: The Halogen Occultation Experiment, *J. Geophys. Res.*, **98**, 10 777-10 797.

Timofeyev, Yu. M., D. V. Ionov, V. V. Ionov, A. M. Shalamiansky, N. F. Elansky, A. S. Elokhov, A. M. Gruzdev, and O. V. Postylyakov, 1999: Delta Characterisation of GOME Data Products with the Russian Monitoring Network, in *ERS-2 GOME Data Products Delta Characterisation Report 1999*, J.-C. Lambert and P. Skarlas (Eds.), 104 pp., 61-76.

Van Roozendael, M., C. Hermans, Y. Kabbadj, J.-C. Lambert, A.-C. Vandaele, *et al.*, 1995: Ground-Based Measurements of Stratospheric OClO, NO_2 and O_3 at Harestua, Norway (60°N, 10°E) during SESAME, in *Proc. 12th ESA Symp. on European Rocket and Balloon Programmes & Related Research, Lillehamer 1995*, ESA SP-370, 305-310.

Vaughan, G., H.K. Roscoe, L.M. Bartlett, F. O'Connor, A. Sarkissian, M. Van Roozendael, J.-C. Lambert, P.C. Simon, K. Karlsen, B.A. Kåstad Høiskar, D.J. Fish, R.L. Jones, R.A. Freshwater, J.-P. Pommereau, F. Goutail, S.B. Andersen, D.G. Drew, P.A. Hughes, D. Moore, J. Mellqvist, E. Hegels, T. Klupfel, F. Erle, K. Pfeilsticker, and U. Platt, 1997 : An intercomparison of ground-based UV-Visible sensors of ozone and NO_2, *J. Geophys. Res.*, **102**, 1411-1422.

Wagner, T., C. Leue, M. Wenig, and U. Platt, GOME NO_2 Validation Studies, in *ERS-2 GOME Data Products Delta Characterisation Report 1999*, J.-C. Lambert and P. Skarlas (Eds.), 104 pp., 87-97.

VI DOAS ISSUES

By Michel Van Roozendael, Vincent Soebijanta, Caroline Fayt,
and Jean-Christopher Lambert

Contact: M. Van Roozendael
Space Aeronomy Institute of Belgium (BIRA-IASB)
Avenue Circulaire 3, B-1180 Brussels, Belgium
E-mail: michelv at iasb.be

Investigation of DOAS Issues Affecting the Accuracy of the GDP Version 3.0 Total Ozone Product

M. Van Roozendael, V. Soebijanta, C. Fayt, and J.-C. Lambert

Space Aeronomy Institute of Belgium (IASB-BIRA)
Avenue Circulaire 3, B-1180 Brussels, Belgium

Abstract: This report is concerned with the quantification of DOAS-related error sources affecting the accuracy of the GDP version 3.0 total ozone product. The study addresses the following issues: choice of ozone absorption cross-section reference data, determination of GOME slit function, accuracy of wavelength calibration of both reference data and measured GOME spectra, determination of ozone absorption effective temperature, treatment of the Ring effect, and use of ozone air mass factor at a single wavelength (325 nm). An error budget is proposed whereby it is concluded that, owing to fortunate cancellation of several sources of bias in the retrieval process, systematic errors other than those related to climatological AMF issues (not treated here) should not contribute significantly to the bulk uncertainty of the product.

VI.1 INTRODUCTION AND OBJECTIVES

The GOME Data Processor (GDP) in all versions including the currently tested version 3.0 implements the widely used differential optical absorption spectroscopy technique (DOAS, Platt, 1994). The two main advantages of the DOAS approach are (1) its conceptual simplicity, and (2) the fact that heavy computations are not needed on-line (thus allowing fast processing). In addition the method is weakly sensitive to radiance calibration errors and to degradation problems since it works on restricted wavelength intervals (e.g. GOME total ozone is retrieved in the 325-335 nm window).

Working with the DOAS approach, we assume that in an optically thin atmosphere the mean optical path of scattered photons can be considered as independent of the wavelength within the relatively small spectral interval selected for the fit (325-335 nm for GDP O_3). As a direct implication, the retrieval process can be separated in two steps independent of each other: (1) the DOAS spectral fit to molecular absorption features which provides slant columns integrated along the effective path of nadir scattered photons, and (2) the conversion of these slant columns into vertical columns based on calculated air mass factors (AMFs).

The ozone slant optical density ($\tau_{O_3}^{slant}$) is related to the vertical column density (V_{O_3}) by the simple equation:

$$\tau_{O_3}^{slant} \cong \sigma_{O_3}(T_{eff}).V_{O_3}.AMF_{O_3}^{325nm}$$

where $\sigma_{O_3}(T_{eff})$ is the temperature-dependent ozone absorption cross-section, and $AMF_{O_3}^{325nm}$ a single wavelength effective AMF calculated according to the following expression:

$$AMF_{O_3}^{325nm} = \frac{\tau_{O_3}^{slant}}{\tau_{O_3}^{vertical}} = \left. \frac{-\log\left(I^{+O_3}/I^{-O_3}\right)}{\int \sigma_{O_3}^{z}\,[O_3]_z\,dz} \right|_{325nm}$$

where I^{+O_3} and I^{-O_3} are simulated nadir radiances calculated with and without ozone respectively.

The use single wavelength AMFs in the DOAS approach is convenient since heavy multi-wavelengths radiative transfer calculations are avoided. However this approximation is not strictly valid due to relatively large O_3 absorption at 330 nm, especially for elevated solar zenith angles (SZA>80°). Nevertheless it has been shown in previous studies (see e.g. Burrows et al., 1999a) that vertical columns can be retrieved with good accuracy (better than 2%) in most practical conditions, using AMFs calculated at the single effective wavelength of 325 nm. The main difficulty and still the likely main error source in the GDP O_3 product is the relatively large dependency of the AMF on both the O_3 total column and profile shape. In its current state, the GDP version 3.0 implements a column-resolved climatology of AMFs calculated from the available TOMS v.7 O_3 profile climatology. However validation results (see Chapter IV of the present issue) still show significant seasonalities in comparisons between the GOME and ground-based total ozone, that call for further analysis.

Main issues to be dealt with in future studies are the current limitations in our ability to account for clouds, aerosol and O_3 profile shape and total column dependencies in the AMF calculations. However at a presumably lower level of uncertainties, there are several additional effects that also require to be further analysed, including the most appropriate approach for dealing with Ring effect as well as the role of remaining inaccuracies in laboratory cross-sections and GOME spectra themselves. These particular DOAS related issues are addressed in the present chapter.

VI.2 OZONE ABSORPTION CROSS-SECTIONS AND GOME SLIT FUNCTION ISSUES

VI.2.1 Introduction

Among other factors, the accuracy of the slant column retrieval relies primarily on the accuracy and suitability of laboratory absorption cross-section data that are used as a reference in the retrieval process.

Ozone absorption cross-sections have been measured in the laboratory as a function of the wavelength and temperature by a number of groups (see Orphal (2002) for a comprehensive review of the available data sets). Recently some debate has been raised concerning the choice of the most suitable O_3 absorption cross-sections to be used for GOME retrieval. In the present section we focus on testing two well-established data sets of temperature dependent O_3 absorption cross-sections currently available from the literature, namely the data published by Burrows et al. (1999b) and those from Bass and Paur (1995).

VI.2.2 Cross-sections data sets

GOME Flight Model data (FM98)

These cross-sections have been measured at 5 different temperatures during the pre-flight calibration of GOME using the GOME flight model (Burrows et al, 1999b). These data hereinafter referred to as FM98, have been used in our study without any further adjustment other than wavelength shift corrections (see VI.2.5).

Bass and Paur data (B&P)

The temperature dependent O_3 cross-sections measured at high resolution (better than 0.025nm) by Bass and Paur (1985) have been recently recommended as a standard for use in remote-sensing applications (see Orphal, 2002). In contrast to FM98 data, the high resolution B&P data must be degraded to the lower resolution of GOME before being used in the retrieval process. To this aim the slit function of GOME must be evaluated with optimal precision, which is subject of the following section.

VI.2.3 Analysis of the GOME slit function in channel 2

Reference data are generally measured in the laboratory at higher resolution than in the field. This is e.g. the case for the Bass-Paur O_3 absorption cross-sections of which the resolution is quoted as better than 0.025 nm, while the resolution of GOME is of the order of 0.15 nm FWHM in channel 2. In order to properly adjust laboratory data to the resolution of the field instrument, a good knowledge of the instrumental slit function and of its eventual variation with the wavelength is needed. The convolution of laboratory data using inappropriate line shapes may result in poor DOAS fits and eventually in systematic errors in the retrieved slant columns due to spectral shape mismatch between reference data and atmospheric spectra. Good knowledge of the instrumental slit function is also a key parameter for the calculation of the undersampling cross-sections (Chance, 1998).

The GOME slit function has been measured at discrete wavelengths during the pre-flight calibration period and is documented in the GOME Users Manual (1995). More recently, the determination of the GOME slit function has been revisited by Caspar and Chance (1997) using a non-linear least-squares (NLLS) fit approach where the resolution of a highly resolved solar atlas (Kurucz, 1984; Chance and Spurr, 1997) was adjusted by convolution until best matching with GOME solar spectra. In this work the GOME slit function was assumed to be Gaussian in shape but its width was allowed to vary along the GOME channels. Results of this analysis applied to the channel 2 of GOME are displayed in Figure 49. One can see that the GOME slit function is optimal around 340 nm and rapidly degrades away from this wavelength especially towards the UV edge of the channel.

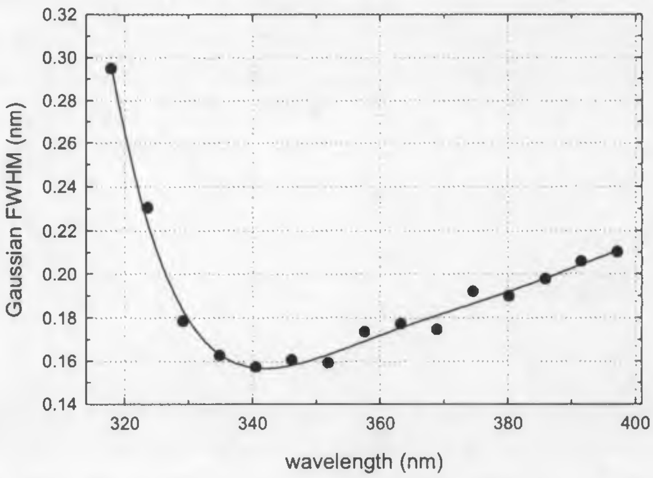

Figure 49 - **Wavelength dependence of the GOME slit function in channel 2, determined by NLLS fit to the Kurucz et al. solar spectrum (see Caspar and Chance, 1997, for a description of the method). The line-shape of the GOME slit function is assumed to be a Gauss function.**

If we take a closer look at the results of this analysis, as in Figure 50(a) where the residuals of the NLLS procedure are displayed, we see immediately that the quality of the fitting process is not constant over the channel. Clearly best residuals are found around 340 nm, while significantly poorer fits are obtained both at smaller and larger wavelengths. The larger residual features below 330 nm can be attributed to (1) the presence of low frequency spectral structures (mainly due to etalon effects) in GOME spectra not corrected by the level 0-1 processing, and (2) the existence of O_3 differential absorption structures in the solar reference atlas, both effects not fully eliminated by the high-pass filtering used in our analysis. At larger wavelengths, however, etaloning structures are largely reduced in size and should not interfere significantly. Therefore a possible explanation for the increasing residuals at large wavelengths could be, that the assumed (Gaussian) line shape is not fully appropriate to represent the GOME slit function at least in certain regions of channel 2.

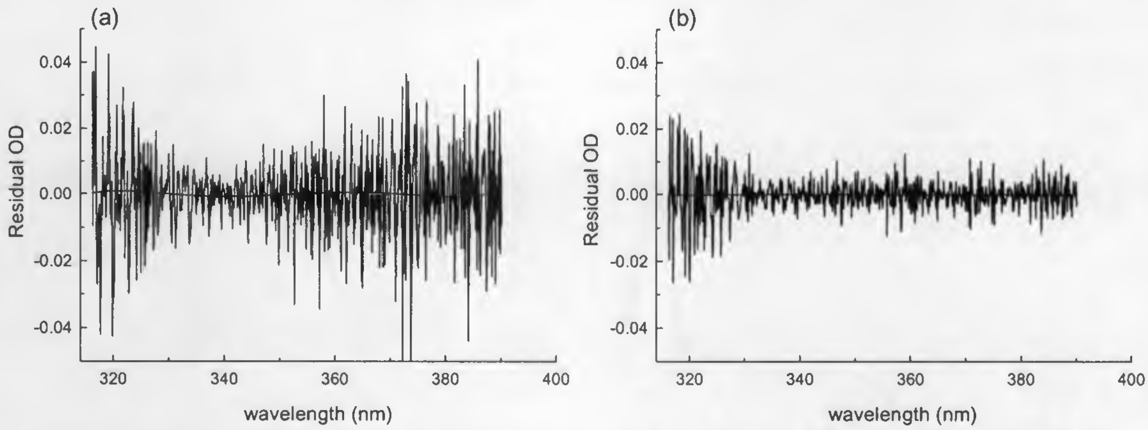

Figure 50 - **Residual of the NLLS fit procedure used to evaluate the width of the GOME slit function in channel 2. (a) Residuals obtained with a Gaussian profile, and (b) using an asymetric Voigt profile (see text).**

Since the high resolution structure of the solar spectrum is known from the literature with good precision, the instrumental slit function (F_{GOME}) can in principle be derived by simple de-convolution of the measured GOME solar irradiance:

$$F_{GOME} = \mathrm{I}_{\mathrm{Solar}}^{\mathrm{GOME}} \div I_{\mathrm{Solar}}^{\mathrm{high\ resolution}}$$

where the symbol ÷ stands here for the process of de-convolution, which can be achieved in practice by simple division in the complex Fourier space:

$$F_{GOME} = invFT\left[\frac{FT(\mathrm{I}_{\mathrm{Solar}}^{\mathrm{GOME}})}{FT(I_{\mathrm{Solar}}^{\mathrm{high\ resolution}})}\right]$$

Although mathematically straightforward, the method requires careful adjustment in practice to avoid noise amplification problems (see e.g. Press et al., 1991, p. 429). Despite these limitations, we were able to successfully derive, by de-convolution of measured GOME spectra, the instrumental line shape at 3 wavelengths of channel 2 (315, 340 and 380 nm). These line shapes are represented in Figure 51 in comparison to a (reference) Gaussian profile of 0.15 nm FWHM. Despite the residual noise, this analysis clearly reveals the existence of distortions in the GOME slit function along channel 2, which are related to limitations in the imaging quality of the GOME spectrometer.

After various attempts using different analytical functions, we found that the FFT-derived line shapes can be satisfactorily fitted throughout the whole channel 2 using a Voigt profile parameterised differently on each side of the line center (therefore allowing to account for the asymmetry of the GOME slit function). Using the Voigt line shape instead of the simple Gauss profile in the NLLS fit procedure significantly improves residuals as can be seen in Figure 50(b). The asymmetric Voigt profile requires the definition of 4 parameters, the Gaussian width and the ratio of the Lorentz and Gaussian widths on each side of the line center. The optimal parameterisation found in this work for GOME channel 2 is displayed in

Figure 52. This parameterisation has been used for optimal convolution of the Bass and Paur O_3 absorption cross-section.

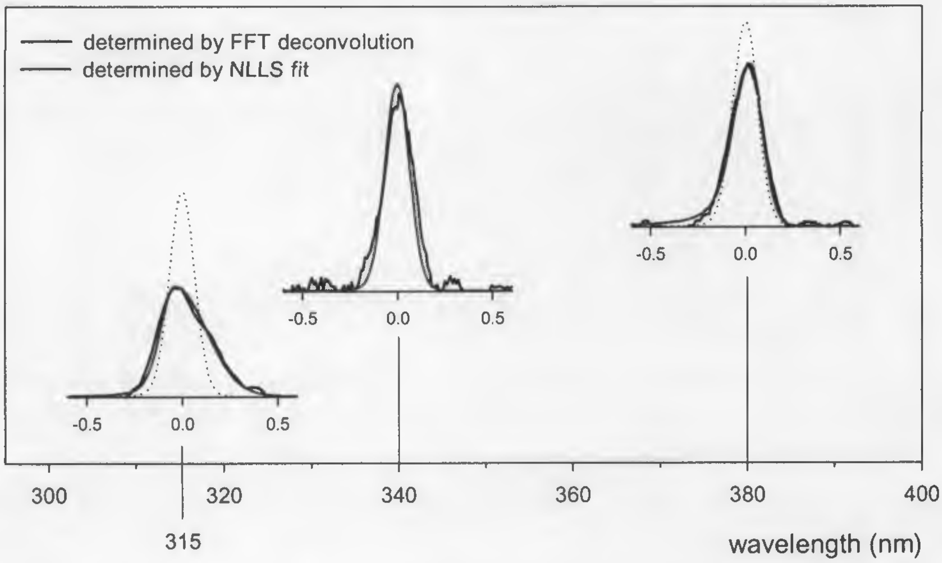

Figure 51 - **Slit function of the GOME instrument determined at 3 wavelengths of channel 2 using two methods: Fourier transform de-convolution (black lines), and NLLS fit to the Kurucz (1984) spectrum using and asymmetric Voigt line shape (red lines). A Gaussian profile of 0.15 nm FWHM is overlaid in each case for reference (dotted lines).**

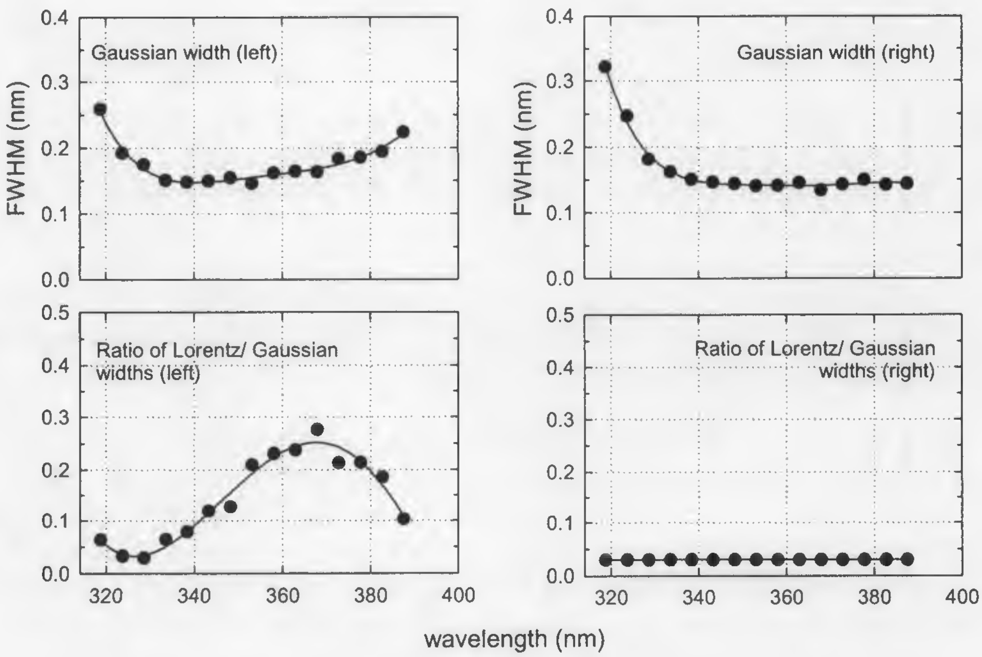

Figure 52 - **Characterisation of the GOME slit function in channel 2, using an asymmetric Voigt line shape defined by 2 independent parameters on each side of the line center. The ratio of Lorentz to Gaussian widths on the right-hand side is kept to a constant value (0.03). Solid lines are high order polynomial curves fitted to the measured points.**

VI.2.4 GOME data sets and DOAS settings

The subset of GOME data used in this study is for the most part the one selected for the GDP 3.0 delta-validation exercise (this issue). It includes approximately 2250 orbits selected for optimum coincidence with correlative ground-based stations of the NDSC. The data set covers the period from 1996 until 2001.

The evaluation programme used to retrieve O_3 slant columns and other parameters from GOME is the Windoas software of BIRA-IASB (Van Roozendael et al., 1999; see also http://www.oma.be/GOMEBrO/WinDOAS-SUM-210b.pdf). O_3 slant columns derived from the GDP and from Windoas have been shown to differ by less than a fraction of a percent when using identical settings (W. Thomas, private communication).

Unless otherwise stated, the DOAS settings applied here are those in use in the GDP 3.0. Main features are as follows:

Fitting interval: 323-335 nm

Wavelength calibration scheme: the wavelength calibration scheme adopted here is the one used by GDP where the wavelength grid of the orbit solar irradiance (as provided by the GDP LVL0-1 extractor) is used as the basic reference grid for all earthshine radiance spectra along the orbit as well as for cross-sections. In the DOAS procedure, the solar irradiance is further allowed to shift in order to compensate for the Doppler shift. It must be noted that with this calibration scheme, possible wavelength shifts of the earthshine radiance spectra along orbits due e.g. to changing thermal stress, are not compensated. As a (better) alternative we therefore recommend the following calibration scheme: use of the wavelength grid of the solar irradiance corrected for the Doppler shift of GOME solar measurements and, in the DOAS procedure, allow for shifting of the earthshine radiance spectra to compensate for both Doppler shift and pixel-dependent shifts.

Cross-sections:

- O_3: GOME FM98 or Bass & Paur, linear temperature dependence accounted for by fitting two cross-sections at different temperatures (see section VI.2.6), Bass and Paur data convoluted to GOME resolution using the wavelength-dependent asymmetric line shape derived in this work.
- NO_2: GOME FM98, shifted by +0.012 nm.
- Ring: calculated using GOME solar irradiance as input, and without molecular filling-in.
- Undersampling: cross-section calculated at DLR/DFD (S. Slijkhuis, private communication)

VI.2.5 Wavelength calibration issues

Wavelength calibration problems affecting both measured spectra and laboratory cross-sections can be a major source of error in DOAS retrievals (see e.g. Aliwell et al., 2002). In the case of GOME spectra, the situation is further complicated by the asymmetry of the slit function identified in section VI.2.3. Figure 53 displays shift values determined using our NLLS wavelength calibration procedure assuming, for the GOME slit function, either a simple Gaussian line shape or the asymmetric Voigt function derived in the previous section. These shifts can, in principle, be interpreted as a measure of the error on the initial wavelength calibration of GOME spectra. It is evident though that the results obtained depend on the assumptions made about the shape of the GOME slit function, and that this puts practical limitations on the achievable accuracy of the wavelength calibration for GOME. As shown in Figure 54, the DOAS fit to O_3 absorptions features is highly sensitive to spectral shift errors. In the typical example analysed here (GOME orbit 14329, pixel 1129), a shift of 0.004 nm was large enough to produce a change of 1% in the O_3 column and 3°K in the retrieved effective temperature. Clearly the important parameter for DOAS is the relative alignment of the cross-sections with respect to the measured spectra. Fortunately this relative alignment can in fact be easily derived from the DOAS fit itself with enough of accuracy. As long as the wavelength calibration of measured spectra can be considered as stable (not necessarily accurate), a constant shift can be applied for long-term processing. The validity of this assumption, which has been used with GDP 3.0, will be further investigated in section VI.3.

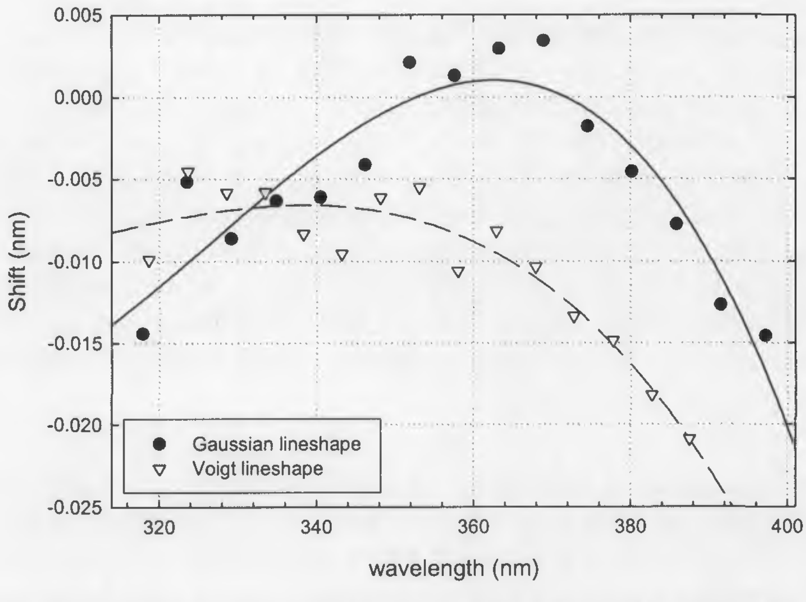

Figure 53 - **Shift values w.r.t. the GOME initial wavelength grid determined by the BIRA-IASB NLLS wavelength calibration procedure, assuming for the GOME slit function a Gaussian lineshape (black dots) and an asymmetric Voigt lineshape (open triangles).**

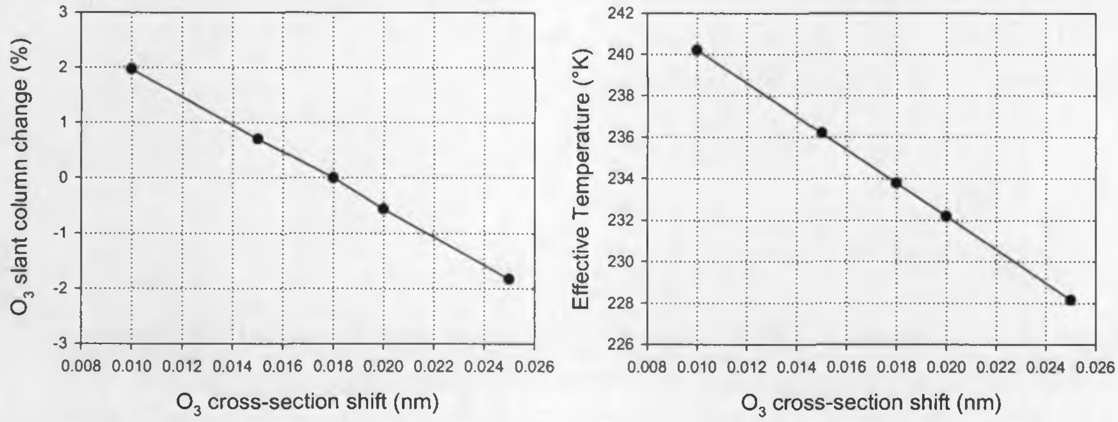

Figure 54 - **Sensitivity of DOAS-retrieved O_3 slant column and effective temperature, with O_3 absorption cross-section shift varying from 0.01 to 0.024 nm (FM98 O_3 cross-sections).**

VI.2.6 Ozone retrievals using GOME FM98 and B&P cross-sections at GOME resolution

In this section the B&P and FM98 absorption cross-sections have been tested as to their ability to provide stable DOAS fits results, working at the GOME nominal resolution. A convolution using the wavelength-dependent slit function determined in section VI.2.3 has been applied to the B&P data as part of the pre-processing procedure.

VI.2.6.1 Stability of results with respect to the choice of the temperature of the fitted cross-sections

One difficulty in retrieving total ozone in the Huggins bands is the temperature dependence of the O_3 cross-sections. In order to account for this dependency, the GDP version 3.0 uses an approach first suggested by A. Richter (U. Bremen), which consists in fitting a linear combination of two O_3 absorption cross-sections. We assume that the temperature dependent absorption cross-section can be linearly expanded as follows:

$$\sigma_{O_3}(T_{eff}) \cong \sigma_{O_3}(T_0) + \frac{\partial \sigma_{O_3}}{\partial T}.\Delta T \qquad (1)$$

Assuming linear dependency throughout the range of stratospheric temperatures, the first order derivative coefficient is a simple function of the difference between two cross-sections (e.g. measured at 241° and 221°K):

$$\frac{\partial \sigma_{O_3}}{\partial T} \approx \frac{1}{20}.(\sigma_{O_3}^{241} - \sigma_{O_3}^{221}) = \frac{1}{20}\Delta\sigma_{O_3} \qquad (2)$$

In the DOAS fitting procedure, two cross-section vectors are introduced ($\sigma_{O_3}^{241}$ and $\Delta\sigma_{O_3}$) from which two pieces of information are retrieved, the O_3 slant column (SCD) and the O_3 absorption effective temperature (T_{eff}):

$$\tau_{O_3}^{slant} \cong \sigma_{O_3}^{241}.C_1 + \Delta\sigma_{O_3}.C_2 \qquad (3)$$

with: $$\begin{cases} SCD_{ozone} = C_1 \\ T_{eff} = 241 + 20.\dfrac{C_2}{C_1} \end{cases}$$

As long as the assumption of linear dependency in temperature is satisfied, the retrieval should in principle be independent of the choice of the temperatures selected for use in the DOAS fitting procedure. In Figure 55, we have tested the respective behaviour of the GOME FM98 and B&P data sets from this point of view. One arbitrarily selected GOME spectrum (orbit 14329, pixel 1129) has been analysed using different combinations of absorption cross-sections. The temperatures used in each case are indicated on the x-axis in blue for GOME FM98 (bottom axis) data and in red for the B&P original data (top axis). For these tests, the wavelength shift applied to the O_3 cross-sections was included as an additional parameter in the DOAS fit. Four parameters have been used for diagnostic purposes: the RMS of the least-squares fit residuals, the percent change in O_3 slant column relative to the column obtained using the FM98 241-221°K combination (GDP 3.0 settings), the retrieved effective temperature and the O_3 cross-section shift.

Results obtained with the FM98 show excellent stability in the sense that the values retrieved for each test parameter are virtually independent of the couple of cross-sections selected for processing. This stability is not only an indication of the good overall consistency of the GOME FM98 data set, but it also provides confirmation that the assumption of linear dependency in temperature is largely adequate for the present purpose. In contrast, results obtained with the B&P data show a much larger variability. Differences in O_3 slant columns as large as 6% can be obtained depending on the combination of cross-sections selected for retrieval, mostly as a result of the instability of the derived effective temperatures. This can be seen more clearly in Figure 56, where O_3 slant column differences have been normalised at the same effective temperature (233.6°K), using the known temperature dependence of the O_3 differential cross-sections (3%/10°K). Looking at the fit residuals, the best combination seems to be obtained using B&P cross-sections at 243° and 218°K. In this case the DOAS fit converges towards an effective temperature smaller than the one derived from FM98, by about 7°K. Normalised at the same temperature, the difference in O_3 slant column less than +2%. If the B&P quadratic parametrisation is used instead of the original cross-sections, the scatter of the results is naturally decreased, but fitting residuals are clearly poorer. After normalisation for the temperature (Figure 56), the mean difference between parameterised B&P and FM98 data is +3.5%.

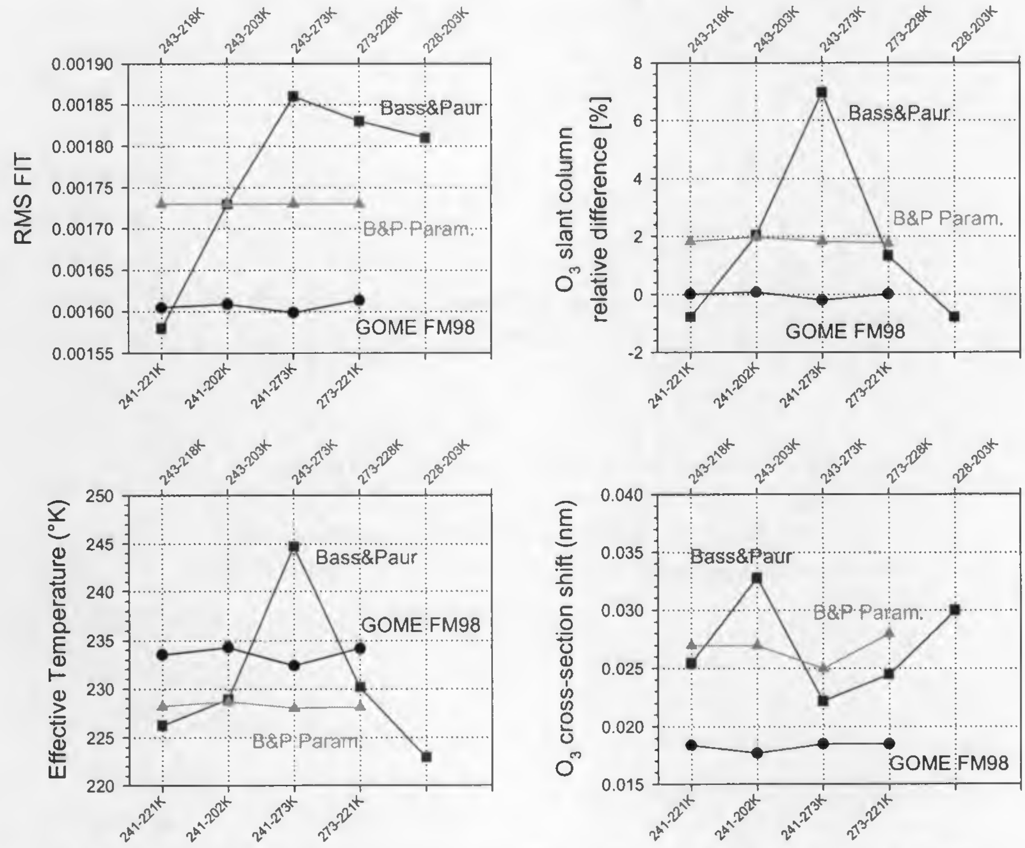

Figure 55 - **RMS fit residuals, O_3 slant column relative differences, effective temperatures and O_3 cross-section shifts obtained after DOAS retrieval of the pixel 1129 of the GOME orbit 14329, using different combinations of O_3 absorption cross-section data sets.**

Since several space and ground-based total ozone measuring instruments (like TOMS or Dobson and Brewer spectrometers) are based on the use of the B&P data, the question has often been raised whether the use of different O_3 cross-sections could be the source of a bias between GOME and other instruments. From our analysis, it might be concluded that GOME O3 retrieval using FM98 cross-sections might be underestimated by 2 to 3.5% relative to evaluations using B&P data. However it must be kept in mind that this difference only applies to differential cross-sections in the 325-335 nm region. Since other instruments usually use different inversion algorithms working in different wavelength regions, this conclusion cannot be safely generalised.

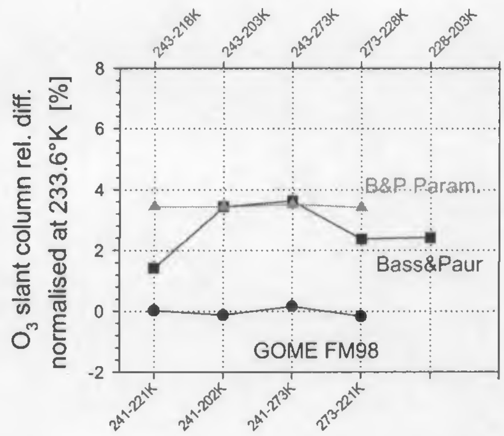

Figure 56 - **O_3 slant column difference relative to the evaluation obtained with cross-sections FM98 (221-241°K), when using different combinations of O_3 absorption cross-sections. All differences are normalised to the temperature of 233.6°K.**

VI.2.6.2 Stability of the DOAS retrieval along a complete orbit

For this exercise, spectra from GOME orbits 14329, 15621, 16928 and 18248 (all from 1998) have been processed for all pixels with solar zenith angles lower than 85°. The results are given in Figure 57, red dots denoting results obtained with the FM98 data (241° and 221°K) and blue dots results obtained with B&P data (243° and 218°K).

The parameters tested are the same as in the previous exercise: RMS fit residuals, O_3 cross-section shift, relative differences in O_3 slant columns and effective temperatures. They are plotted as a function of the GOME solar zenith angle (SZA) taken positive for the Northern Hemisphere and negative for the Southern Hemisphere, in order to display the systematic SZA dependency of the O_3 cross-section shift obtained with the FM98 data (see red dots in the lower left plot). This variation likely results from a drift in the GOME wavelength registration due to changing thermal stress on the instrument along the orbit (in the GDP procedure the calibration of the earthshine radiance is taken as constant, while the solar irradiance is shifted). The tight compactness of the O_3 shift values obtained with the FM98 data is again a good indication of the stability of the DOAS fit when using the GOME cross-sections. Results of Figure 57 also confirm the overall better quality/stability of the DOAS fits using FM98 instead of B&P data (smaller residuals, better stability of the derived shift values). As already discussed in the previous section, the difference in O_3 column is small (<1%) but not representative since larger differences may be obtained depending on the choice of temperature vectors used in the retrieval (cf. Figure 55).

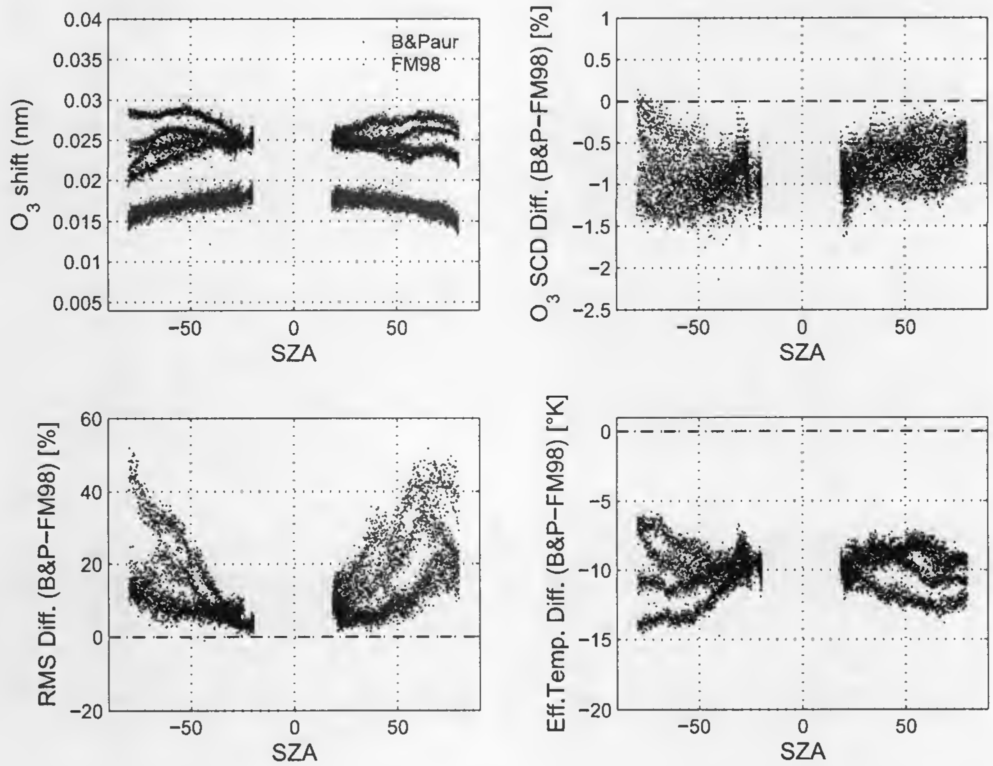

Figure 57 - **Ozone cross section shift, relative difference in RMS fit residuals, ozone slant column differences and effective temperature differences obtained after analysis of the GOME orbits 14329, 15621, 16928 and 18248 using the GOME FM98 and the Bass & Paur oaonz absorption cross-sections.**

VI.2.7 O_3 retrievals using GOME FM98 and B&P cross-sections at reduced resolution

One possibility suggested for retrieval of O_3 is to reduce the effective spectral resolution. A recent study for the METOP/GOME-2 mission (J.B. Burrows, private communication), has shown that increasing the FWHM up to about 0.6 nm can be acceptable in the Huggins band without much loss of information. The main aim in degrading the resolution is to reduce the sensitivity of the retrieval to line shape uncertainties.

Test results shown in Figure 58 have been obtained using spectra degraded to the resolution of 0.6 nm FWHM. They definitely do not show any improvement compared to initial tests at GOME nominal resolution (Figure 55), at least in terms of DOAS fit stability using B&P data. On the other hand, the relative differences in O_3 slant columns after temperature normalisation, displayed in Figure 59, tend to be more constant around +2.5% for B&P relative to FM98.

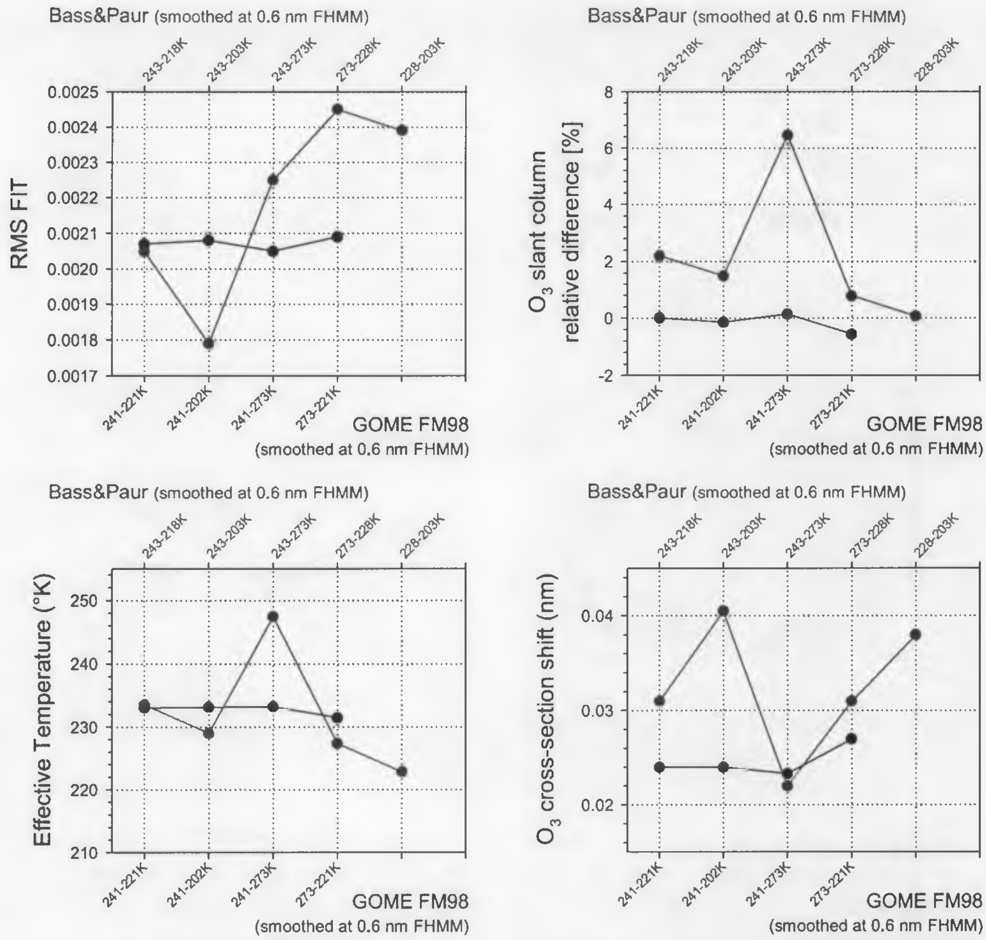

Figure 58 - **Same as** Figure 55, **but using data degraded to the resolution of 0.6 nm FWHM.**

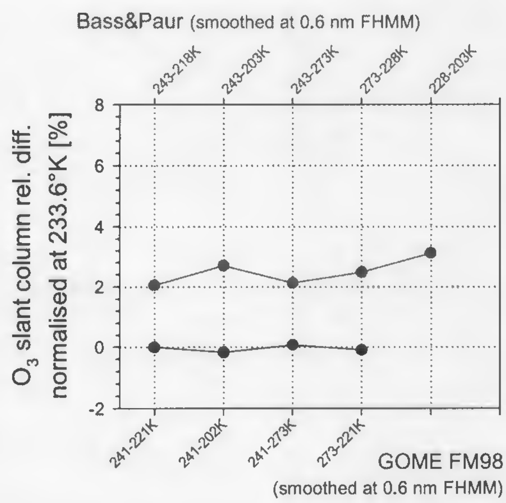

Figure 59 - **Same as** Figure 56, **but using data degraded to the resolution of 0.6 nm FWHM.**

VI.2.8 Impact of the solar I_0 effect

The so-called solar I_0 effect first pointed out by P.V. Johnston (unpublished results, see also Aliwell et al., 2002) is responsible for small distortions in measured atmospheric absorption features (in comparison with laboratory absorption cross-sections), which are related to the highly structured nature of the solar spectrum. To date, the impact of the solar I_0 effect on the GOME total ozone retrieval has been considered negligible compared to other error sources. However, this issue has been raised again recently within the GSAG.
A technique to correct for the I_0 effect has been proposed by Johnston (see Aliwell et al., 2002 for a description), which consists in a special treatment applied to the cross-sections when convolving them at the resolution of the measuring instrument. In order to evaluate the impact of the I_0 effect on GOME O_3 retrieval, we have generated two sets of absorption cross-sections (GOME FM98 241K and 221K) with and without I_0 correction. In order to allow application of the solar-I_0 correction procedure, the original FM98 cross-sections were first de-convolved using a FFT method similar to the one described in section VI.2.3. The resulting data were used to process our four working GOME orbits (14329, 15621, 16928 and 18248). As shown in Figure 60, the use of solar-I_0 corrected cross-sections improves residuals (10-15% at large solar zenith angles) while effective temperatures are lowered by about 2.5°K. The impact on the retrieved O_3 slant columns is well below 1%.

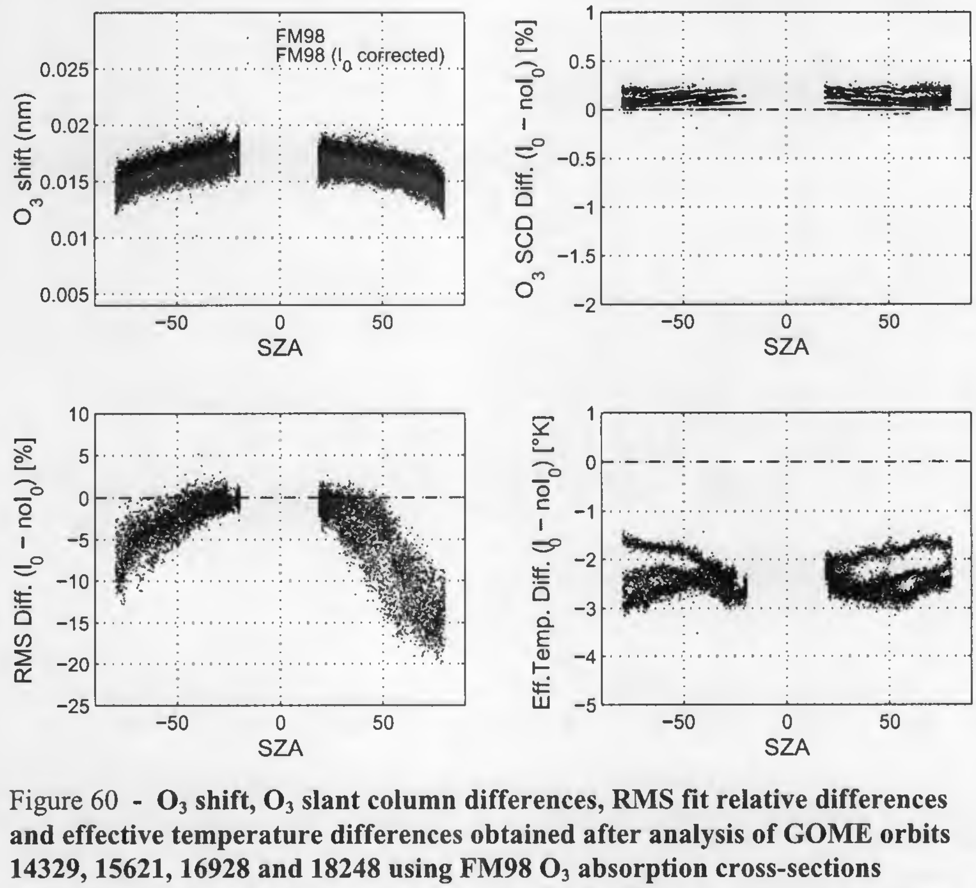

Figure 60 - **O_3 shift, O_3 slant column differences, RMS fit relative differences and effective temperature differences obtained after analysis of GOME orbits 14329, 15621, 16928 and 18248 using FM98 O_3 absorption cross-sections convoluted with and without correction for the I_0 effect. Accounting for the solar-I_0 effect improves residuals and produces smaller effective temperatures.**

VI.3 LONG-TERM STABILITY OF THE GOME SPECTRAL CALIBRATION

The need to shift in wavelength the O_3 absorption cross-sections to correct for uncertainties in the absolute calibration of both GOME and laboratory data has been discussed earlier in this report (section VI.2.5). DOAS fit residuals are extremely sensitive to this shift (cf. Figure 57), which also means that the position of the measured O_3 absorption features can be used in principle to test the stability of the wavelength calibration of GOME spectra. Indeed, as long as the wavelength registration of GOME spectra is stable in time, we expect the O_3 cross section shift to remain constant.

In previous versions of GDP, GOME spectra were calibrated in wavelength using lamp measurements. With GDP version 3.0, a new calibration method has been introduced based on a cross-correlation algorithm where the position of the solar lines measured by GOME is adjusted by comparison with a reference solar spectrum.

Our idea here was to test both methods using the atmospheric ozone absorption as a wavelength reference. To this aim we have processed the series of GOME orbits selected for the current GDP3.0 Delta Validation campaign (this issue) using DOAS settings where the shift of the O_3 cross-section (FM98) was switched on in the least-squares fitting procedure. Results of this analysis performed using level-1 data calibrated with and without the cross-correlation method are displayed in Figure 61. One can conclude that for the limited wavelength region concerned by the O_3 fitting (325 – 335 nm) the lamp calibration for now offers the best stability with fluctuations generally smaller than 0.003 nm. The situation might change in the future after optimisation of the cross-correlation algorithm, currently in progress at DLR. From the present analysis, we recommend to apply a shift of +0.017 nm to the GOME FM98 cross-sections, instead of the 0.012 nm shift currently implemented in GDP.

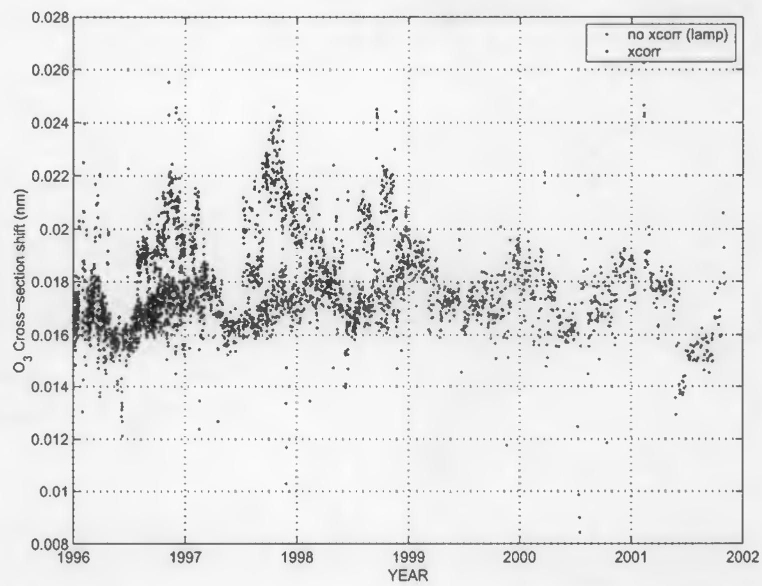

Figure 61 - **1996-2001 time evolution of the orbit-averaged O_3 cross-section shift determined from analysis of the GOME orbits selected for the GDP3.0 Delta-Validation exercise (this issue). Results obtained using GOME level-1 data calibrated with (blue dots) and without (red dots) the cross-correlation method are compared.**

VI.4 DOAS-FITTED O_3 ABSORPTION EFFECTIVE TEMPERATURE

In previous versions of the GOME data processor, the ozone absorption temperature was forced using the MPI 2D temperature climatology (Bruehl and Crutzen, 1991). With GDP version 3.0 another algorithm has been implemented whereby temperature dependent absorption cross-sections are allowed to adjust themselves to the measured O_3 absorption features. As a result, GDP 3.0 simultaneously retrieves two ozone parameters: the O_3 slant column and an associated effective absorption temperature. In principle this approach should represent an improvement in the data processing since the need for extra information on the atmospheric temperature is avoided. We may also expect from the algorithm a better adjustment to real atmospheric variability. However the method also requires some validation in order to assess the geophysical consistency of the retrieved temperatures and verify that no significant bias can be introduced at this stage of the inversion.

Attempts to validate the GDP effective temperatures on individual orbits have already been presented in Chapter IV. In this paper, a climatological approach has been adopted in order to try and derive more representative figures. O_3 absorption effective temperatures appropriate to the geometry of GOME observation have been calculated based on the time/latitude O_3 profiles climatology of Fortuin and Kelder (1998) combined to the ECMWF temperature climatology of Trenberth (1992) for the troposphere and CIRA for the stratosphere. These reference climatological temperatures are represented for each month as a function of the latitude in Figure 62 (black lines), where there are also compared to effective temperatures derived from DOAS analysis of GOME data (red squares and green triangles).

GOME data presented here were obtained from analysis of the complete GDP 3.0 delta validation set of 2257 orbits covering the 1996-2001 period, followed by the calculation of monthly-averages sorted in bins of 10° latitude. The plots show that latitudinal structures of the monthly averaged temperatures are well captured by the DOAS evaluations. This demonstrates that the method is sensitive to actual variations of the atmospheric temperature. However it is also clear that, in comparison to climatological values, retrieved GOME DOAS temperatures tend to be systematically overestimated by approximately 10K when using the GDP 3.0 analysis settings (red squares). Taking into account the known temperature dependency of the O_3 differential cross-sections in the 325-335 nm region (3%/10K), the inferred temperature bias directly translates in a 3% systematic overestimation of the O_3 slant column. What are the possible reasons for this problem? The role of the solar-I_0 effect has already been pointed out in section VI.2.8. Although it can explain a positive bias of about 2.5K, this is not enough to resolve the present discrepancy. Uncertainties in the O_3 cross-sections can be considered as unlikely since the accuracy of the temperature measurements in the laboratory were quoted to better than 1°K by Burrows et al. (1999b). Problems or shortcomings in the data evaluation: we have tested a series of potential sources of distortion that may be responsible for a temperature offset. Undersampling effect, NO_2 cross-section alignment, non-linearity of the O_3 cross-section temperature dependence were all found to have a negligible impact on the retrieved effective temperatures. As already noted in section VI.2.5, one important parameter is the wavelength alignment of the O_3 cross-sections. In GDP 3.0, a shift of +0.012 nm was applied to the FM98 data while our analysis suggests that a shift 0.017 nm would be more appropriate (see section VI.3). Using this latter shift instead of the nominal GDP 3.0 settings improves the situation as can be seen in Figure 62 (green triangle). Nevertheless a positive bias of about 5K persists after optimisation of the wavelength alignment suggesting that another error source is still playing. As will be shown in the next section, inappropriate handling of the Ring effect is likely to be responsible of a large part the remaining bias in the retrieved temperatures.

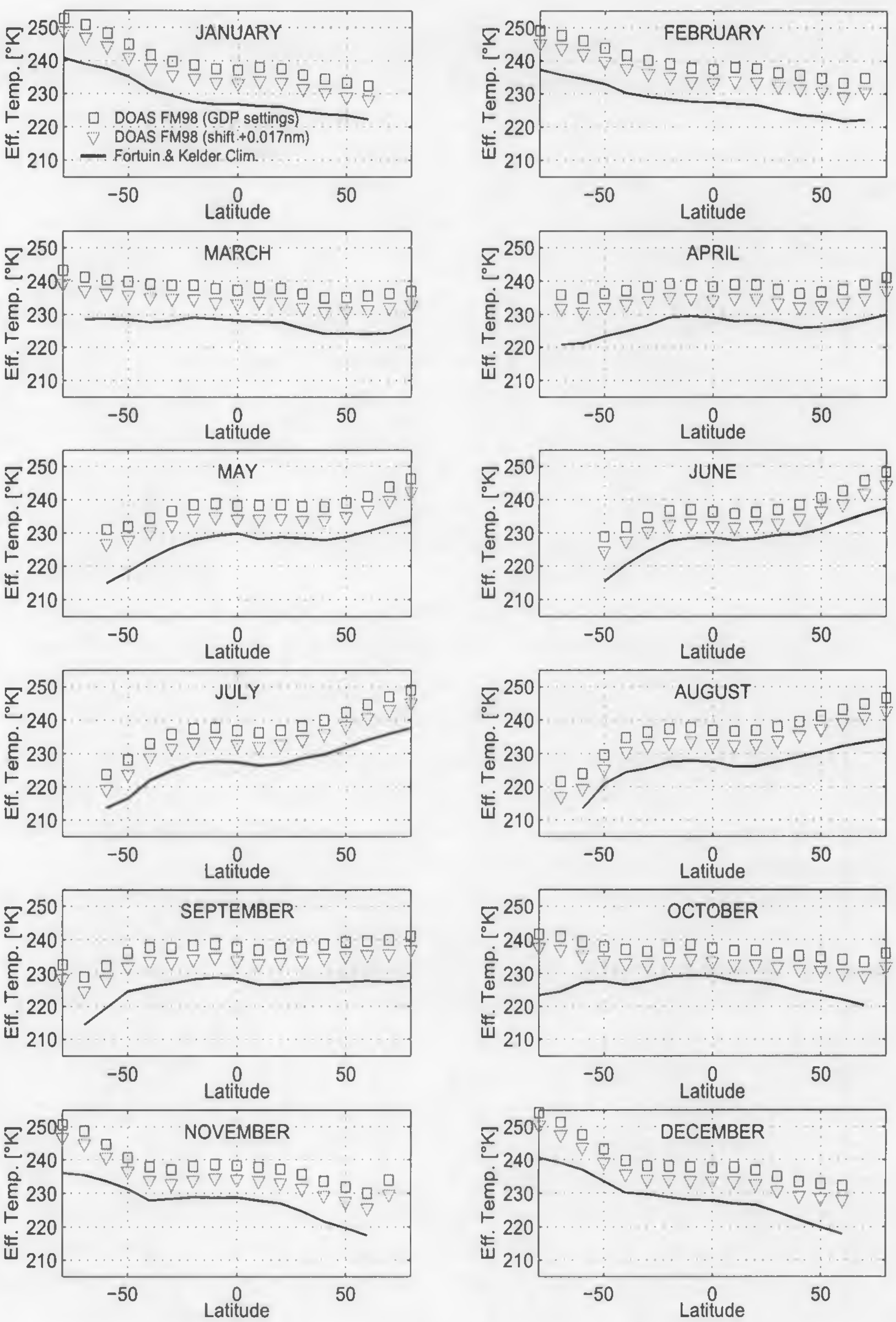

Figure 62 - **Monthly averaged O_3 absorption effective temperatures derived from DOAS analysis of GOME spectra (1996-2001 average), compared to climatological values calculated using the Fortuin and Kelder (1997), Trenberth (1992) and CIRA atmospheric databases. DOAS retrieved temperatures using GDP 3.0 analysis settings are systematically overestimated by 5 to 10°K. Part of the discrepancy can be resolved when the wavelength alignment of the O_3 cross-section is optimised.**

VI.5 TREATMENT OF THE RING EFFECT

VI.5.1 Introduction

The Ring effect first described by Grainger and Ring (1962) manifests itself by a reduction of the depths of absorption lines in scattered light observations compared to direct sunlight. Several studies (e.g. Fish and Jones, 1995; Joiner et al., 1995; Vountas et al., 1998, Sioris and Evans, 1999) have demonstrated that the main process responsible for the observed filling-in of absorption lines is Rotational Raman scattering (RRS) by molecular O_2 and N_2. One can therefore consider that in any scattered light observation, the measured intensity includes one (highly structured) elastic component due to Rayleigh and Mie scattering, plus one (much broader) inelastic component due to Raman scattering:

$$I^{\text{measured}} = I^{\text{elastic}} + I^{\text{Raman}} \quad (1)$$

In first approximation, the impact of Raman scattering on atmospheric (DOAS) observations can be understood according to the following simple considerations. Accounting for an effective atmospheric attenuation (τ_a) that applies to both elastic and inelastic components (but with different contributions due to the different mean optical paths of elastically and inelastically scattered photons), we can write:

$$I^{\text{measured}} = I_0^{\text{solar}} \exp(-\tau_a) + I^{\text{Raman}} \exp(-\tau_a') \quad (2)$$

In this equation, the parameter of interest for O_3 retrieval is τ_a, i.e. the slant optical density that would be measured in the absence of Raman scattering. In DOAS-type retrievals, the Ring effect is usually treated as a pseudo-absorber through use of calculated or measured Ring cross-sections. A rigorous and direct approach to account for the effect of Raman scattered light in DOAS evaluations has been proposed by Vountas et al. (1998). It relies on radiative transfer simulations of nadir radiances including and excluding Raman scattering. The method is based on the calculation of Ring cross-sections that are added to the usual DOAS equation according to the following expression, which directly derives from Eq. (2):

$$\log(I^{\text{measured}}) = \log(I_0^{solar}) - \tau_a + \log\left(\frac{I^{total}}{I^{elastic}}\right) \quad (3)$$

The last term $< \log\left(\frac{I^{total}}{I^{elastic}}\right) >$ is the calculated Ring cross-section, the amplitude of which can be fitted together with molecular absorption cross-sections in the DOAS procedure. Ideally this modelled Ring cross-section should be calculated using realistic atmospheric parameters (O_3 profile, solar zenith angle, albedo, cloud top height etc.). However due to the complexity and of this approach for operational processing, a simpler method is usually used in DOAS evaluations of O_3 as well as other trace species. One assumes (see e.g. Chance and Spurr, 1997), that a good approximation of the Ring cross-section can be obtained from calculation of a source term for Raman scattering (I^{Raman}) derived by simple convolution of the solar spectrum with Raman cross-sections. With this method the need for radiative transfer simulations including Raman scattering is claimed to be avoidable. Most importantly one also assumes that the filling-in of telluric absorption lines (molecular Ring effect) is negligible in comparison to the filling-in of the intense solar lines, and one uses the following equation as a basis for DOAS evaluations:

$$\log(I^{measured}) = \log(I_0) - \tau_a + \frac{I^{Raman}}{I_0} \quad (4)$$

where the Ring cross-section is given by the ratio I^{Raman}/I_0. This is the method currently implemented in the GDP for total ozone retrieval. An alternative procedure where a scaled Raman spectrum is directly fitted to the Intensities has also also been used by some authors:

$$I^{measured} - I^{Raman} = I_0 \cdot \exp(-\tau_a) \quad (5)$$

Both of these approaches appear to work well in practice in the sense that they allow good correction of the high frequency Ring structures observed in scattered light spectra. However if we take a closer look at the equations written above, it can be easily seen that neither Eq. (4) nor Eq. (5) can be satisfactorily derived from Eq. (2). In effect a more correct derivation of the DOAS equation, written in terms of a simple solar-convolved Ring cross-section (I^{Raman}/I_0), can be obtained by the following expansion of Eq. (2) where small terms have been linearised:

$$\log(I^{measured}) = \log(I_0) - \tau_a \left\{ 1 - \frac{I^{Raman}}{I_0} (1 - \frac{\tau_a'}{\tau_a}) \right\} + \frac{I^{Raman}}{I_0} \quad (6)$$

This equation is to our point of view very instructive because it shows in a simple way how Raman scattering influences DOAS retrievals of trace species when a simple Fraunhofer Ring cross-section is used. One can see that Raman scattered light is not only responsible for the well-known Ring structures (the I^{Raman}/I_0 term), but that it also perturbs the molecular absorption features. This effect is globally known from the literature as molecular Ring since its net effect is to reduce the depth of atmospheric absorption features. In fact the molecular Ring term (the expression between brackets) must be understood as the superposition of two effects: (1) an offset term which simply results from the presence of the Raman light and can be seen in first approximation as a simple stray-light term. This term is directly related to the fraction of Raman light available. Since Raman scattering typically contributes several percents to the total scattered light, its magnitude is clearly not negligible. (2) since the Raman scattered light is essentially generated at low altitude in the atmosphere, it also encounters some molecular absorption on its way up to the satellite and this absorption effectively acts in reducing the size of the offset term by the ratio τ_a'/τ_a .

VI.5.2 Radiative transfer simulations and test of various Ring correction approaches

In this section, we describe results of model simulations performed with the aim to test on realistic cases the considerations developed above and also to better evaluate the likely impact of Ring effect on the accuracy of the current GDP total ozone product.

Over the last few years, radiative tranfer models have been designed both in Europe and in the US, which allow computation of RRS in a multi-layer scattering atmosphere (Joiner et al., 1995; Vountas et al., 1998; Spurr, 2002). The tool used in our study is SCIATRAN version

2.1, a radiative transfer model developed at the University of Bremen in the context of the SCIAMACHY experiment (Rozanov et al., 1997; Buchwitz et al., 2000; Vountas et al., 1998; see also the web site http://www.iup.physik.uni-bremen.de/sciatran) for radiance calculations in the UV, visible and near-infrared ranges, with capabilities for inclusion of Raman scattering processes. In order to investigate the sensitivity of the effects to different typical atmospheric conditions, the simulations have been performed using as input the climatological O_3 and temperature models previously described in section VI.4. Top-Of-Atmosphere (TOA) radiances have been generated with and without Raman scattering, in the wavelength range 320-340 nm. The simulations included O_3 absorption (with a quadratic parameterisation of its temperature dependence) as well as NO_2 absorption, and were performed at solar zenith angles typical of GOME measurements at the grid points of the 2D time-latitude climatological model.

Simulated radiances were inverted using the BIRA-IASB Windoas software with analysis settings representative of those used by the GDP version 3.0 (see section VI.2.4). In the present analysis, we have focused on the determination of the possible range of errors on the retrieved O_3 slant columns when using different methods to account for the Ring effect. Following the developments described in section VI.5.1, reference slant columns (τ_a) are those that would be retrieved in the absence of Ring effect. Therefore they were derived by DOAS analysis of nadir radiance spectra calculated without Raman scattering in the model. In the plots below the relative differences in O_3 slant column calculated by reference to the pure-elastic case are presented. Results are sorted according to months and latitudes, separately for Northern and Southern hemispheres.

Six different Ring correction methods have been tested, most of them having been used or proposed in the literature. Note that our purpose at this stage is not to propose any new or optimised method for Ring effect correction. This will be the subject of further studies to be performed as part of our upcoming activities on O_3 retrieval algorithms:

1. "Exact method": Ring cross-sections calculated according to Eq. (3) using model calculations fully consistent with the simulated scenes (atmospheric profiles and solar zenith angle).
2. "Fraunhofer Ring correction": Ring cross-sections calculated by simple convolution of the solar source spectrum according to Chance and Spurr (1997) as used in the GDP 3.0
3. "Intensity fitting correction": Raman source spectrum fitted to intensities according to Eq. (5)
4. "Eigenvectors approach": use of two Ring cross-section eigenvectors derived by Principal Component Analysis of a set of Ring cross-sections calculated for different atmospheric conditions and solar zenith angles. This method was proposed by Vountas et al. (1998)
5. "Fixed Molecular Ring": single Ring cross-section calculated according to Eq. (3) but for a fixed atmosphere and solar zenith angle.
6. "SZA-dependent Ring": Ring cross-section calculated for a fixed atmosphere but as a function of the solar zenith angle. The appropriate Ring vector is interpolated on-line from the input matrix at the solar zenith angle of the fitted spectrum.

The results of the synthetic data analysis are displayed in a series of plots presented in between Figure 63 and Figure 70, which we will now discuss in more details.

For the analyses of Figure 63, Ring cross-sections fully consistent with synthetic spectra calculations were used (method 1). These results are essentially given for reference since, according to Eq. (3), a perfect correction of the Ring effect is expected in this case, as confirmed to a very large extent in the figure. The points where small deviations are found correspond to conditions of large solar zenith angle where the DOAS approximation tend to fail.

Results shown in Figure 64 and Figure 65 are representative of the situation encountered with the GDP and most other GOME total ozone retrieval algorithms (e.g. GOFAP) where a simple solar-convolved Ring cross-section is used (method 2). They illustrate the error due to neglecting the impact of molecular filling-in terms in Eq. (6). In all simulations, the differences show a marked seasonality, which can be easily understood as resulting from the variation of the $\tau_a^{'}/\tau_a$ ratio, mainly related to solar zenith angle changes. This solar zenith angle dependency is clearly apparent in Figure 65. Note the compact relationship obtained between the O_3 slant column errors and the SZA, despite the fact that our simulations covered a broad range of O_3 columns and profile shapes. If confirmed by further simulations, this relative in-sensitivity of the molecular Ring effect to the actual O_3 profile might be used to design a simplified yet accurate Ring effect correction.

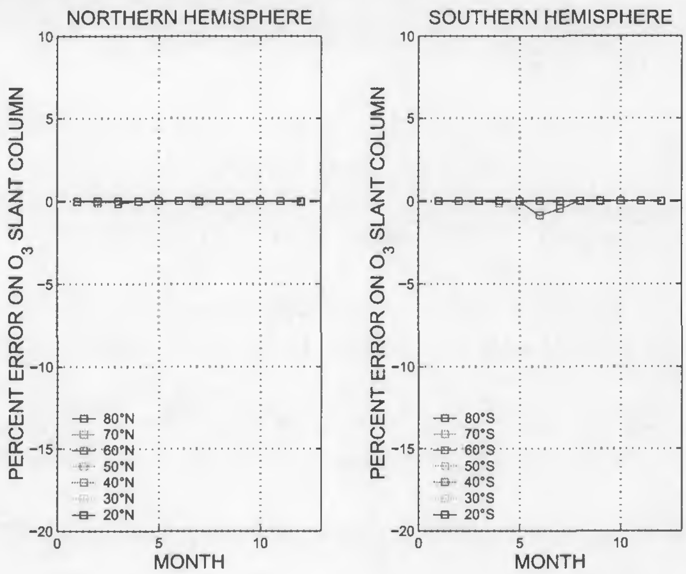

Figure 63 - **Calculated error on O_3 slant column retrieval, as applied to synthetic spectra including Raman scattering. Method 1: The Ring effect is corrected using calculated cross-sections fully consistent with forward model simulations.**

In Figure 66, the error on O_3 slant column retrievals when using a simple (Fraunhofer-only) Raman correction directly applied to measured intensities (method 3) is presented. As can be seen, O_3 columns are overestimated with this method; a behaviour that was to be expected from Eq. (5), since telluric absorptions in the Raman term are neglected in this simple approach.

Results displayed in Figure 67 have been obtained using two Ring cross-sections, derived from Principal Component Analysis of a set of Ring cross-sections calculated for a series of different atmospheric conditions (method 4). The two first eigenvectors of this analysis basically correspond respectively to the solar- and molecular- Ring contributions in the total Ring effect, as described by Vountas et al. (1998). Note the very large instability of the results obtained using this 2 Ring-eigenvectors approach for total ozone retrieval, especially at large solar zenith angles. In our opinion, the likely reason for this behaviour is related to the fact that the second Ring eigenvector, being very close in shape to the O_3 absorption cross-section, strongly correlates with the latter, which produces the observed large bias.

As illustrated in Figure 68, the average bias of the O_3 slant column retrieval can be somewhat reduced, still using a single Ring cross-section, if this cross-section is calculated including molecular absorption for one given standard reference. However the errors obtained in this case still show significant seasonal dependencies. Again, as can be seen in Figure 69, these seasonal signatures mostly result from a solar zenith angle dependency.

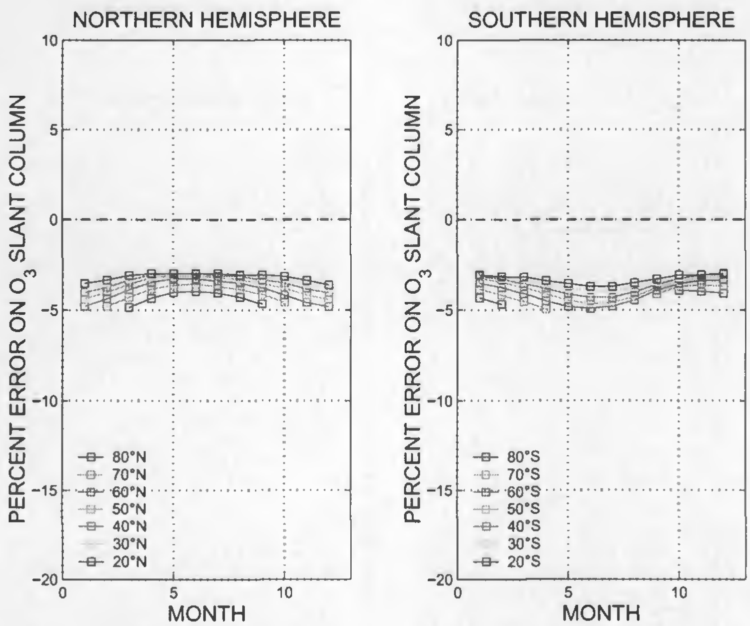

Figure 64 - **Calculated error on O_3 slant column retrieval, as applied to synthetic spectra including Raman scattering. Method 2: Ring effect is corrected without accounting for molecular filling-in, according to Chance and Spurr (1997). These results are representative for the settings used in GDP 3.0.**

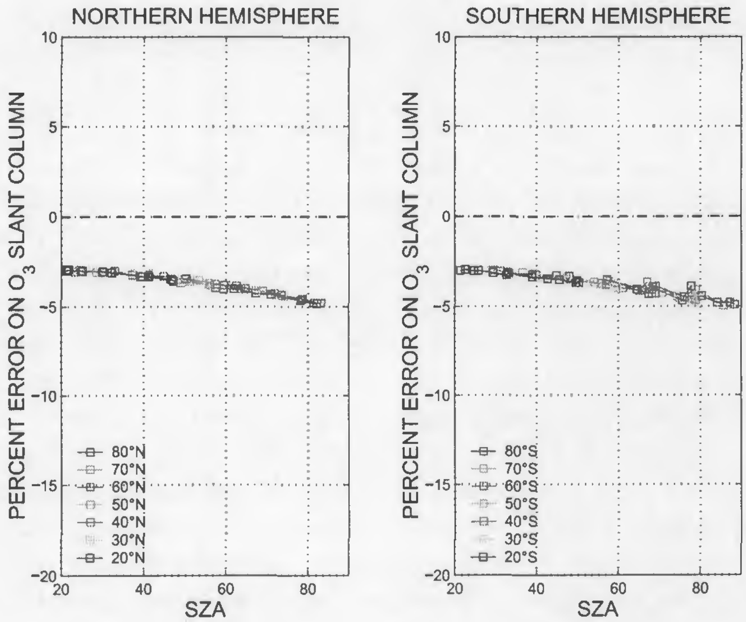

Figure 65 - **Same as in** Figure 64, **except that the results are plotted as a function of the solar zenith angle.**

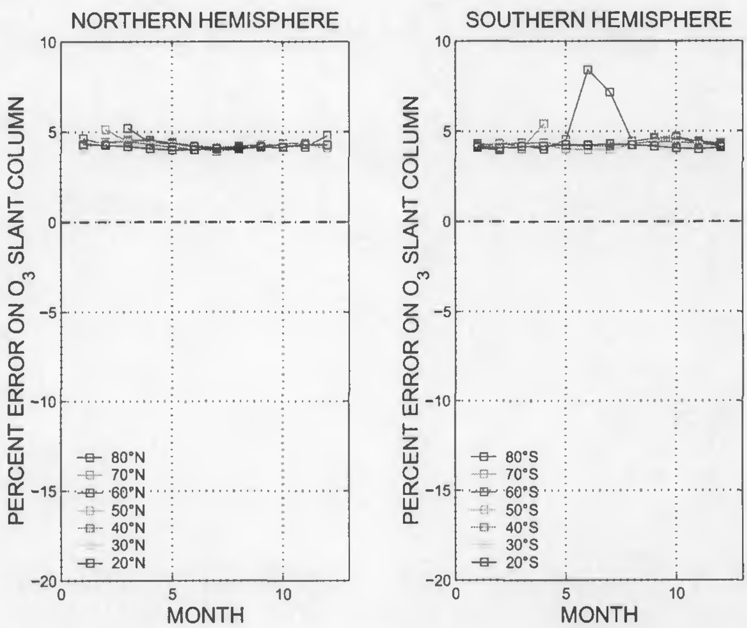

Figure 66 - **Calculated error on O_3 slant column retrieval, as applied to synthetic spectra including Raman scattering. Method 3: The Ring effect is treated by direct fitting of a Raman source spectrum to the nadir intensities, following Eq. (5).**

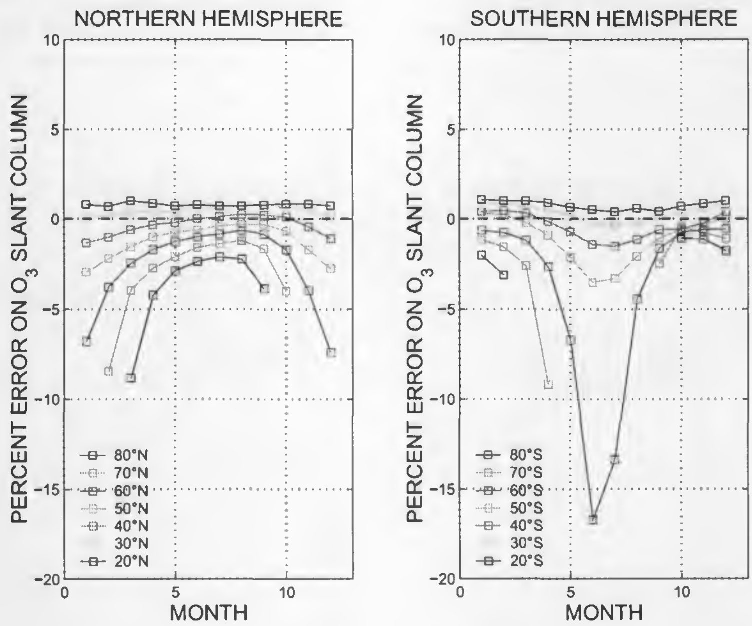

Figure 67 - **Calculated error on O_3 slant column retrieval, as applied to synthetic spectra including Raman scattering. Method 4: The Ring effect is treated by fitting 2 Ring cross-section eigenvectors, according to Vountas et al. (1998).**

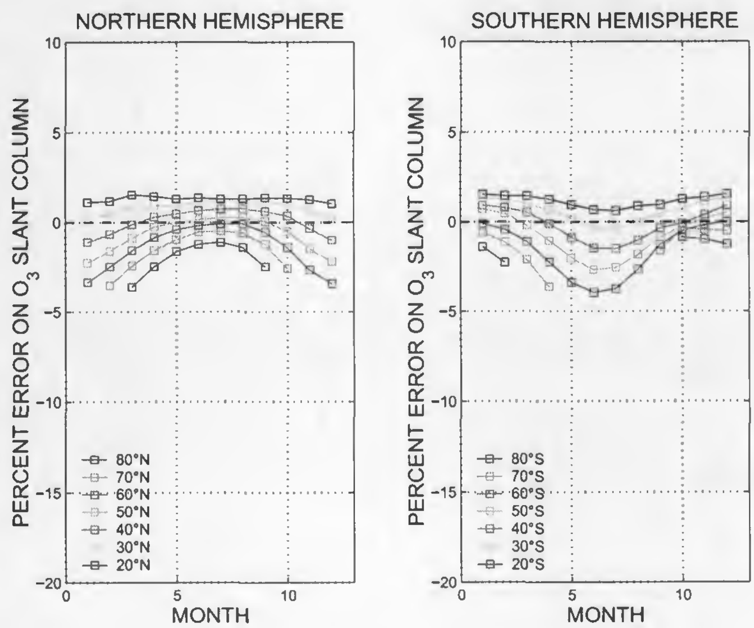

Figure 68 - **Calculated error on O_3 slant column retrieval, as applied to synthetic spectra including Raman scattering. Method 5: The Ring effect is corrected using a single cross-section (fixed atmosphere and solar zenith angle) calculated from radiative transfer simulations including Raman scattering.**

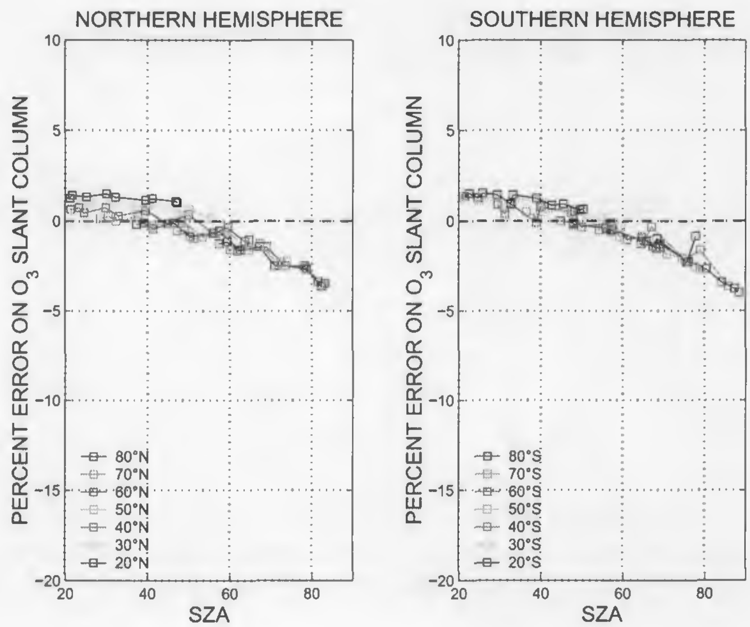

Figure 69 - **Same as in** Figure 68**, except that results are plotted as a function of the solar zenith angle.**

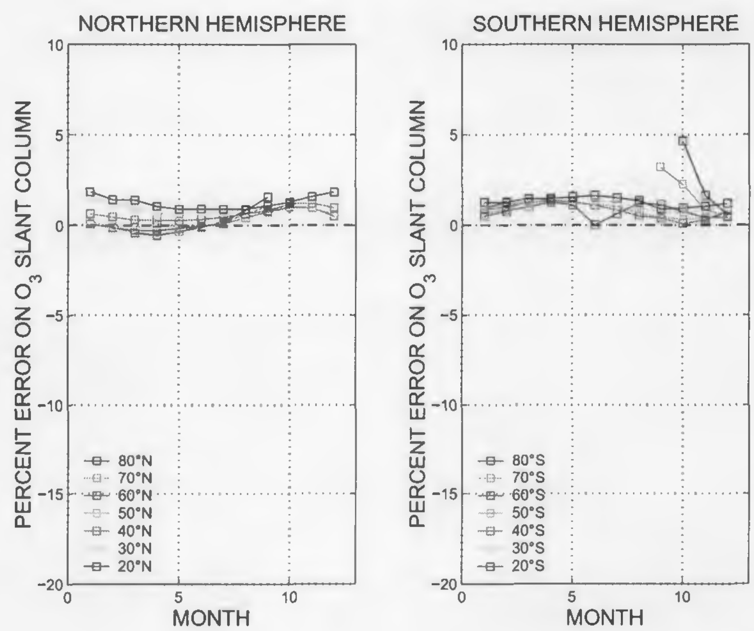

Figure 70 - **Calculated error on O_3 slant column retrieval, as applied to synthetic spectra including Raman scattering. Method 6: The Ring effect is corrected using solar zenith angle dependent cross-sections including molecular filling-in, calculated for a fixed atmospheric model (50°N, June).**

For the last exercise described in this study (method 6), a modified DOAS algorithm has been used where a two-dimensional matrix of Ring cross-sections (wavelength-SZA) could be introduced as an input to the fitting procedure. In this evaluation, the Ring cross-section was adjusted on each analysed spectrum according to the current GOME solar zenith angle, by interpolation through the Ring matrix. With this procedure the solar zenith angle dependency of the Ring cross-section could be accounted for, while the dependency on the atmospheric profiles was still neglected. The results (Figure 70) show a significant error reduction in comparison to other methods, with differences in O_3 SCD relative to the pure elastic case reaching 1-2% for most grid points of the Fortuin and Kelder climatology (excluding winter-spring Antarctic conditions). Further reduction of the errors would require explicit treatment of the O_3, P, T profile dependency of the Ring effect (as for Method 1). Additional simulations would also be needed to investigate the impact of clouds, albedo and maybe other atmospheric parameters. Such work definitely goes beyond the purpose of the present study.

VI.5.3 Application to GOME total ozone evaluations

The encouraging results obtained using a simple solar zenith angle dependent Ring correction (Method 6) have lead us to test its implementation on real GOME measurements. To this aim, the 2250 Delta-validation orbits have been reprocessed using our modified Ring correction plus a set of I_0-corrected and re-aligned GOME FM98 O_3 cross-sections (see sections VI.2.8 and VI.3). These results were binned according to month and latitude as described in section VI.4. Revised effective temperatures and the relative differences between our improved evaluation and the original GDP 3.0 O_3 slant columns are displayed in Figure 71 and Figure 72 respectively.

In comparison to results shown in Figure 62, one can seen that the inclusion of molecular Ring effect in the DOAS evaluation together with the use of properly aligned and I_0-corrected O_3 cross-sections leads to a reduction of the retrieved effective temperatures, down to a value that, in average, matches much better the temperatures derived from the climatology. At this stage, the exact role played by molecular Ring on the determination of effective temperatures is not clearly understood, but one may guess that part of the temperature bias in GDP 3.0 O_3 slant columns comes from the non-inclusion of O_3 absorption features in the Ring effect. The net impact of not-including molecular Ring effect might therefore be a complex one, since resulting from the combination of a negative bias due to disregard of molecular terms in Eq. (6) (cf. also Figure 64) and a positive bias due to overestimation of the effective temperature. In effect the differences in O_3 slant columns between our (hopefully improved) evaluation and the original GDP 3.0 are relatively small (less than 2%) with the exception of high latitude regions where larger differences can be found.
This analysis sets up a budget of DOAS-related errors that likely affect the accuracy of the GDP 3.0 total ozone product. There remains a last DOAS issue concerned by the present study, which we now consider.

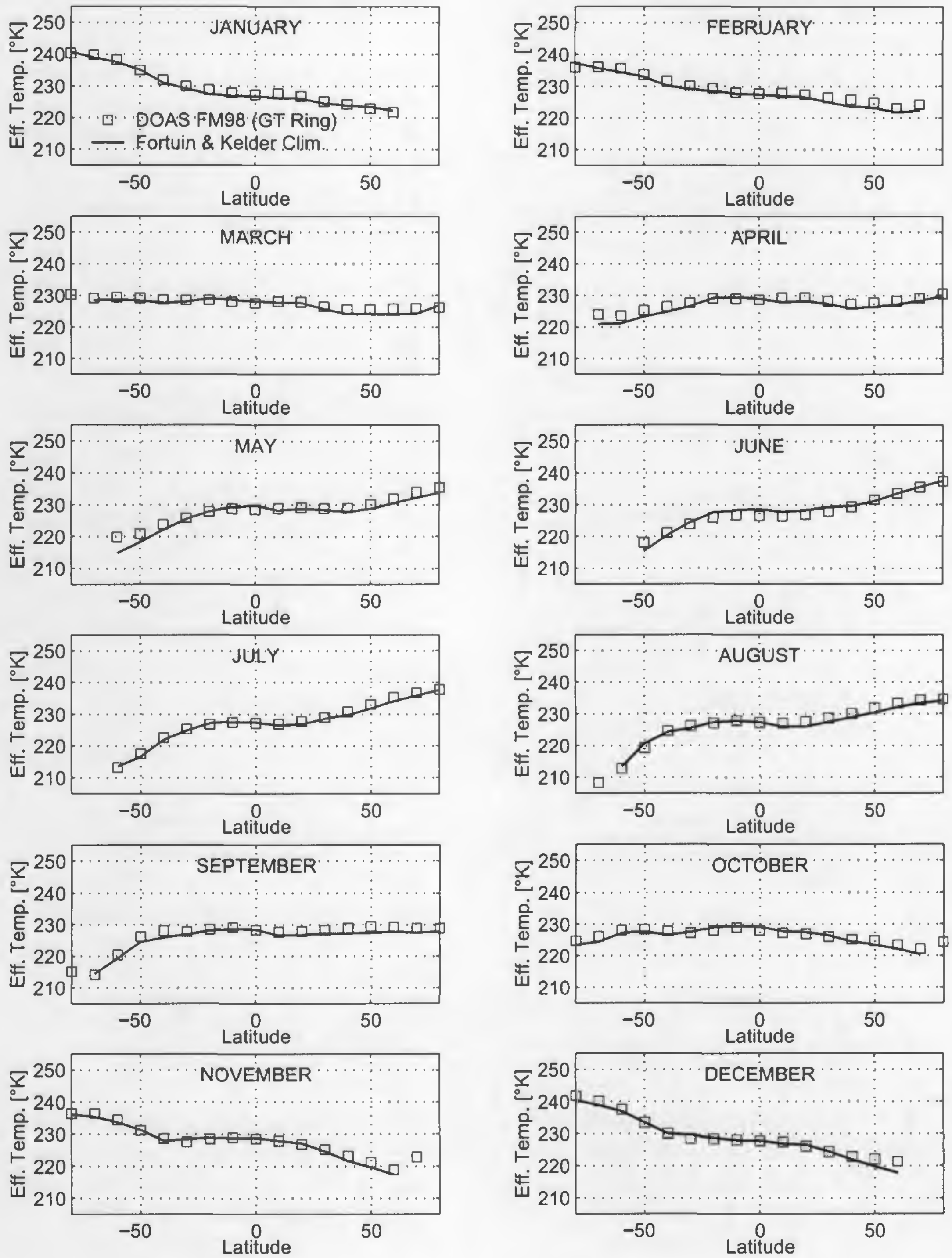

Figure 71 - **Monthly averaged effective temperatures derived from DOAS analysis of GOME spectra (1996-2001 average), compared to climatological temperatures calculated using the using the Fortuin and Kelder (1997), Trenberth (1992) and CIRA atmospheric data. The DOAS evaluation used for this analysis includes a Ring effect correction that accounts for molecular Ring effect and its solar zenith angle dependency (see text).**

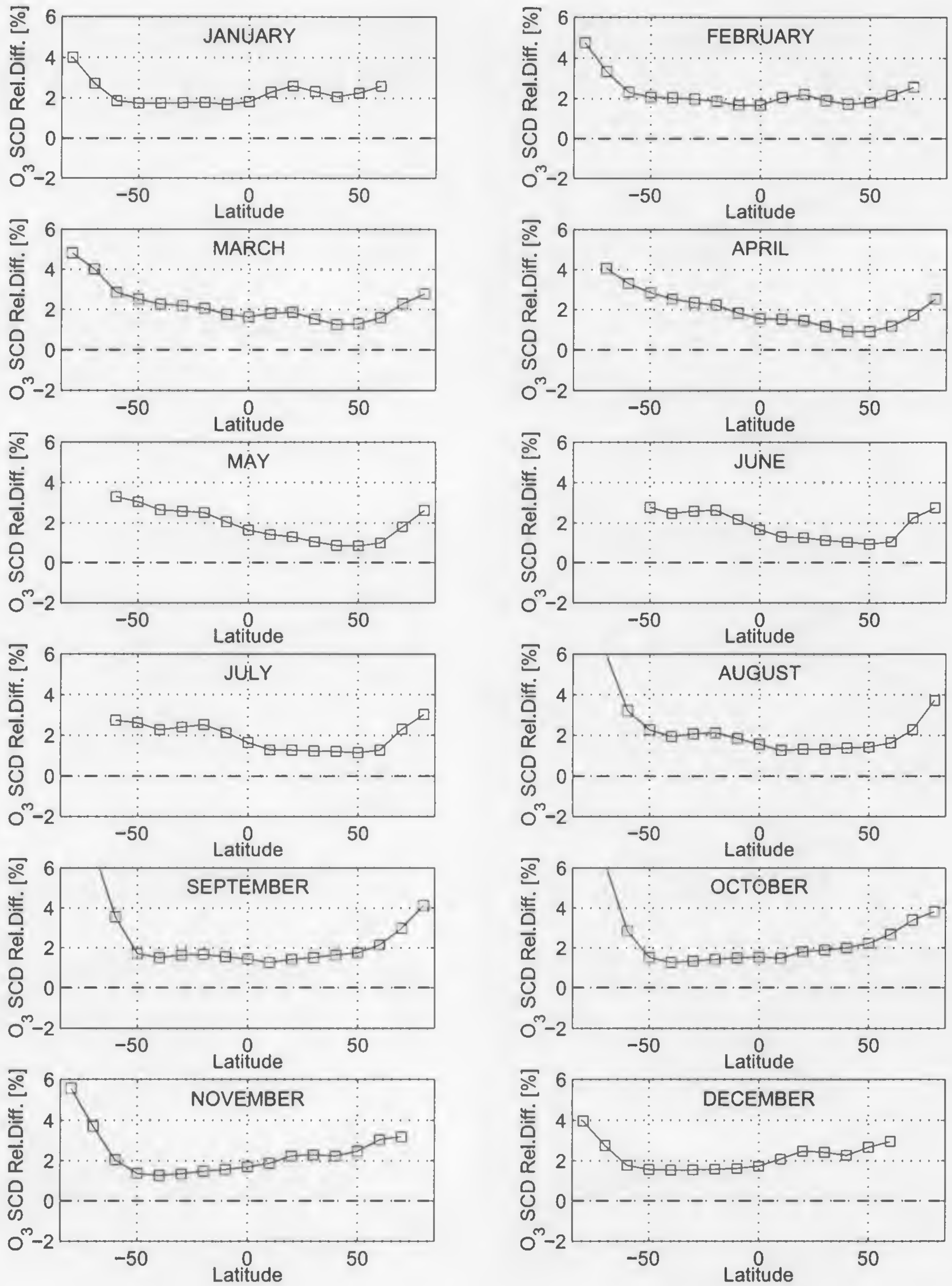

Figure 72 - **Percent differences in O_3 slant columns retrieved from GOME using a DOAS algorithm accounting for molecular Ring and its solar zenith angle dependence, relative to the original GDP 3.0 O_3 slant column product.**

VI.6 USE OF A SINGLE WAVELENGTH AMF

As explained in the introduction of this report, the DOAS approach used in the GDP is based on the assumption that the radiative transfer properties of the atmosphere can be considered as wavelength-independent over the width of the fitting window selected for processing. In other words, this means that the spectral fitting to absorption features can be decoupled from radiative transfer calculations. For total ozone retrieval in the 325-335 nm range, a single air mass factor (AMF) is computed at the most representative wavelength of 325 nm (Burrows et al., 1999a).

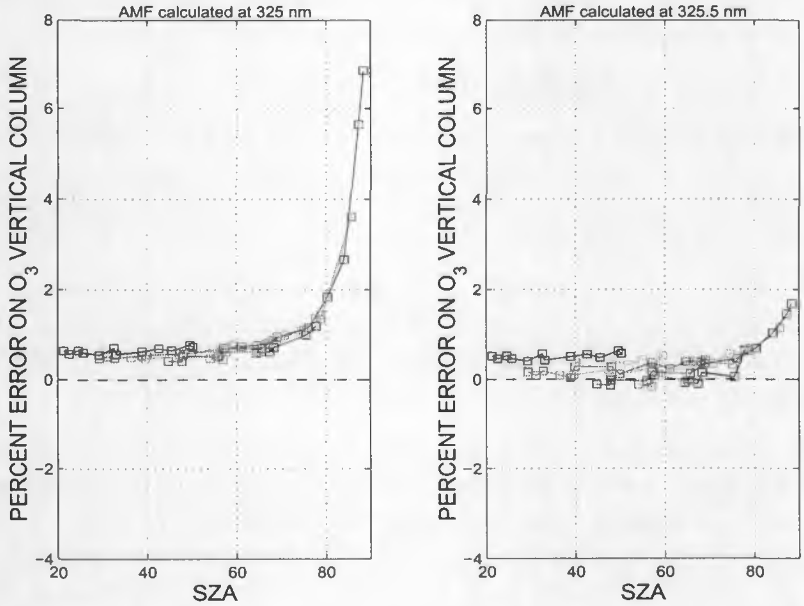

Figure 73 - **Calculated error on O_3 vertical columns retrieved from DOAS evaluations in the 325-335 nm region, using a single AMF calculated at 325 nm (left panel) and 325.5 nm (right panel).**

In order to test the validity range of this assumption, we have generated a set of synthetic spectra without Raman scattering (based on the same inputs and tools as for previous simulations), from which O_3 vertical columns have been retrieved by DOAS using consistent AMFs calculated at 325 nm. The errors on these synthetic retrievals are displayed in Figure 73, as a function of the solar zenith angle. One can conclude in agreement with previous studies that the error introduced by the single-AMF approximation remains small (less than 2%) up to a solar zenith angle of about 80°. However significantly larger deviations seem to be found above 80° SZA, independently of the atmospheric profiles used. It is interesting to note that this (positive) error is opposite in sign to the (negative) error one would expect from the non-inclusion of molecular Ring effect at large SZA (see previous section): another example of possible error cancellation in a simplified DOAS retrieval scheme.

Repeating the same exercise using AMFs calculated at 325.5 nm instead of 325 nm seems to improve the situation at large solar zenith angles, to the expense of more variability at higher solar elevations. This result might have to be considered in future evaluations using a DOAS approach.

VI.7 CONCLUSION

In this report, the impact of several DOAS-related error sources that may affect the accuracy of the GDP 3.0 total ozone product has been investigated. Addressed issues include:

- The choice of the best-suited temperature-dependent O_3 absorption cross-sections data set for GOME retrieval;
- The optimal determination of the GOME slit function in channel 2;
- The accuracy of the wavelength calibration of both reference data and measured GOME spectra;
- The determination of the O_3 absorption effective temperatures;
- The treatment of the Ring effect;
- The estimation of errors due to the use of a single-wavelength AMF.

Main findings can be summarised as follows:

- O_3 slant columns retrievals in the 325-335 nm region using the O_3 cross-section data set measured at five different temperatures with the GOME flight model (Burrows et al., 1999b) show a higher degree of internal consistency compared to equivalent retrievals using the Bass and Paur (1985) cross-sections.
- O_3 retrievals in the 325-335 nm region using Bass and Paur cross-sections give slant columns approximately 2% larger compared to retrievals using the Burrows et al. cross-sections. However, it must be stressed that this difference cannot be considered as representative for the Huggins bands as a whole, meaning that it cannot be used to conclude about possible bias between GOME and other instruments (e.g. TOMS) due to the use of different cross-sections, since these instruments also use different retrieval algorithms working at different wavelengths.
- The lineshape of the GOME slit function, analysed by Fourier transform de-convolution and by NLLS fit to a high resolution solar spectrum, is found to be strongly asymmetric on both edges of channel 2. This limits the absolute accuracy of the GOME wavelength calibration.
- An inappropriate wavelength shift applied to the O_3 cross-sections in GDP 3.0 produces a positive bias of 5°K of the retrieved effective temperature, corresponding to a systematic positive bias of 1.5% of the O_3 slant columns.
- The absence of correction for the solar I_0 effect is likely to be responsible for a systematic overestimation of the effective temperatures by 2.5°K.
- Non-inclusion of molecular absorption in the Ring correction scheme used by GDP 3.0 is likely to be responsible for a systematic negative bias of the slant columns, of about 5-10%, partly compensated by a 5°K overestimation of the effective temperature.
- The use of a simple DOAS approach based on air mass factors calculated at 325 nm is likely to be responsible for a positive bias of the retrieved columns at elevated solar zenith angles (larger than 80°).

To summarise, the budget of the systematic error sources identified in this study is given in Table 1. It is striking that, when combined together, the various errors tend to cancel to a remarkable degree. It must be stressed however that the values quoted in Table 1 are only meant to be representative of bulk effects. We do not expect the cancellation to be perfect in all cases, and it is therefore likely that some of the effects reported here contribute at least partly to the cyclic signatures (seasonal, meridian, SZA and column dependences) identified in validation results.

Table 1 - Summary of DOAS-related systematic error sources identified as affecting total ozone retrievals by the GDP version 3.0

Systematic error source	**Percent error**	
	SZA < 80°	**SZA > 80°**
O_3 absorption cross-sections	± 2 %	± 2 %
Wavelength shift of the O_3 cross-sections	+1.5 %	+1.5 %
Solar I_0-effect	-0.2 %	-0.2 %
Direct impact of non-inclusion of molecular Ring	- 3 %	- 5 %
Indirect impact of non-inclusion of molecular Ring on effective temperature determination	+1.5 %	+1.5 %
O_3 AMF calculated at 325 nm	+1 %	+5 %
Total bias (excluding cross-section error)	0.3 %	2.3 %

VI.8 REFERENCES

Aliwell, S.R., M. Van Roozendael, P.V. Johnston, A. Richter, T. Wagner, B. Arlander, J.P. Burrows, D.J. Fish, R.L. Jones, J.-C. Lambert, I. Pundt, K. K. Tornkvist, Analysis for BrO in zenith-sky spectra : An intercomparison exercise for analysis improvement, J. Geophys. Res., 2002 (in press).

Bass, A.M., and R.J. Paur, The Ultraviolet Cross-Sections of Ozone, I, The Measurements, in: Atmospheric Ozone, edited by C. S. Zerefos and A. Ghazi, pp. 606-610, D. Reidel, Norwell, Mass., 1985.

Bruehl, C., and P. Crutzen, The MPI Two Dimensional Atmospheric Model – Trace Gas Profiles, Max-Planck Institute for Chemistry, Mainz, Germany, private communication, 1991.

Buchwitz, M., et al., User's Guide for the Radiative Transfer Program SCIATRAN, Version 1.2, Institute of Remote Sensing, University of Bremen, FB1, Germany, May 2000.

Burrows, J.P., M. Weber, M. Buchwitz, V. Rozanov, A. Ladsatter-Weisenmayer, et al., The Global Ozone Monitoring Experiment (GOME): Mission Concept and First Scientific Results, J. Atmos. Sci., 56, 151-175, 1999a.

Burrows, J.P., A. Richter, A. Dehn, B. Deters, S. Himmelmann, S. Voigt, and J. Orphal, Atmospheric Remote-Sensing Reference Data from GOME: 2. Temperature-Dependent Absorption Cross Sections of O_3 in the 231-794 nm Range, J. Quant. Spectrosc. Rad. Transf. 61, 509-517, 1999b.

Caspar, C., and K. Chance, GOME wavelength calibration using solar and atmospheric spectra, Proc. Third ERS Symposium, Florence, Italy, 1997, ESA SP-414, pp. 609-614, 1997.

Chance, K. and R.J.D. Spurr, Ring effect studies: Rayleigh scattering, including molecular parameters for rotational Raman scattering and the Fraunhofer spectrum, Applied Optics, 36, 5224-5230, 1997.

Chance, K., Analysis of BrO measurements from the Global Ozone Monitoring Experiment, Geophys. Res. Lett., 25, 3335-3338, 1998.

Fish, D. and R. Jones, Rotational Raman scattering and the Ring effect in zenith-sky spectra, Geophys. Res. Lett., 811-814, 1995.

Fortuin, J.P.F., and H. Kelder, An ozone climatology based on ozonesonde and satellite measurements, J. Geophys. Res., 103, 31709-31734, 1998.

GOME Users Manual, Ed. F. Bednarz, ESA Publications Division, ESA SP-1182, 1995.

Grainger, J.F., and J. Ring, Anomalous Fraunhofer Line Profiles, Nature, 193, 762, 1962.

Joiner, J., P. Barthia, R. Cebula, E. Hilsenrath, R. McPeters, and H. park, Rotational Raman scattering (Ring effect) in satellite backscatter ultraviolet measurements, Applied Optics, 34, 4513-4525, 1995.

Lambert, J.C., et al., GDP 3.0 Delta Validation Report, document in preparation, 2002.

Orphal, J., A critical review of the absorption cross-sections of O_3 and NO_2 in the 240-790 nm region, ESA Technical Note MO-TN-ESA-GO-0302, 2002.

Paur, R.J., and A.M. Bass, The Ultraviolet Cross-Sections of Ozone, II, Results and Temperature Dependence, in: Atmospheric Ozone, edited by C. S. Zerefos and A. Ghazi, pp. 611-616, D. Reidel, Norwell, Mass., 1985.

Platt, U., Differential Optical Absorption Spectrocopy (DOAS), in *Air Monitoring by Spectroscopic Techniques*, chap. 127, edited by M. W. Sigrist, pp.27-84, John Wiley, New York, 1994.

Press, W.H., B.P. Flannery, S.A. Teukolsky, W.T. Vetterling, Numerical Recipes in C, The Art of Scientific Computing, Cambridge University Press, Cambridge, USA, 1991.

Rozanov, V.V., D. Diebel, R.J.D. Spurr, and J.P. Burrows, GOMETRAN: A radiative transfer model for the satellite project GOME – the plane-parallel version, J. Geophys. Res. 102, 16683-16695, 1997.

Sioris, C., and W. Evans, Filling in of Fraunhofer and gas absorption lines as caused by rotational Raman scattering, Applied Optics, 38, 2706-2713, 1999.

Spurr, R.J.D., Discrete Ordinate Theory in a Stratified Medium with First Order Rotational Raman Scattering: A General Quasi-Analytical Solution, submitted (2002).

Thomas, W., D. Loyola, R. Spurr, GOME Level 1 to 2 Algorithms Description, ER-TN-DLR-GO-0025, Iss./Rev. 3/A, April 10, 2002

Trenberth, NCAR/TN-373+STR, 191pp., 1992.

Van Roozendael, M., C. Fayt, J.-C. Lambert, I. Pundt, T. Wagner, A. Richter, and K. Chance, Development of a bromine oxide product from GOME, Proc. ESAMS'99-European Symposium on Atmospheric Measurements from Space, ESTEC, Noordwijk, The Netherlands, 18-22 January 1999, WPP-161, p. 543-547, 1999.

Vountas, M., V.V. Rozanov, and J.P. Burrows, Ring effect : Impact of rotational Raman scattering on radiative transfer in earth's atmosphere, J. Quant. Spectrosc. Rad. Transfer, 60, 943-961, 1998.

VII CONCLUSION

The correctness of upgrades of GOME Data Processor level-1-to-2 to version 3.0, as well as their effect on GOME data products, have been investigated using different methods based on auto-correlation studies, on comparisons with correlative measurements, and on independent retrieval software tools.

The following data products and auxiliary information have been verified:

- Ozone data: slant and vertical column amount, effective absorption temperature, air mass factor, cloud fraction, and ghost vertical column;
- Nitrogen dioxide data: slant and vertical column amount, air mass factor.

In general, it is confirmed that modifications implemented in GDP 3.0 produce expected changes in the data products. However, it must be kept in mind that reported studies rely on a limited set of orbits and therefore unverified effects can not be ruled out.

Level-1 calibration: Compared to the spectral calibration technique used in GDP 2.7, the new cross-correlation method has only a slight effect on the level-2 data products. A GOME/EGOI calibration study performed at KNMI (not reported in the present document) on GDP solar and earthshine spectra extracted with versions 1.50 and 2.0 of the GDP extractor, confirms that there is no significant change in spectral window 323.13-336.22 nm where ozone is fitted. The cross-correlation technique is an improvement for the ICFA window. Nevertheless, DOAS studies in Chapter 6 point out that the lamp calibration offers so far the best stability of the spectral registration in the ozone fitting window, with fluctuations generally smaller than 0.003 nm.

Total ozone: The main objective of this GDP upgrade has been met: cyclic differences – seasonal, meridian, solar zenith angle and column dependences – between GOME and correlative total ozone data reduce by about 40-50% in amplitude. The improvement is remarkable during the Antarctic ozone hole condition where the 20% overestimation of the lowest column values by GDP 2.7 reduces to a 10% overestimation with GDP 3.0. The improvement is driven mostly by changes in the ozone air mass factor.

Total nitrogen dioxide: As expected, the total nitrogen dioxide data product has not significantly changed. For the first time, a quantitative assessment of the pole-to-pole agreement with NDSC/UV-visible network data is proposed. The quantitative agreement between GOME and total NO_2 data records is within a few 10^{14} molec.cm^{-2} for clean-troposphere stations from the tropics to the middle latitudes, and within 1-1.5 10^{15} molec.cm^{-2} at the poles during springtime. Over polluted areas, the difference can exceed 1-2 10^{15} molec.cm^{-2} and exhibits a seasonal variation of the same order of magnitude, correlating with seasonal cycles of tropospheric NO_2 predicted by modelling results. The accuracy of the air mass factor and of the effective absorption temperature remain major issues.

DOAS issues: The following DOAS-related error sources affecting the accuracy of GDP 3.0 total ozone have been studied: choice of ozone absorption cross-sections, determination of GOME slit function, accuracy of wavelength calibration of both reference data and measured GOME spectra, determination of ozone absorption effective temperature, treatment of the Ring effect, and use of single wavelength ozone air mass factor. Combined together, the various errors tend to cancel to a remarkable degree although not perfectly. It is likely that some of the reported effects contribute at least partly to the cyclic signatures still present in GDP 3.0 validation results.

Documentation: Existing documentation on GDP and on the quality of GDP data products was updated: DLR Technical Notes, GOME Data Disclaimer, GOME validation web site.

Operation: As a result of the general improvement of GOME data products, the new version of the level-0-to-1 and level-1-to-2 segments of GDP was implemented in the operational processing chain. Reprocessing of the whole GOME data record will be completed by the end of 2002. Data from 2002 onwards will be (re)processed with a new GDP level-2 version 3.1, which corrects for the AMF convergence problem mentioned in Section I.3 of the introduction. All reprocessed products can be used within the limitations outlined in the existing literature and updated in the present report.

VIII ANNEXE – DATA DISCLAIMER FOR GOME LEVEL-1 AND LEVEL-2 DATA PRODUCTS: NOVEMBER 2002

Introduction

Since the beginning of GOME operation aboard ERS-2 in 1995, the assessment of the quality of products generated by the GOME Data Processor (GDP), established at the German Processing and Archiving Facility (D-PAF), has been a continuing activity aimed at achieving data products having their theoretically achievable errors. This process and the algorithm improvement have benefited from the validation exercises involving the scientific community. The involved scientific groups have expertise in the development of retrieval algorithms and the measurement of trace constituents from other relevant instrumentation.

The operational products produced by the GDP are defined as:

- Level-1 data: Earthshine spectral radiance at the Top of the Atmosphere at the GOME viewing solid angle; Extra-terrestrial solar spectral irradiance.

- Level-2 data: Vertical Column amount of O_3 (Dobson Unit); Vertical Column amount of NO_2 (molecule cm-2); Cloud Fractional Coverage.

An intensive validation campaign for GOME products was conducted during the commissioning phase. Reported in an ESA publication (ESA WPP-108), studies carried out by more than 20 different groups highlighted a number of critical aspects of the GDP data products. As a result, recommendations were made for modifications to the GDP, data analysis, instrument operations, data processing, and data distribution. Some of these recommendations were implemented during the first months of 1996. Since then, several other important issues have been identified. Consequently further GDP modifications have been recommended and some of them implemented.

Before proceeding to the implementation of any major GDP changes in the operational processing chain, it is essential to verify the accuracy and effectiveness of the modification and to assess the quality of the new data product. Such 'delta' validation campaigns have been executed by a sub-group of the GOME Validation Group, with a limited but representative validation data set. Results were discussed during dedicated meetings in May and June 1996 and in January 1998 at the D-PAF and in May and July 1999 and in January and April 2002 at ESRIN.

Complementarily, detailed validation and algorithm improvement studies have been carried out by a wider community and reported on many occasions during conferences and workshops as well as in the open literature.

Based on the results of the above-mentioned studies, the present disclaimer summarises the status of the current GDP data quality, referring to version 2.2 for GDP level-0-to-1 and version 3.0 for GDP level-1-to-2.

Current Data Quality of GOME level 1-Product

The level-1 data products exhibit good wavelength stability indicating a high instrument precision.

GOME level-1 products are affected by spectral and radiometric distortions of instrumental origin, which change with time. The solar irradiance measurements exhibit an anticipated and in this sense normal, slow degradation in the UV (channels 1 and 2), which can optionally be corrected by the GDP extraction software. In addition, the degradation is superimposed by a seasonal variation of sensitivity depending on the solar azimuth at the sun diffuser. The errors impact the retrieval of ozone and other constituents in a relatively minor way, thanks to the use of the DOAS retrieval technique.

The accuracy of the Earth's reflectivity (i.e., the ratio between Earth radiance and solar irradiance) is considered to be about 3% except in the UV.

Solar Irradiance

The validation of GOME solar irradiance data is based on comparisons with SOLSTICE and SSBUV measurements in the 240-400 nm spectral range, on auto-correlation studies of GOME data, and on comparisons with high-resolution solar spectrum atlas data.

Deviations at the beginning of the GOME Instrument lifetime:

Despite the better agreement with SOLSTICE measurements, the GOME irradiance measurement in its channel 1 is considerably lower, by 5 % to 10 %. In channel 2, the agreement is better but the accuracy of GOME data is limited by etalon features (modulation of +/- 2 %).

The average deviation of GOME data from the SOLSTICE data on 3-Jul-1996 and the rate of linear decay between 3-Jul-1995 and 14-Jan-1996 are given in the following table:

Wavelength range	Average deviation	Linear decay
240 - 250 nm	5.8 %	3.5%/100 days
250 - 300 nm	5.1 %	1.5%/100 days
300 - 370 nm	0.8 %	0.5%/100 days
370 - 400 nm	2.4 %	0%/100 days

Deviations at mid 1999:

The average deviation of GOME data from the SOLSTICE V12 data on 1-Jan-1999 and the rate of linear decay in 1998 are given in the following table:

Wavelength range	Average deviation	Linear decay
240 - 250 nm	-51 %	4.7 %/100 days
250 - 300 nm	-25 %	1.7 %/100 days
300 – 350 nm	-9 %	0.7 %/100 days
350 - 400 nm	-4 %	0.3 %/100 days

The observed degradation in the UV was expected and is similar to the degradation observed in other relevant instruments. It can optionally be corrected by the extraction software. Note that the solar azimuth on the solar diffuser is different for January and July data, which affects the sensitivity in the spectral region below 260nm by about 6%. Therefore, the linear decay presented in the tables above must be considered as an upper limit.

Deviations till 2001:

The following table shows the yearly mean percentage degradation of GOME channels (basis = 3-Jul-1995) in the period from 1996 to 2001.

Wavelength range	1996	1997	1998	1999	2000	2001
240-250 nm	-0.2 %	-9.4 %	-22.8 %	-48.8 %	-60.6 %	-55.6 %
250-300 nm	-0.1 %	-3.0 %	-7.6 %	-16.9 %	-35.7 %	-47.8 %
300-350 nm	0 %	-1.6 %	-3.5 %	-5.3 %	-9.1 %	-25.1 %
350-400nm	0 %	-0.5 %	-1.4 %	-1.8 %	-2.3 %	-7.7 %
400-600 nm	0 %	-0.6 %	-1.3 %	-0.7 %	+1.2 %	+1.7 %
600-790 nm	0 %	-0.1 %	-1 %	-2.2 %	-1.4 %	+2.3 %

Earthshine Radiance

The Earthshine radiance product suffers from the same instrument degradation as the Solar Irradiance product.

A correction for the GOME instrumental response to polarisation (PC) is required for the radiance products. This PC has been determined assuming that single scattering is dominant below 300 nm. The polarisation of the up-welling radiation from the atmosphere has been determined as follows:

i) for wavelengths below 300 nm, it is assumed that the Rayleigh scattering determines the degree of polarisation;

ii) for wavelengths greater than 300 nm, experimental values for the degree of polarisation have been determined from the detector arrays in channels 2, 3 and 4 and their corresponding polarisation monitoring device (PMD);

iii) a polynomial is then fitted to the four "measurements" of the degree of polarisation, with a parameterisation based on model calculations between 300 and 350 nm, providing individual values of the degree of polarisation.

After the degradation correction of the polarisation measurements, the accuracy of the radiometric calibration of GOME between 350 and 790 nm is considered to be about 3% except in the UV where it is limited to 5 % due to pre-flight calibration uncertainties and to the remaining effects of atmospheric polarisation. Below 350 nm the Earth's radiance has not yet been fully validated.

One aspect of the radiance error results from inadequacies in the polarisation-correction procedure implemented in the level-1 extractor software. The interpolation of the small p values in the region between 350 nm (measured PMD1 polarisation value) and 300 nm (theoretical polarisation value) is not fully satisfactorily.

Discontinuities in the absolute radiance values are observed between channels and are real. This is caused by the serial readout of the detectors, which means that although all array pixel detectors have the same integration time, the read-out of the first array detector pixel is 93 ms shifted in time compared with the 1024th array detector pixel. This effect occurs in a pronounced fashion for earthshine scenes having significant albedo changes in the field of view of the first and of the last pixel of the detector. An option in the extraction software is available to create an effective average scene for the four channels.

Current Data Quality of GOME level-2 products

Vertical column amount of ozone

GDP total ozone has been validated from pole to pole by comparison with well understood, controlled and documented ground-based measurements from SAOZ/DOAS UV-visible spectrometers, Brewer and Dobson spectrophotometers, and UV filter radiometers, and with global data from the TOMS satellite sensor and from modelling/assimilation tools. GDP retrievals have also been compared with retrievals from independent DOAS algorithms and from the TOMS V7 algorithm.

The spectral fitting of ozone slant columns in the UV region from 325 to 335 nm works well. GOME gives a consistent global picture of the total ozone field and results in temporal and spatial structures similar to those from other sensors. The studies do not reveal any long-term drift of quality.

The agreement of GDP level-2 total O_3 data product with the other sources of O_3 data varies with both latitude and season. At Northern middle latitudes, the average agreement is within ±2-3%. At higher latitudes, a solar zenith angle (SZA) dependent difference appears. In addition a dependence of the GDP data product on the ozone column values has been identified. Latitude, season, SZA and column dependences are coupled in the final data product.

The average deviation of GOME from ground-based data does not exceed ±2-4% for SZA below 70°. At lower sun elevation, the average error ranges from -8% to +5% depending on the season. Lowest total ozone values are overestimated by GOME by 5-10% during ozone hole conditions.

The two-step DOAS approach adopted in GDP consists of the spectral fitting of slant column amount, followed by its conversion into vertical column amount using a calculated Air Mass Factor (AMF). Compared to GDP 2.7, GDP 3.0 includes a new determination of effective absorption temperature derived by spectral analysis, better atmospheric databases, and AMFs determined iteratively using a neural network trained on column- and latitude-classified atmospheric profiles and measurement parameters. All upgrades result in a reduction by about 30-50% of the amplitude of the GOME total ozone dependence on the SZA, the latitude, the season, and the ozone column amount.

The remaining dependence is attributed to the limited treatment of the atmospheric profile shape effect in GDP and to the partial unsuitability of the particular spectral analysis when the atmosphere becomes optically thick. Satellite ozone AMFs in the UV are sensitive to the shape of atmospheric profiles and to the total ozone amount. GDP 3.0 AMFs are determined using column- and latitude-classified atmospheric profiles, which therefore may differ from the actual, highly variable atmospheric profile shape. The two-step approach of GDP is well suited for relatively small absorptions which have a constant AMF across a selected spectral window. This assumption breaks down for ozone in the UV. As a result the difference between GOME vertical column ozone data and ground-based measurements exhibits a monotone solar zenith angle dependence when the air mass factor is calculated at the centre wavelength of the DOAS fit window (330 nm). Model calculations have shown that this latter effect is minimised by using the AMF at 325 nm.

Under very occasional circumstances of high ozone values (> 500 DU) at low sun elevation (SZA > 85°), the iterative AMF algorithm might not converge to a realistic AMF value, leading to unrealistically high ozone values (e.g. 700 DU) that could be identified and filtered out easily. The affected ground pixels are estimated to be in the order of 0.01% of a single orbit, randomly distributed on 1% of the GOME products from 1995 through 2001. Therefore no reprocessing of those historical data is foreseen in the near future. This problem has been solved and the data from 2002 onwards will be (re)processed with a new GDP level-2 version 3.1.

3.2 Vertical column amount of nitrogen dioxide

GOME GDP total nitrogen dioxide has been validated from pole to pole by comparison with well-understood, controlled and documented data retrieved from ground-based measurements from a network of SAOZ/DOAS UV-visible spectrometers and Fourier Transform Infrared spectrometers, and with global data from the HALOE and POAM satellite sensors and from both tropospheric and stratospheric modelling tools. GDP retrievals have also been compared with GOME NO_2 DOAS retrievals performed by members of the validation sub-group.

The inclusion in the fitting NO_2 window (425-450 nm) of the absorptions of O_4 and H_2O, coupled with a number of software improvements, results in the GOME total nitrogen dioxide being in reasonable agreement with ground-based and other satellite measurements: within ±5 10^{14} molec.cm^{-2} in areas of low tropospheric NO_2 and within ±8 10^{14} molec.cm^{-2} in areas of very low slant column of NO_2. Although it is difficult to evaluate precisely the accuracy of this product due to various problems such as the diurnal photochemical variation of NO_2, the overall accuracy is estimated to fall within the 5% to 20% range. GOME total NO_2 is affected by larger errors under particular circumstances, e.g., over polluted areas and in the South Atlantic Anomaly.

The relatively small NO_2 absorption in its selected fitting window implies that retrieval using the two-steps DOAS approach of GDP is well suited to generate accurate data products. However, NO_2 AMFs and effective absorption temperatures are strongly affected by variations in tropospheric burden of NO_2 especially for high pollution conditions in the boundary layer. Atmospheric parameters currently in use in GDP introduce a fictitious latitudinal/seasonal variation of a few percent superimposed on the geophysical variations in NO_2.

Conclusions

As a consequence of the anticipated degradation of the instrument and resultant changes of in-flight calibration parameters, a dynamic or temporally dependent database has been developed to provide the optimal calibration of the level-1 data. The database describes the temporal behaviour of GOME calibration parameters and was validated before implementation.

The present errors in the level-1 product have a negligible impact on the quality of the total column of ozone and nitrogen dioxide density derived by the DOAS in level-1-to-2 processing. The reason is that many errors arising from the changes in calibration parameters cancel because the DOAS algorithm uses the irradiance divided by the radiance spectra as its input.

Present quality of level-2 products makes them usable for a variety of geophysical research studies. Reprocessing of the complete data set with GDP 3.0 is anticipated by the end of 2002.

The present understanding of the GOME data quality is based on the validation results presented in Frascati (January 1996, May and July 1999, January and April 2002), Florence (March 1997), Noordwijk (January 1999) and during GOME science & algorithms workshops, on the existing literature, and on the findings of a sub-group of the GOME validation group, which investigated the quality of the GOME data after the successive implementations of major changes in GDP.

The improvement of GDP and the consequent validation work are still going on. This report presents only an overview of the current situation. Further improvement and detailed validation results based on an extended data set are expected in the future.

Documentation

The available ESA documentation for the GOME system comprises:

- GOME WWW site: http://earth. esa.int/gome
- GOME Interim Science Report (ESA-SP 1151, 1993)
- GOME Users manual (ESA-SP 1182, 1995)
- Product Specification Document of the GOME Data Processor (ER-PS-DLR-GO-0016, issue 4A, April 10th, 2002)
- GOME Level 0 to 1 Algorithms Description (ER-TN-DLR-GO-0022, issue 5B, April 10th, 2002)
- GOME Level 1 to 2 Algorithms Description (ER-TN-DLR-GO-0025, issue 3A, April 10th, 2002)
- GOME Software Databases for Level 1 to 2 Processing (ER-TN-IFE-GO-0018, issue 3A, April 10th, 2002).
- Proceedings of GOME Geophysical Validation Campaign Final Results Workshop, ESA-ESRIN, Frascati, 24-26 January 1996 (ESA WPP-108, 1996).

- Proceedings of 3rd ERS Scientific Symposium, Florence, Italy, 17-20 March 1997 (ESA SP-414, Vol. 2, 1997).
- GOME Data Improvement Validation Report (Ed. B. Greco, ESA/ESRIN APP/AEF/17/GB, 1998).
- Proceedings of European Symposium on Atmospheric Measurements from Space, ESA-ESTEC, Noordwijk, The Netherlands, 18-22 January 1999 (ESA WPP-161, 2 Vol., 1999).
- Update Report for GDP 0-to-1 Version 1.5 and GDP 1-to-2 Version 2.4 (ER-TN-DLR-GO-0043, 1999).
- ERS-2 GOME Data Products Delta Characterisation Report 1999 (Ed. J.-C. Lambert and P. Skarlas, IASB, Brussels, Issue 1.0, November 1999).
- ERS-2 GOME GDP 3.0 Implementation and Delta Validation (Ed. by J.-C. Lambert, IASB, Brussels, Issue 1.0, November 2002).

In addition a growing scientific literature is available at the GOME WWW site and at the GOME Validation WWW site (http://www.oma.be/GOME). Links to other relevant GOME sites are also provided.

Contact point

To order GOME products, or for further information, please contact the ESRIN Help & Order desk:

ESRIN Earth Observation Help and Order desk:

Via Galileo Galilei CP 64
I - 00044 FRASCATI, Italy
phone: +39 6 941 80 666
fax: +39 6 941 80 272
e-mail: eohelp at esrin.esa.it

GOME WWW site: http://earth.esa.int/gome